Technische Universität München
Institut für Organische Chemie und Biochemie

Max-Planck-Institut für Biochemie
Abteilung Strukturforschung
Biologische NMR-Arbeitsgruppe

Structural and biochemical characterization of proteins involved in cancer

Madhumita Ghosh

Vollständiger Abdruck der von der Fakultät für Chemie der Technischen Universität München zur Erlangung des akademischen Grades eines

Doktors der Naturwissenschaften

genehmigten Dissertation

Vorsitzender: Univ.-Prof. Dr. Dr. A. Bacher
Prüfer der Dissertation:
1. apl. Prof. Dr. Dr. h. c. R. Huber
2. Univ.-Prof. Dr. J. Buchner

Die Dissertation wurde am 02.12.2004 bei der Technischen Universität München eingereicht und durch die Fakultät für Chemie am 18.01.2005 angenommen.

Dedicated to my mom

Publications

Parts of this thesis have been or will be published in due course:

Madhumita Ghosh, Sreejesh Shanker, Igor Siwanowicz, Karlheinz Mann, Werner Machleidt, and Tad A. Holak

Proteolysis of insulin-like growth factor binding proteins (IGFBPs)

Biological Chemistry (2005) ***386:*** *85-93*

Madhumita Ghosh, Srinivas K. Kumar, Loyola D'Silva, Tad A. Holak, and Saeed R. Khan

Novel boronic and cyano chalcone derivatives as inhibitors of the p53-MDM2 pathway

Manuscript submitted to Journal of Medicinal Chemistry

Narasimharao Nalabothula, Oliver Popp, **Madhumita Ghosh**, Loyola D'Silva, Shirley Gil-Parrado, Werner Machleidt Tad A. Holak

Identification of cleavage sites of calpain in G1 cyclin-dependent kinase inhibitor p19^{INK4d}

Manuscript submitted to Biochemistry

Igor Siwanowicz, Grzegorz Popowicz, **Madhumita Ghosh**, Louis Moroder, Loy Dsilva, Joma Joy, Sudipta Majumdar, Magdalena Wisniewska, Sue M. Firth, Robert C. Baxter, Robert Huber and Tad A. Holak

Molecular architecture of the insulin-like growth factor binding proteins (IGFBPs)

Manuscript under preparation

Table of contents

Introduction

Cancer, considered to be one of the major challenges to mankind is responsible for about quarter of all deaths in the developed nations. It is lethal because a large proportion of all cancers spread beyond the reach of surgery, when first detected. After decades of disappointment and enormous investment of time and capital, limited success has been achieved in treating some cancer types. Cancer remains a disease of high unmet clinical need where life expectancy can often be short. The completion of the human genome sequence, rapid improvements in our understanding of the molecular basis of cancer and the introduction of new technologies for assessing transcriptional and proteomic changes provide new opportunities for addressing the practical challenges of cancer.

Scope of this work

Tumours are diverse and heterogeneous, but they all share the ability to proliferate beyond the constraints limiting growth in normal tissue. Mammalian cells have multiple safeguards to protect them against the potentially lethal effects of carcinogenetic transformation. One such defence mechanism is the tumour suppressor protein p53. The loss of p53 activity due to the increased expression of its negative regulator, murine double minute clone 2 (MDM2) protein results in uncontrolled proliferation of damaged cells (Oliner et al. 1992). Hence, a novel class of chalcone derivatives were characterized as possible MDM2 antagonists using NMR spectroscopy (Chapter 5.1). Till date since only the first 100 residues of MDM2 in complex with the p53 peptide has been structurally defined (Kussie et al. 1996), in order to gain some structural insight we looked into the longer N terminus constructs and the C terminal region of MDM2 which binds to pRb (Xiao et al. 1995). Chapter 5.2 gives an overview of some preliminary investigations performed.

Extracellular mitogens like insulin-like growth factors (IGFs) stimulate signalling pathways leading to cellular division and proliferation. Deregulation of these survival factors result in uncontrolled cell growth and suppressed apoptosis, which constitute the first step in neoplastic development (Pollak, et al. 2004). Realizing the importance of IGFBPs' in regulating the freely available IGFs in circulation, it is imperative to gain more knowledge in IGFBPs domain organization and the structural requirements for complex formation with IGFs. The conclusions of this work add on towards structure based drug design for tumours with high IGF

mitogenic activity. Details are given in Chapter 5.3.

Many proteases, which are present in tumor microenvironments, including metalloproteinases or caspases, can digest IGFBPs and release free ligand. Production of such proteases by cancer cells might therefore increase IGF-I receptor signalling (Pollak 1998). Calpains are Ca^{2+}-dependent cysteine proteases, which play a role in the cell cycle, specifically in the G_1 to S phase transition. Rules that govern calpain cleavage specificity are poorly understood. Hence we performed proteolytic studies on IGFBPs and the CDK inhibitor, $p19^{INK4d}$ in order to understand the cleavage pattern followed by calpain. The results are discussed in Chapters 5.3.2 and 5.3.3.

The aim of this thesis was to structurally and biochemically characterize the above-described proteins. To achieve the tasks various biochemical and biophysical methods were employed. Nuclear magnetic resonance spectroscopy experiments were undertaken to search for binding sites of small molecular weight compounds as potential inhibitors of protein-protein interactions. Inhibitor binding efficiency was also determined by the isothermal titration calorimetry (ITC). Laboratory work was based on the biochemistry and molecular biology techniques described in Chapter 4.

2. Biological Background

2.1. The mammalian cell cycle

The mammalian “cell-division cycle” denotes a sequence of events by which cells accurately duplicate their genetic material (chromosomal replication) and then divide (chromosomal segregation) into two genetically identical daughter cells. These events are regulated by biochemical pathways defined as checkpoints that halt the cell cycle in response to cellular stress. Since the processes of DNA replication and cell division occur at distinct and regulated time intervals, the cell cycle can be conceptually divided into four phases (Fig. 2.1) as shown in the tabular form below in Table 2.1.

2.1.1. Cell cycle checkpoints

The eucaryotic cell division cycle requires the presence of extracellular growth factors or mitogens for its progression (Fig. 2.1). Cells respond to these stimulations only in the G_1 phase

Table 2.1 *Cell cycle phases in somatic cells*

G_1 (gap-1)	This covers longest phase of the cell cycle during which cells prepare for replication. It is the gap between M phase and S phase and gives way to S phase.
S (synthesis phase)	This phase occupies about half of the cell cycle time (10-12 hours) during which the genetic material is duplicated and a complete copy of each of the chromosomes is made.
G_2 (gap-2)	This is the shortest gap phase, which occurs after the DNA synthesis and before mitosis.
M (mitosis phase)	A relatively brief phase of the cell cycle (around 1 hour) where, chromosome segregation and cell division takes place, whereby the duplicated chromosomes are distributed equally to the two daughter cells.
G_0 (G-zero)	Under unfavorable conditions, cells withdraw from the cycle at the early G1-stage into a non-proliferating, quiescent, or resting phase of the cell cycle called G_0.

(and also in G_0) of the cell cycle. The final decision of the cell to proceed with the cell division or enter the quiescent state depends on the extra- or intracellular environment of the cell. Such a decision is made in the late G_1 phase of the cell cycle and is termed as the "G_1/S transition checkpoint" or "restriction point" (R-point) (Fig. 2.1). The R-point is of crucial importance since after passing this point, cells are committed to DNA replication and cycle until completion, even if the extracellular signals that stimulate cell growth and division are removed (Sherr and DePinho 2000). Checkpoints operate during the gap phases and ensure that the cells are competent to undergo DNA replication (G_1/S checkpoint) and that replication of the DNA has been successfully completed before cell division (G_2/M check point). Cells can arrest transiently at the checkpoints to allow for DNA repair or undergo programmed cell death, if the damage is irreparable. The mechanisms inducing delay in cell cycle progression or apoptosis are closely

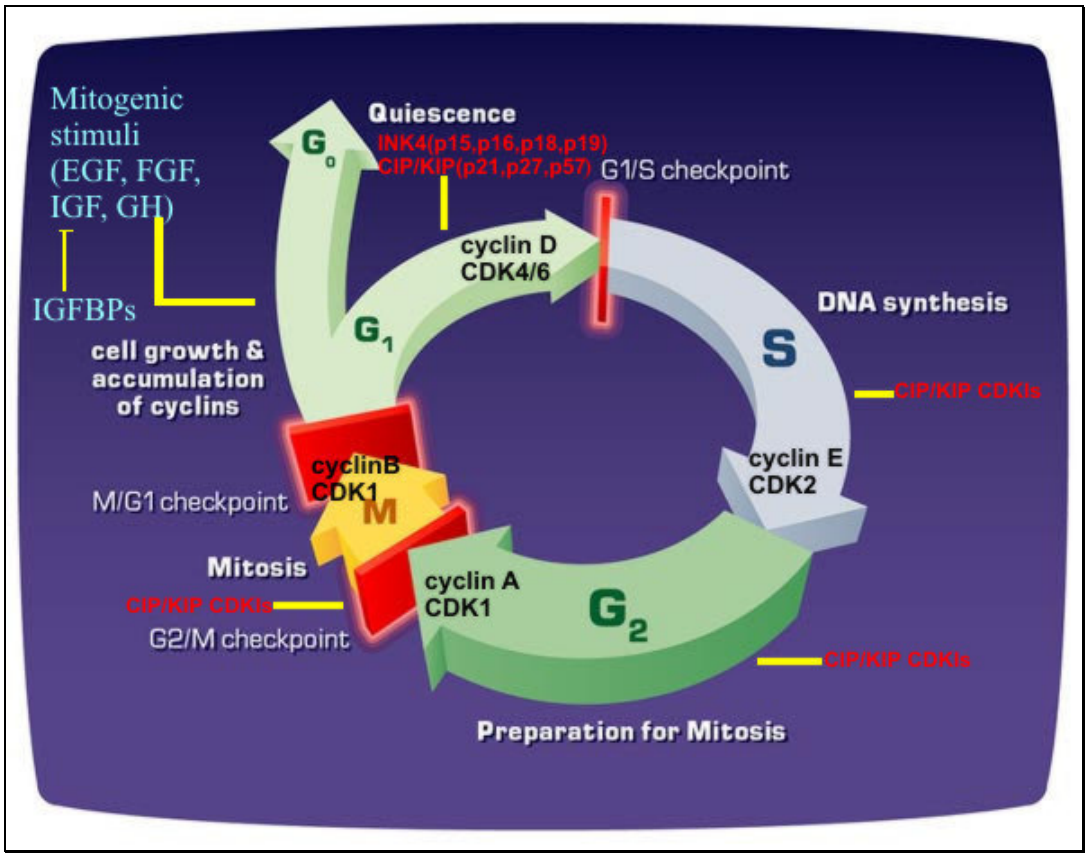

Figure 2.1 *Schematic representation of highly regulated and well organized cell cycle checkpoints. The cell cycle phases, driven by the precisely controlled cyclins and cyclin-dependent kinases in the respective phases are shown. Also mitototic signals in the G_1 and G_0 phase are depicted.*

interconnected via key regulatory tumor suppressors, such as p53 and pRb (Fig. 2.2) (Sherr 1996; Lundberg and Weinberg 1998; Vermeulen et al. 2003).

2.1.2. Gap 1 (G_1) phase

The progression of the cell cycle is controlled by regulation of protein phosphorylation by specific protein kinase complexes, consisting of a catalytic subunit called cyclin-dependent kinases (CDKs) and a regulatory subunit called cyclins (Fig. 2.2). CDK activation requires the binding of a cyclin partner in addition to site-specific phosphorylation by CDK activating kinase (CAK) (Vermeulen et al. 2003). The cyclin-CDK complexes are negatively regulated by the binding of CDK inhibitors (CDKIs), which consist of two families, the INK4 inhibitors and the Cip/Kip inhibitors (Sherr and Roberts 1999). There are four known members of INK4 protein

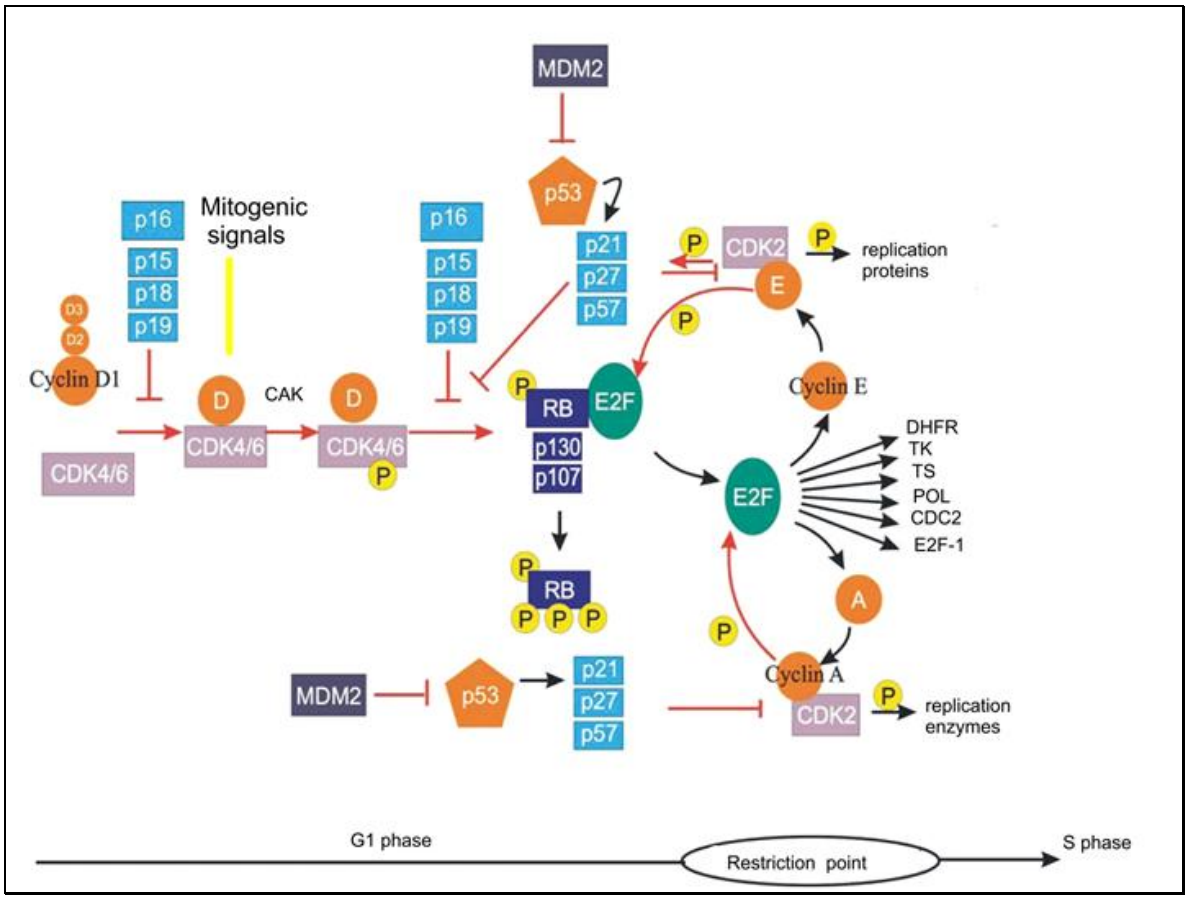

Figure 2.2 *Restriction point control. The tumor suppressors most frequently targeted in human cancers are highlighted. Overexpression of the oncogene, Mdm2 would inhibit the p53 mediated cell regulation. The CDK-cyclin complex and their inhibitors are also shown.*

family: $p16^{INK4a}$, $p15^{INK4b}$, $p18^{INK4c}$ and $p19^{INK4d}$; and the Cip/Kip family has three members: $p21^{Waf1/Cip1}$, $p27^{Kip1}$ and $p57^{Kip2}$. Mitogenic signals affect extracellular signal simulating proliferation, leading to cyclin D activation, which are growth factor sensors (Fig. 2.2). The INK4 family members function only at G_1 to inhibit cyclinD-CDK4/6, whereas the Cip/Kip family serves as CKIs in all the four phases of the cell cycle (Sherr and Roberts, 1999). Activated cyclinD-CDK4/6 holoenzyme phosphorylates pRb and other pRb like pocket proteins; p130, p107 which leads to the release of E2F transcription factors, which then, in turn transcribe many genes that encode proteins (like DHFR, dihydro folate reductase; TK, thymidine kinase; TS, thymidylate synthase; POL, DNA polymerase α; CDC2, cyclin dependent kinase 1) required for S-phase entry (Sherr and Roberts 1999; Malumbres et al. 2000). The increase in E2F

transcriptional activity promotes completion of pRb phosphorylation by cyclin E-CDK2 that establishes a positive feed back loop and ensures irreversibility of G_1/S checkpoint transition. This renders entry into the S-phase independent of mitogenic stimulations. Furthermore, cyclin E-CDK2 facilitates cell cycle progression through induction of $p27^{Kip1}$ phosphorylation (Sherr and DePinho 2000).

2.1.3. Synthesis (S) phase

Phosphorylation of components of the DNA replication machinery by cyclin A-CDK2 is important for initiation of DNA replication. The synthesis of cyclin A is activated by E2F, but as a negative feed back loop, E2F activity is inhibited by cyclin A-CDK2 via phosphorylation of the E2F heterodimerisation partner DP1 (Johnson et al. 1999). Additionally, cyclin D-, E-, and A-dependent kinases are negatively regulated by Cip/Kip family members: $p21^{Waf1/Cip1}$, $p27^{Kip1}$ and $p57^{Kip2}$.

2.1.4. Cell cycle in cancer

The ability of normal cells to undergo cell-cycle arrest after damage to DNA is crucial for the maintenance of genomic integrity. Normally, in adult tissue, there is a delicate balance between cell proliferation (cell division) and apoptosis (programmed cell death) resulting in a steady state. Aberrations in this equilibrium by dysregulation of the cell cycle checkpoint are hallmarks of malignant transformations, leading to the development of tumors (Sherr 1996). Principally, deregulation of the cell cycle can be caused by induction of positive regulators (oncogenes) or by inactivation of inhibitory factors (tumor suppressor genes). Most of the cancers are a result of cell cycle deregulation due to mutation of the tumor suppressors; hence cancer is rightfully called the “disease of the cell cycle”.

2.2. MDM2 as an oncogene

MDM2 (murine double minute 2) was first identified as the gene amplified on double minute particles in a transformed murine cell line. The *Mdm2* gene was found to be located on small, acentric extrachromosomal nuclear bodies, called double minutes. These 1-2 megabase fragments contained three expressed genes, of which the product of the second gene, which was *Mdm2,* was found to have transforming abilities when overexpressed. Later it was found that the

transforming potential of the *Mdm2* gene product was attributed to its ability to bind to the transactivation domain of the tumour suppressor protein p53, and thereby inhibit both p53 mediated G1 arrest and apoptosis (Oliner et al. 1992; Oliner et al. 1993; Chen et al. 1996). Moreover, the MDM2 levels have been shown to be abnormally up regulated in a variety of human tumours such as sarcomas that retain wild type p53 activity (Oliner et al. 1992). This suggests that MDM2 overexpression can be oncogenic because of the resulting p53 inactivation. MDM2 acts negatively on p53 in three different ways:

1. MDM2 binds to the transactivation domain of p53 and inhibits its transcriptional activity.
2. MDM2, which acts as an ubiquitin ligase, promotes p53 degradation through ubiquitin mediated proteolysis pathway.
3. Finally, on binding to p53, MDM2 favours export of p53 into the cytoplasm since it contains a nuclear export signal.

The MDM2 mediated p53 ubiquitination is subject to a feedback loop, in which the p53 protein binds to the regulatory region of the *Mdm2* gene and stimulates the transcription of this gene into messenger RNA, which is then translated into protein. This MDM2 protein then binds to p53 and stimulates the addition of ubiquitin groups to the carboxy terminus of p53, which is then degraded. This lowers the concentration of p53 and reduces transcription of the *Mdm2* gene, closing the feedback loop and allowing p53 levels to rise again.

2.2.1. *Mdm2* gene structure

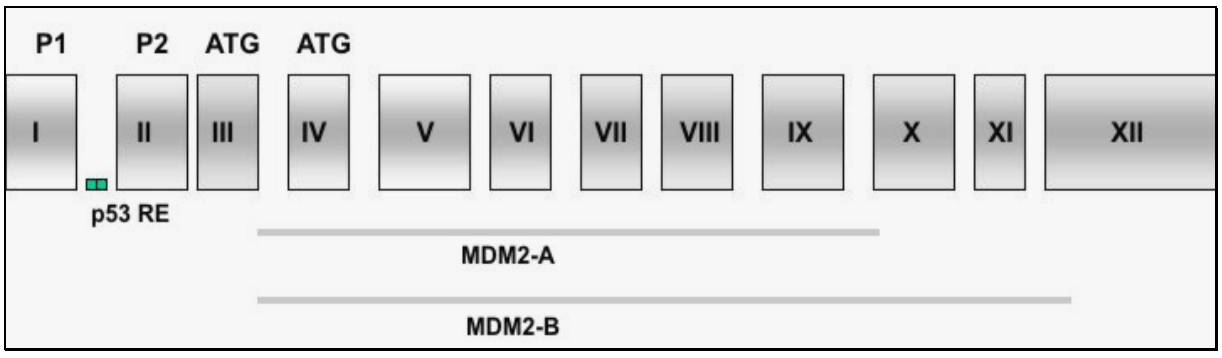

Figure 2.3 *Schematic representation of the gene structure of Mdm2, highlighting the various exons. Also shown are the regions coding for the major transcrips of the Mdm2 gene.*

The murine *Mdm2* gene is about 25-kilobase (kb) in size. Both murine and human *Mdm2* genes consist of 12 exons (Montes de Oca Luna et al. 1995) that can generate many different proteins. The *Mdm2* gene has two different promoters of which the second promoter is p53 responsive (Fig. 2.3). These promoters lead to transcripts, which may initiate translation at different ATG codons (Barak et al. 1994; Zauberman et al. 1995) generating two proteins, the full-length p90 and a shorter protein p76 that initiates at an internal ATG (Olson et al. 1993; Perry et al. 1993). The shorter protein, p76 lacks the p53 binding domain (Fig. 2.3). Moreover, there are several different isoforms of *Mdm2* mRNA transcripts and expression analyses of these transcripts in various cancer types and normal tissues have revealed alternative as well as aberrant splicing of *Mdm2*. These aberrant splicing generate numerous short MDM2 proteins (Bartel et al. 2004) which lack the p53 binding domain, nuclear localization and export signals, the p300 binding domain and even the acidic domain. In humans, MDM2-A and MDM2-B are the two major splice variants that delete exons 4-9 and 4-11, respectively. Though the biological significance of these splice variants are yet unclear but these short MDM2 proteins may function as dominant negatives inhibiting the function of full length MDM2 and amplifying the activity of p53 (Iwakuma and Lozano 2003).

2.2.2. MDM2 protein domains

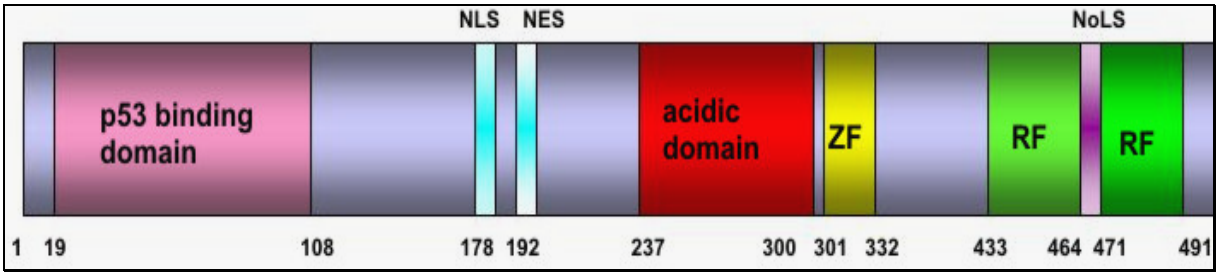

Figure 2.4 *MDM2 domain representation. The initial 100 residues of the N-terminal binds p53, this is followed by nuclear localization signal (NLS) and nuclear export signal (NES). Acidic domain occupies the central region, the zinc finger (ZF) domain is from residues 301-332 and the RING finger (RF) domains are in the C-terminus. Also a nucleolar localization signal (NoLS) is located in this terminus.*

Human MDM2 is 55.23 kDa phosphoprotein that has several domains conserved between species (Fig. 2.4). The first conserved domain, in the amino terminus of MDM2, consists of the

first 100 residues of this terminus that is sufficient to bind the α-helix present in the NH_2 terminal transactivation domain of p53 (Chen et al. 1993; Kussie et al. 1996). Other motifs include the nuclear localization signal (NLS) and nuclear export signal (NES), which mediates MDM2's ability to shuttle back and forth between the nucleus and the cytoplasm (Roth et al. 1998). A central acidic domain comprises of 40% glutamic acid and aspartic acid residues and is responsible for binding the histone acetyl transferase, p300/CBP (CREB-binding protein) and contributes in ubiquitin mediated p53 degradation (Argentini et al. 2001; Zhu et al. 2001). Downstream of the acidic domain is the zinc finger (ZF) domain of unknown function, followed by the conserved cysteine rich RING finger (RF) domain which functions as the E3 ligase to ubiquitinate p53 at several lysine residues (Rodriguez et al. 2000). RING finger domain is also known to be responsible for interactions with other proteins, DNA or RNA. Amino acids 464-471 can also function as nucleolar localization signal (NoLS) (Lohrum et al. 2000), although the biological significance of this regulation is to be elucidated.

2.2.3. p53 protein motifs

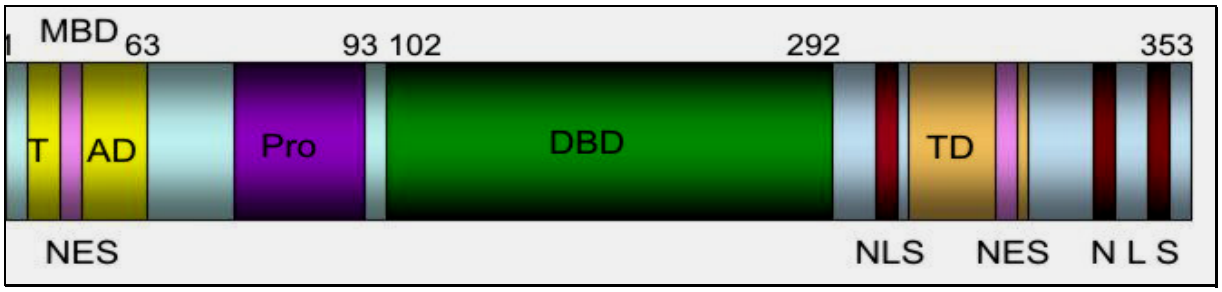

Figure 2.5 *p53 domain organization. The NH_2 terminal domain of p53 comprises of the transcription activation sub domain (TAD) and the proline rich sub domain; a central sequence specific DNA binding core domain (DBD) and a carboxy-terminal region that contains a tertramerization domain (TD) and nuclear localization signals. Nuclear export of p53 is regulated by signals in the amino and carboxy termini. MBD, denotes the MDM2 binding domain.*

Tumour suppressor p53 is a potent transcription factor that has several well defined domains (Fig. 2.5) which allows the tetrameric p53 protein on binding to DNA, to regulate the expression of several genes with different biological functions like cell cycle regulation, apoptosis, DNA repair and differentiation. Thus activation of p53 in response to stress protects

the normal cells from malignant transformation (Wu and Levine 1997; Levine and Fleischli 2000; Vogelstein and Kinzler 2001).

2.2.4. Oncoprotein MDM2 and tumour suppressor p53 interaction

The regions corresponding to residues 17-125 of MDM2 have been crystallized in complex with p53 peptide (15-29) and the biochemical basis of MDM2-mediated inhibition of p53 was further elucidated by the X-ray structure determined at 2.6 Å resolution (Kussie et al. 1996). The structure shows MDM2 forms a deep hydrophobic cleft (about 25 Å long and 10 Å wide), lined with 14 hydrophobic and aromatic residues into which the transactivation domain of p53 binds, thereby concealing itself from the interaction with the transcriptional machinery (Fig. 2.6). The sides of the cleft are formed by two helices, and β-strands are present at its ends.

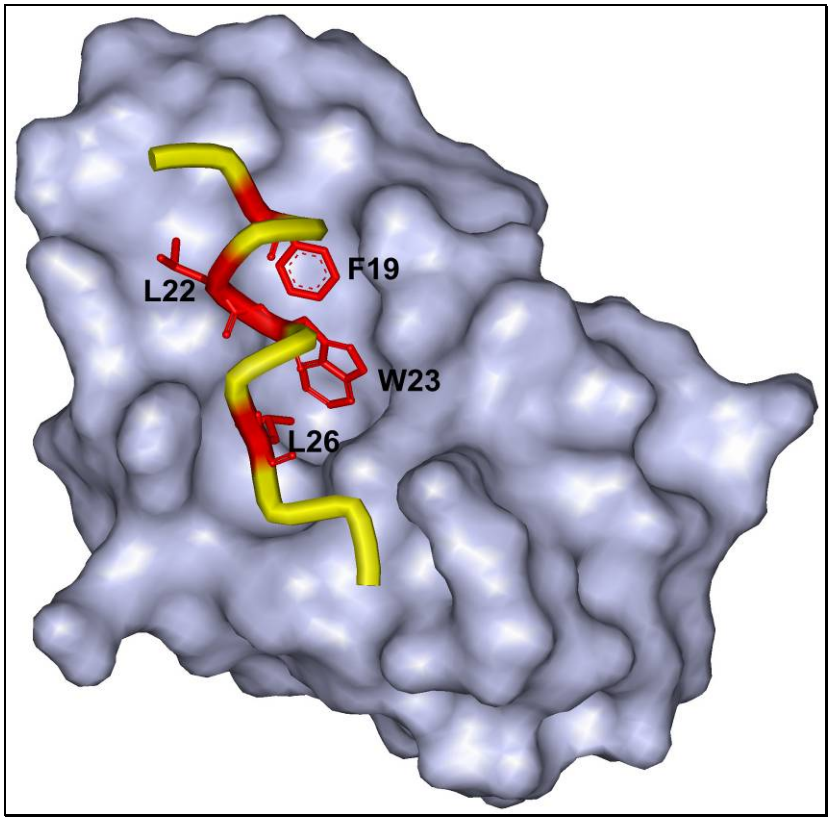

Figure 2.6 *Crystal structure of the complex of MDM2 protein with p53 peptide The MDM2 surface showing the deep hydrophobic cleft (gray) into which the p53 helix fits. The p53 peptide is shown as a solid ribbon and the p53 amino acids that interact with this surface (Phe19, Trp23, and Leu26) are shown in red (Kussie et al 1996).*

Two antiparallel smaller helices form the bottom of the cleft (Fig. 2.7). This interaction interface relies primarily on van der Waals interaction and the buried surface area is essentially hydrophobic in nature and with 70% of the atoms at the interface being nonpolar. The interaction is stabilized by three hydrogen bonds; Trp contributes the most buried one on p53. Experimental measurements of the strength of the p53-MDM2 bond range from a K_d of 60-700 nM depending on the length of the p53 peptide (Kussie et al. 1996; Schon et al. 2002). Site directed mutagenesis studies have shown the importance of p53 residues Leu14, Phe19, Leu22, Trp23 and Leu26, of which Phe19, Trp23, and Leu26 are of prime importance (Chen et al. 1993; Bottger et al. 1997).

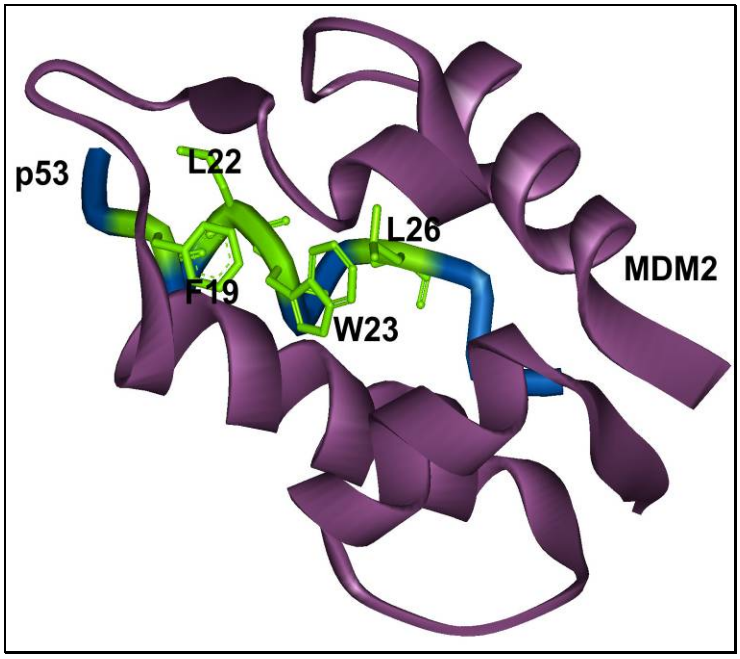

Figure 2.7 *Ribbon structure of MDM2-p53 interaction.*

2.2.5. p53 independent functions of MDM2

Although MDM2 has been extensively characterized as a regulator of p53, there is considerable evidence that MDM2 has p53-independent functions. These proteins can be divided into two groups: those that function upstream of MDM2 (effectors) and that specifically modify MDM2 and those that are downstream of MDM2 (affectors) that are regulated by MDM2 as shown in Table 2. Fig.2.8 shows the various functions of MDM2 besides p53 regulation.

Table 2 *A list of MDM2 modulators and effectors besides p53. Mdm2denotes the* MDM2*gene.*

Effectors	**Effect on MDM2**
ARF	Down regulation of MDM2, sequestration of MDM2 in the nucleolus
Tsg101	Self ubiquitination of MDM2 is lowered
P300/CBP	Stabilizes *Mdm2*
Affectors	**Result of interaction on MDM2**
pRb	MDM2 inhibits the ability of pRb to inhibit E2F function
E2F/DP1	*Mdm2* stimulates E2F/DP1 transcriptional activity and DNA synthesis
Sp1	*Mdm2* inhibits its activity
HDAC1	MDM2-HDAC1 mediated deacetylation of p53 helps in p53's ubiquitination
MTBP	*Mdm2* abrogates MTBPinduced G1 arrest
Numb	*Mdm2* accelerates its degradation
DNA pol ε	MDM2 stimulates its activity

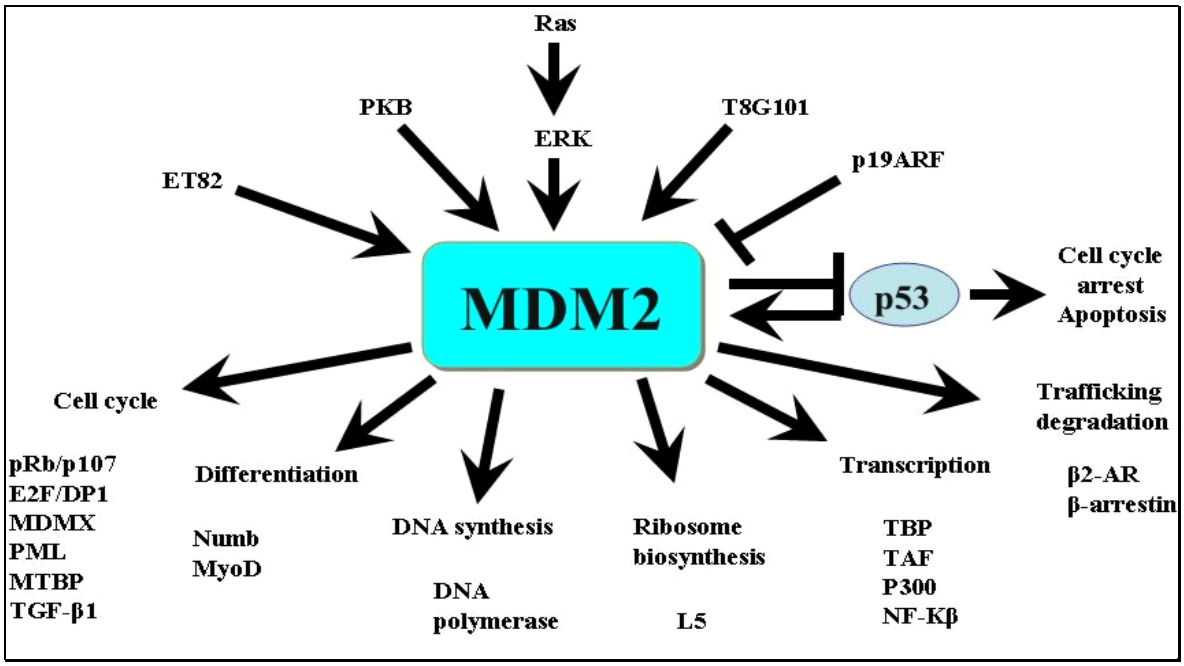

Figure 2.8 *Schematic representations of p53 independent functions of MDM2.*

2.2.6. MDM2 and pRb interaction

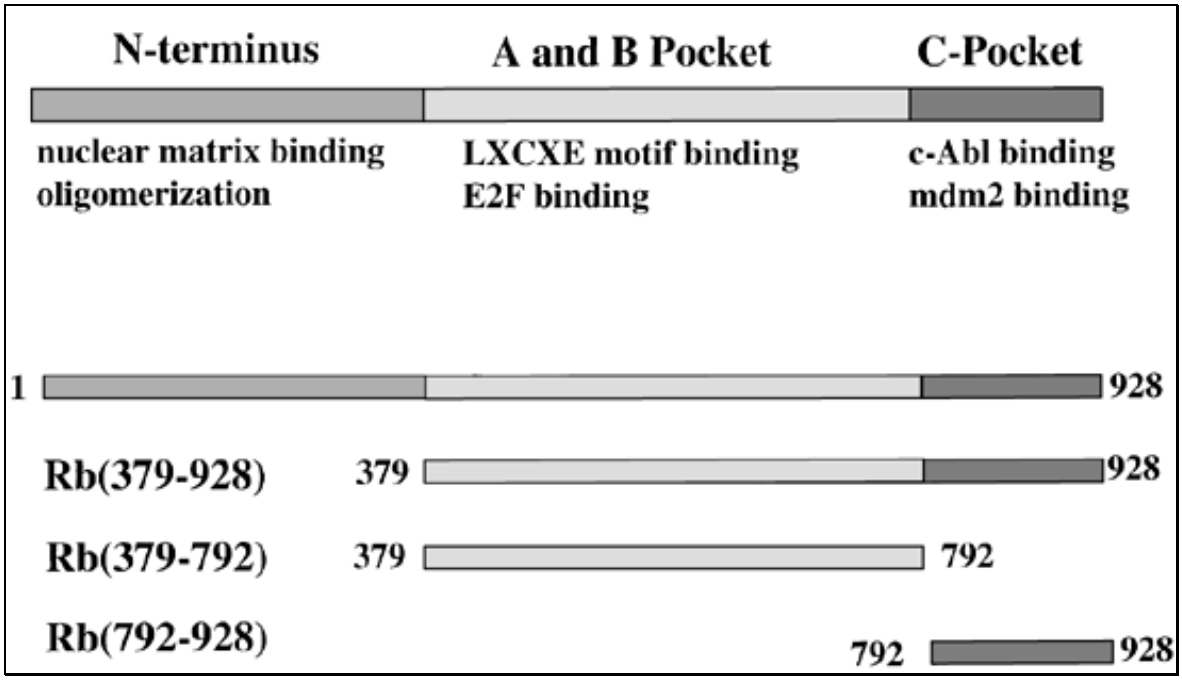

Figure 2.9 *Functional domains of retinoblastoma protein include the N-terminal domain (1-379), A/B pocket and the C-terminal domain (729-928). The large pocket region (379-928), which is needed for pRb to perform growth suppressor activity, and A/B pocket, which is needed for pRb to perform growth suppressor activity, and A/B pocket, which is conserved among all pocket proteins, and chiefly involve in binding of pRb to numerous cellular and viral oncoproteins*

pRb is a tumor suppressor protein that has functions similar to p53, in cell cycle inhibition and cell death. The pRb, carboxy terminal (residues 792-928) has important implications as this fragment together with the small pocket is required for growth suppression activity of pRb and for stable interaction with E2F a, nuclear transcription factor involved in cellular replication and transition of cell cycle from G1/S phase. MDM2 modulates the activity of pRb, by binding to its C-terminal fragment and interferes with the ability of pRb to inhibit E2F. Conversely, pRb also impairs antiapoptotic function of MDM2 on p53-mediated apoptosis through the formation of a trimeric complex with p53 (Hsieh et al. 1999). The functional domain structure of pRb is shown in Fig. 2.9. Biochemical experiments indicate that pRb potentially interacts with more than 100 different cellular proteins; hence a much detailed structure/function mapping is required to clarify the biological relevance of all these interactions.

2.2.7. p19ARF links the tumor suppressor's p53 and pRb

Surprisingly, p53 and pRb are themselves regulated by two proteins encoded by a single genetic locus, INK4a/ARF, the products of which $p16^{INK4a}$ and $p19^{ARF}$, are also potent tumour suppressors. $p16^{INK4a}$ is an inhibitor of cyclin-dependent kinase that function upstream of pRb and restrains cell growth through preventing phosphorylation of pRb. $p19^{ARF}$acts by attenuating MDM2 mediated degradation of p53 (Stott et al. 1998). The interaction of ARF with MDM2 blocks MDM2 shuttling between the nucleus and cytoplasm via the nucleolus. Fig. 2.10 explains this interaction.

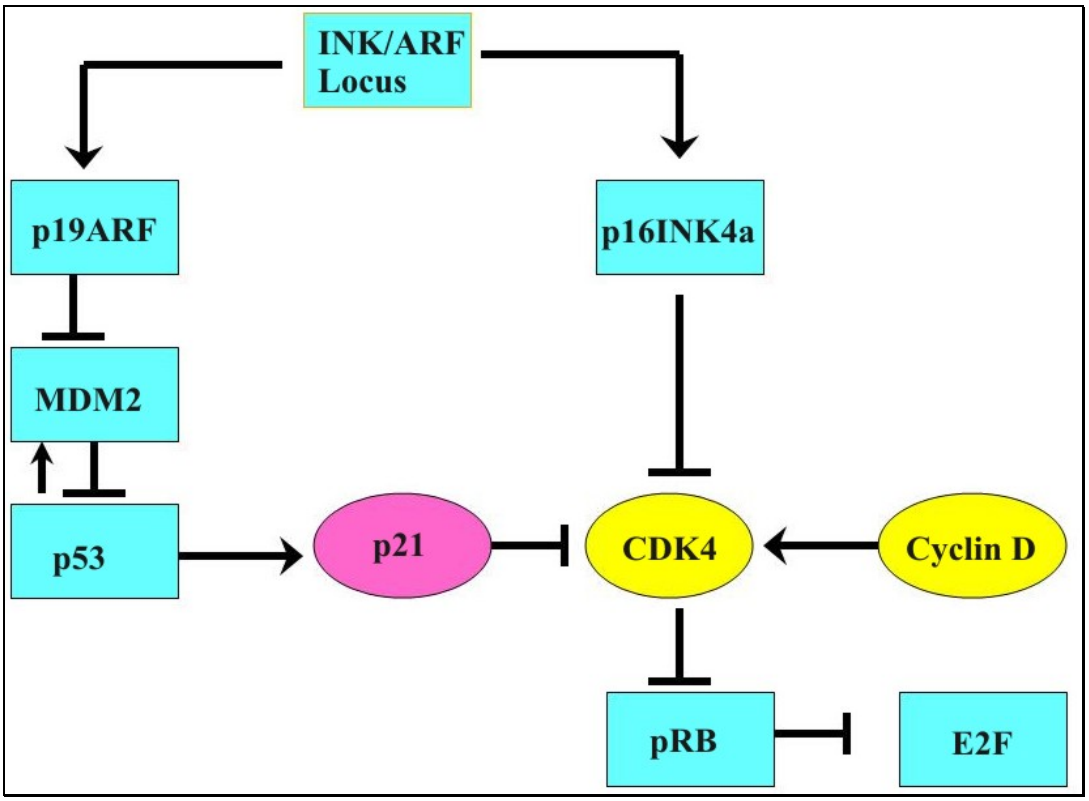

Figure 2.10 *p53- pRb pathway. Increase in p53 levels results in activation transcriptional activation of many apoptotic genes one of which is p21 which contributes to the arrest of cells in G1, through inhibition of cyclin-CDK complexes, with a subsequent accumulation of unphosphorylated form of pRb which arrests the cells in G_1 phase by preventing the release of E2F.*

2.2.8. MDM2 as target for cancer therapy

Blocking the MDM2-p53 interaction in cancer cells is a target for cancer therapy. Elucidation of structural and biochemical information about the MDM2-p53 interaction provides clear picture for designing small lipophilic molecules (since the interaction is hydrophobic) that disrupt the p53-MDM2 interaction and thereby stabilize p53 in the nucleus. Protein-protein interactions are difficult targets for small molecule drug discovery, since such interactions generally involve large and frequently less well-defined, contact surfaces, compared with classical drug targets such as the active sites of enzymes and small ligand receptor sites. But the contact surface of MDM2-p53 is rather small, apolar, and the interface is quite deep; all these features favor the possibility that a small inhibitory molecule might work, which in turn favors an oral administration route.

Despite major efforts, the only inhibitors available for a long time were synthetic peptides, which have demonstrated to be very useful tools to show both in vitro and in vivo, inhibition of MDM2-p53 interaction and induce apoptosis in tumor cells, but they are far from becoming drugs due to their insolubility or impermeability. Recently, Vassilev and his team (Vassilev 2004; Vassilev et al. 2004) demonstrated that a class of synthetic low molecular weight compounds, cis-imidazoline analogs referred to, as Nutlins are potent displacers of recombinant p53 protein from its complex with MDM2. The IC_{50} value determined is between 1.5-3 μM. Although the effects of Nutlins should be characterized further in normal cells, these compounds elegantly demonstrate the potential of structure-based drug selection. In contrast to the rationale design approach, attempts to identify the mechanism of action of known anticancer agents, the chalcones, led to the characterization of their ability to inhibit the MDM2-p53 interaction.

Chalcones are structurally distinct classes of naturally occurring tyrosine kinase inhibitors, which act as anticancer (Dimmock et al. 1999), and antituberculosis agents (Lin et al. 2002). Chalcones, considered as precursors of flavonoids and isoflavonoids, are abundant in edible plants. Chalcones (derived from 1, 3-diphenyl-2-propen-1-one; synthetic derivatives of licorice root compound) have been described in the literature as inhibitors of chemopreventive agents ovarian cancer cell proliferation (De Vincenzo et al. 1995) pulmonary carcinogenesis (Wattenberg 1995) skin carcinogenesis (Yamamoto et al. 1992) and other tumorigenic effects. The chemical structure of chalcones is shown in Fig. 2.11. Recent studies have shown that these chalcones induce apoptosis in variety of cancer cell types, including breast cancers. (Calliste et al.

2001). These broad antitumor properties of chalcones prompted us to synthesize a series of boronic and cyano chalcones and characterize these compounds at the molecular level for investigating the interactions with the p53/MDM2 system. Chalcone synthesis was done using Claisen-Schmidt aldol condensation protocols as previously published (Bois et al. 1999). We used NMR spectroscopy to map their binding sites and calculate their binding affinities.

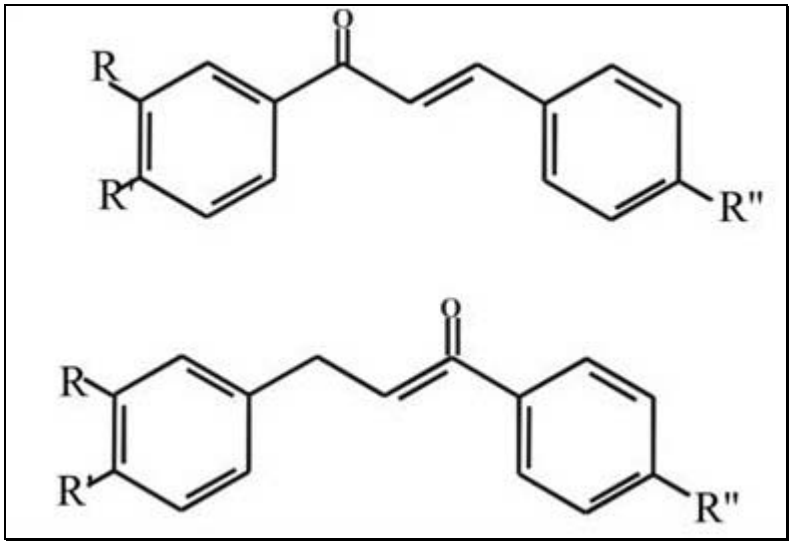

Figure 2.11 *Basic chalcone skeleton used in our study.*

2.3. The IGF system

The insulin-like growth factor (IGF) system is the major control pathway of physiological growth in mammals. The insulin-like growth factors (IGF-I and IGF-II) are small peptide (approx.7.5 kDa) that share a high degree of sequence homology with insulin and have glucose lowering effects. However, beyond these effects, they function as both endocrine and paracrine/autocrine hormones to stimulate cell proliferation, differentiation and survival of various cell types. Dysregulation of the IGF system is associated with many diseases like cancer and diabetes (Bach and Rechler 1996; Bach 1999; Yu and Rohan 2000).

IGFs can exert their biological action by binding to their transmembrane receptors, the type I and type II IGF receptors (IGF-IR and IGF-IIR). Their cellular action is mediated mainly via IGF-IR, which possesses tyrosine kinase activity. In serum and extracellular fluids,

interaction of IGFs with these receptors is stringently regulated by a group of soluble, high affinity IGF binding proteins (IGFBPs), which comprise a family of six related, secreted proteins that bind IGFs with high affinity (Khandwala et al. 2000; Clemmons 2001). They prolong the half lives of the IGFs and by sequestering IGFs away from the type I receptor, IGFBPs, may inhibit mitogenesis, differentiation, survival and other IGF-stimulated events. These binding proteins may alternatively enhance the IGF activity by concentrating the IGFs near their receptors. These opposing effects can be determined by understanding the structures of the binding proteins. Besides these high affinity IGF binding proteins, several IGFBP-related proteins have been described which show little or no affinity for IGF ligands (Hwa et al. 1999). Cleavage of IGFBPs by specific proteases modulates levels of free IGFs and IGFBPs and thereby their actions to interact with IGF-IR. Thus the IGF system comprises of the following:

- IGF receptors, type I and II
- IGF binding proteins (1-6)
- IGFBP proteases

2.3.1. Insulin-like growth factors (IGFs)

IGF-I has characteristics of both a circulating hormone and a tissue growth factor. Most circulating insulin-like growth factors are produced in the liver. Regulation of hepatic IGF-I production is complex (Fig. 2.12). Growth hormone (GH), which is produced in the pituitary gland under the control of the hypothalamic factors growth hormone-releasing hormone (GHRH) and somatostatin (SMS), is a key stimulator of IGF-I production. IGF-II is also expressed both in the liver and extrahepatic sites, but is not tightly regulated by GH. Various IGFBPs are also produced in the hepatic tissues. In IGF responsive tissues, the ligands IGF-I and IGF-II as well as IGFBPs can be delivered through the circulation from the liver by endocrine mechanism, but IGFs and IGFBPs can also be locally produced through autocrine or paracrine mechanisms. These mechanisms often involve interactions between stromal and epithelial-cell subpopulations.

2.3.2. IGF receptors

The IGF receptors are glycoproteins located on the cell membrane. Both IGF-I and IGF-II bind to IGF-I receptor with high affinity (K_D of 1.5 nM and 3.0 nM respectively) (Loddick et al., 1998). IGF-IR is autophosphorylated upon ligand binding and subsequently recruits and

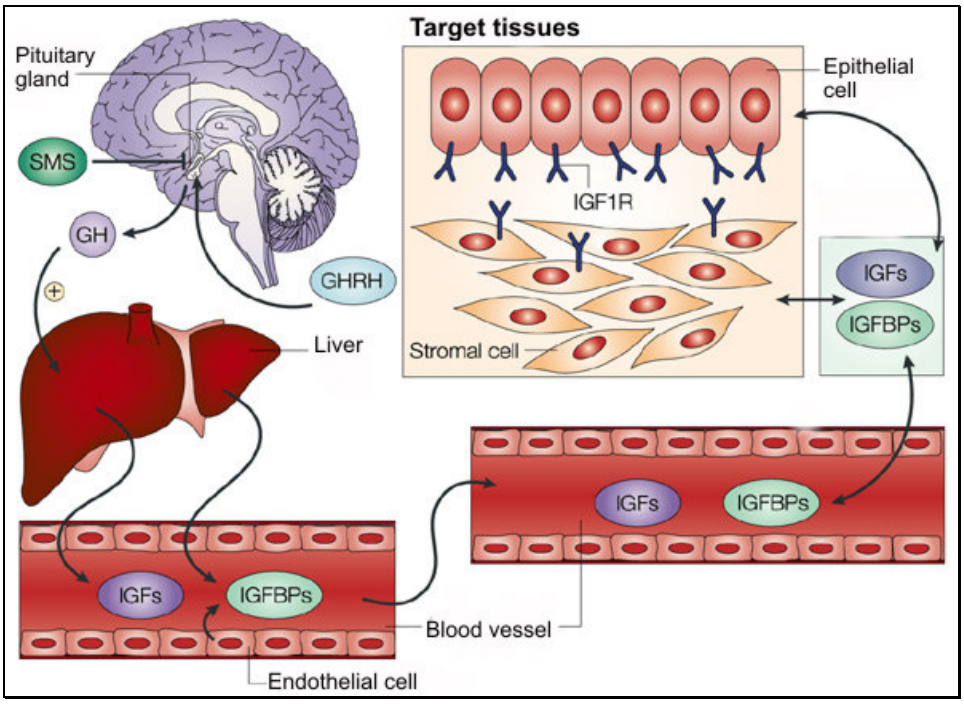

Figure 2.12 *Regulation of circulating and tissue levels of insulin-like growth factors. For details refer text. Adopted from (Lu et al. 2004).*

phosphorylates IRS and Shc proteins as shown in Fig 2.13. Two distinct signal transduction pathways get activated by IGF IR, Ras protein, Raf protein, and mitogen- activated signal protein kinase (MAPK) and the other being phosphoinositol-3-kinase (PI3K). IGF-IIR has no tyrosine kinase activity, and binds only to IGF-II, which results in degradation of IGF-II; hence IGF-IIR acts as an antagonist to IGF II, thereby reducing its biologic activity. Because of this effect, IGF-IIR has been considered to be a potent tumor suppressor molecule.

2.3.3. The IGF-binding protein super family

The precursor forms of all six IGFBPs (Fig. 2.14) have secretary signal peptides between 20 to 39 amino acids, and the mature proteins have between 216 and 289 amino acids. A key conserved structural feature among the six IGFBPs is a high number of cysteines (16-20 cysteines), clustered at the N-terminus (12 cysteines) and also, but to a lesser extent, at the C-terminus. IGFBP-1 to 6 share a high degree of similarity in their primary protein structure

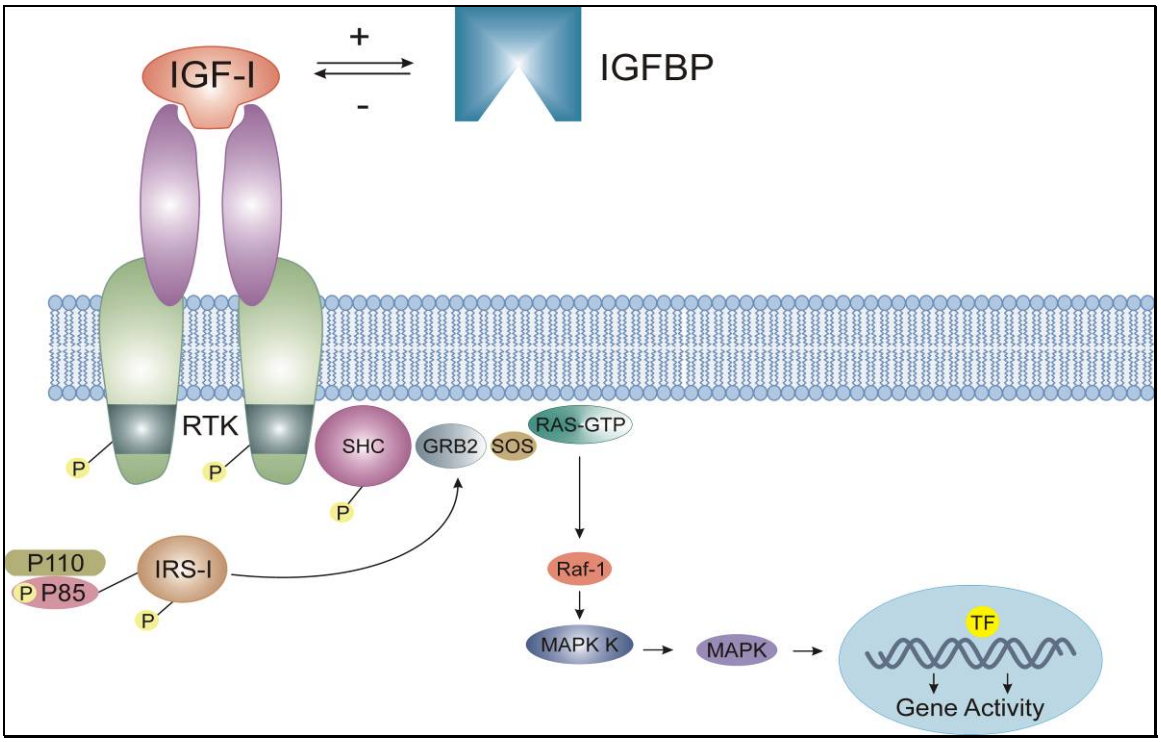

Figure 2.13 *Effects of IGFs and IGF-IR on normal cell growth. The tyrosine kinase activity of IGF-IR activates different signalling pathways as explained in the text.*

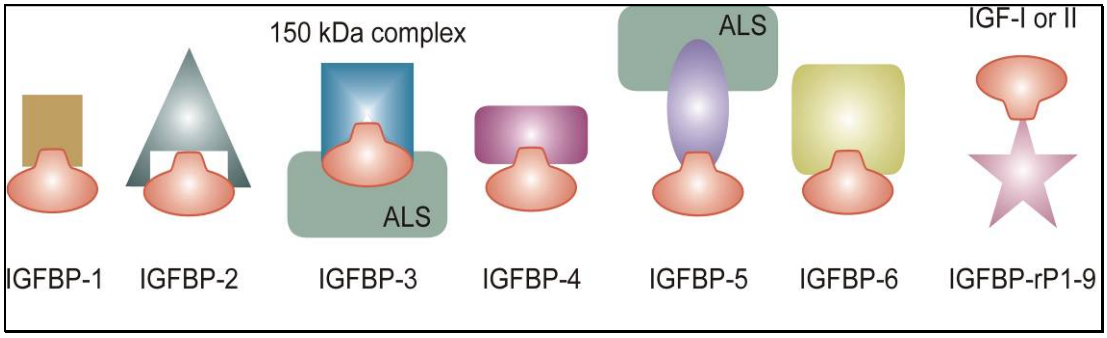

Figure 2.14 *Schematic representation of the six IGFBPs which bind IGFs with high affinity, thereby regulating the bioavailabilty of free IGFs. Also shown are the IGFBP related proteins which show a lower affinity for IGFs.*

(identities around 30-40%), with highest conservation at the N- and C-terminal regions. Most of the IGF-I and IGF-II molecules in serum are found in a 150 kDa ternary complex formed by an IGF, IGFBP-3, and a glycoprotein known as the acid labile subunit (ALS) (Baxter 1994). It has

been shown that these regions participate in the binding to IGFs (Baxter 2000; Payet et al. 2003; Shand et al. 2003) . The central domain shows essentially no structural conservation and contains most of the cleavage sites for specific proteases (Bunn and Fowlkes 2003). The IGFBPs have several potential functions; a few of them are listed in Table 3. They not only regulate IGF action but also stimulate several biological effects that are independent of their ability to bind to the IGFs. These being inhibition or enhancement of cell growth and induction of apoptosis. Fig. 2.15 displays the various modes of action of IGFBPs. The IGF independent functions involve putative IGFBP receptors. Serine/threonine kinase receptors are proposed for IGFBP-3 and -5, but their signaling functions are poorly understood. IGFBP-3 and IGFBP-5 have recently been shown to be translocated into the nucleus compatible with having a nuclear localization sequence (NLS) in their mid-region.

Table 3 *Important functions of IGFBPs*

Functions of IGFBPs
Prolong the half-life of IGFs in circulation
Limit bioavailability of free IGFs to bind IGF receptors
Prevent IGF-induced hypoglycemia
Enhance actions of IGFs by forming a slow-releasing pool of IGFs
Affect cellular proliferation/death via IGFBP receptors
Regulate transport of IGFs between intra- and extravascular spaces
Nuclear functions regulating the cell cycle

IGFBPs can also enhance the IGFs availability by mechanisms, which are yet to be elucidated. IGFBPs were also shown to bind to important viral oncoproteins like HPV oncoprotein E7. This implies additional roles for IGFBPs in the pathways of cell proliferation, apoptosis, and malignant transformation. The properties of IGFBPs however, such as presence of the large unstructured, erratically behaving regions, disulfide-rich folded domains and susceptibility to proteolysis and aggregation (Torres-Aleman et al. 1996; Hwa et al. 1999; Carrick et al. 2001; Clemmons 2001) make these proteins a difficult target for crystallographic as well as NMR structural studies.

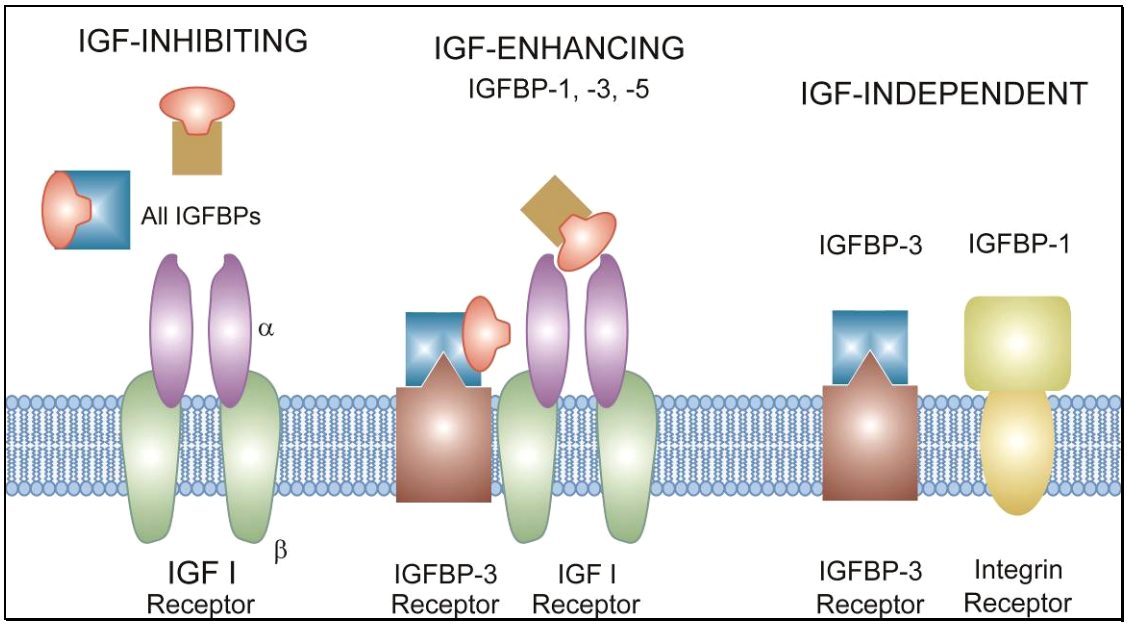

Figure 2.15 *The IGF-dependent and IGF-independent functions of IGFBPs.*

2.3.4. IGFBP degrading proteases

In a variety of physiological conditions, IGFs must be released from their binding proteins so that they can exert their mitogenic and metabolic effects (Fig. 2.16). This is possible principally through decreasing the affinities of IGFBPs for IGFs. These mechanisms include:

- Binding of IGFBPs to extracellular matrix molecules
- Phosphorylation of IGFPs
- Proteolytic degradation of IGFBPs

Of the above mechanisms proteolysis has been considered to be most preferred. These proteinases degrade IGFBPs into fragments with low affinity for IGFs, thereby resulting in an increase in IGF bioavailability and their bioactivity at the cell surface.

2.3.5. IGF system and cancer

IGFs exert strong mitogenic and antiapoptotic actions on various cancer cells. IGFs can also act synergistically with other mitogenic growth factors and steroids to antagonize the effect

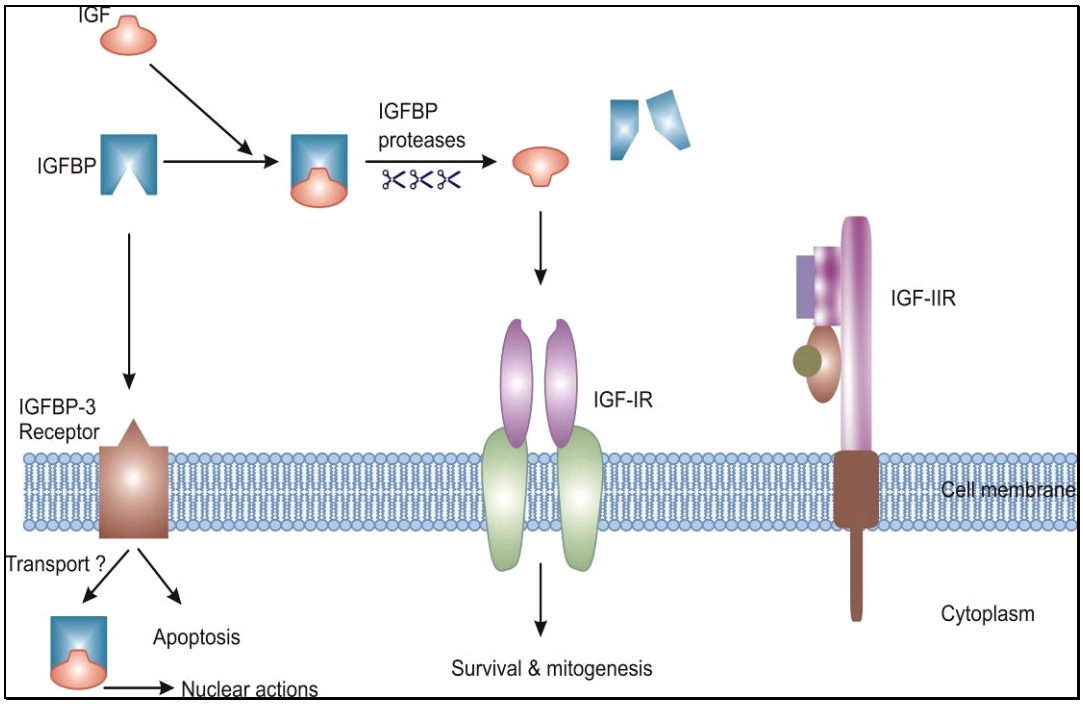

Figure 2.16 *The IGF-IGFBP axis. Certain IGFBP degrading proteases cleave IGFBPs thereby regulating the levels of free IGFs which then bind to the IGF-IR receptor on the cell membrane and bring about the mitogenic effects.*

of antiproliferative molecules on cancer growth. The role of IGFs in cancer is supported by epidemiological studies, which have found that high levels of circulating IGF-I and low levels of IGFBP-3 are associated with increased risk of several common cancers, including those of the prostate, breast, colorectal and lung (Giovannucci 1999). In most situations, the binding proteins suppress the mitogenic action of IGFs and promote apoptosis, however, because of the presence of IGFBP proteases, two in vitro studies (Chen et al.1994; Camacho-Hubner et al. 1991) have found that IGFBPs are able to stimulate the growth of cancer cells. Moreover, certain IGFBPs have IGF independent growth inhibitory or pro-apoptotic influences against which neoplastic cells can develop resistance (Firth and Baxter 2002). The effects of IGFs on cancer cells are mediated through IGF-IR, eliminating IGF-IR from the cell membrane, blocking the interaction of IGFs with IGF-IR, or interrupting the signal transduction pathway of IGF-IR can abolish the mitogenic action of IGFs on cancer cells (Neuenschwander et al. 1995). Thus the IGF family is a complex system which participates in cancer development and requires a careful understanding of it in order to develop diagnostics measures against cancer.

2.3.6. Structural characterization of IGFBPs

As solving the exact mechanisms of the IGFBP-IGF interactions would open possibilities of precise control over cell growth and differentiation *in vitro* and *in vivo*, and it is clear that studies on the binding proteins would greatly benefit from more detailed structural knowledge, we try to explore the domain and subdomain organization of IGFBPs with the aid of NMR spectroscopy. The idea was to gain a more detailed understanding of the IGFBPs domain organization and structural requirements for binding to IGFs. A 6-kDa fragment of an amino-terminal domain of IGFBP-5 was the first structurally characterized (Kalus et al. 1998; Zeslawski et al. 2001). This fragment, miniBP-5 (residues 40-92, numbering of amino acids is for mature proteins), though essential for IGF binding by IGFBP-5, bound IGF with a 10-fold lower affinity than the intact protein, indicating the significance of the remaining domains for stable binary complex formation (Schedlich et al. 2003). It also did not prevent IGF-IGF type I receptor (IGF-IR) interaction, binding on the site of the IGF molecule opposite to the IGF-IR-contacting epitope. Hence, we further tried to understand the stucture of another IGFBP in complex with IGF.

2.4. The calpain system

The calpains form a family of structurally related intracellular multidomain cysteine proteinases containing a papain-resembling catalytic domain. They are unique members of the cysteine protease family of enzymes as most of them require calcium for their activity.

2.4.1. Calpain protease family

The mammalian calpain protease family includes approximately 14 genes (Fig. 2.17) but only two members, μ- and m-calpain, are found in mammalian tissues as stable proteins in amounts sufficient for isolation and study by enzymology and structure based methods (Dear and Boehm 2001; Sorimachi and Suzuki 2001; Goll et al. 2003). The proteolytic activity of most of these calpains depends on the presence of free calcium, while a few other calpains such as p94 (Sorimachi et al. 1989) do not seem to require calcium for their activity. The only known natural/endogenous inhibitors of activated calpains are calpastatins (Takano et al. 1995) and the second cystatin domain of kininogen (Salvesen et al. 1986). The "classic" μ- and m-calpains are

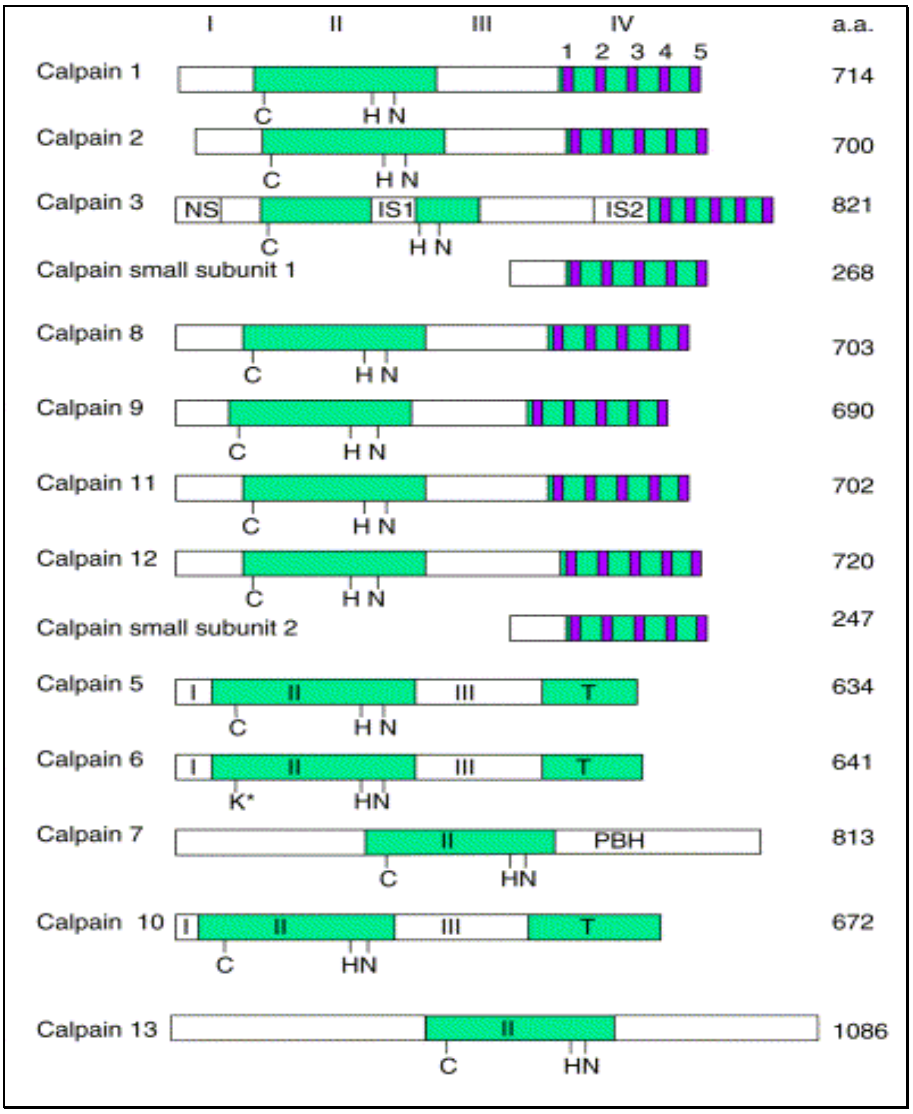

Figure 2.17 *Schematic representation of various mammalian calpains. Domian IV represents the five sets of EF-hands. C, H, N represent the catalytic residues Cys His and Asn. K* represents the unique non-functional Lys residue (instead of Cys) in calpain 6. PBH is a domain homologous to a region of protease PalB. IS-1 and IS-2 are the inserts in the mammalian skeletal muscle specific calpain 3 which has a nuclear translocation like sequence (Huang and Wang 2001).*

the best-characterized calpains, which are heterodimeric proteins, composed of a large 80-kDa catalytic subunit organized in four domains I–IV and a common small 28 kDa regulatory subunit composed of domains V and VI (Fig.2.17). On exposure to calcium, at concentrations of 5–50 μM (μ-calpain) and 200–1000 μM (m-calpain), both calpains become active in vitro. In vivo, however, where the calcium concentrations are in general far below 1 μM (Goll et al. 1992), the

calpain activity might be additionally regulated by other mechanisms such as binding of activators or interaction with phospholipids (Pontremoli et al. 1990; Saido et al. 1992).

2.4.2. Structural insights

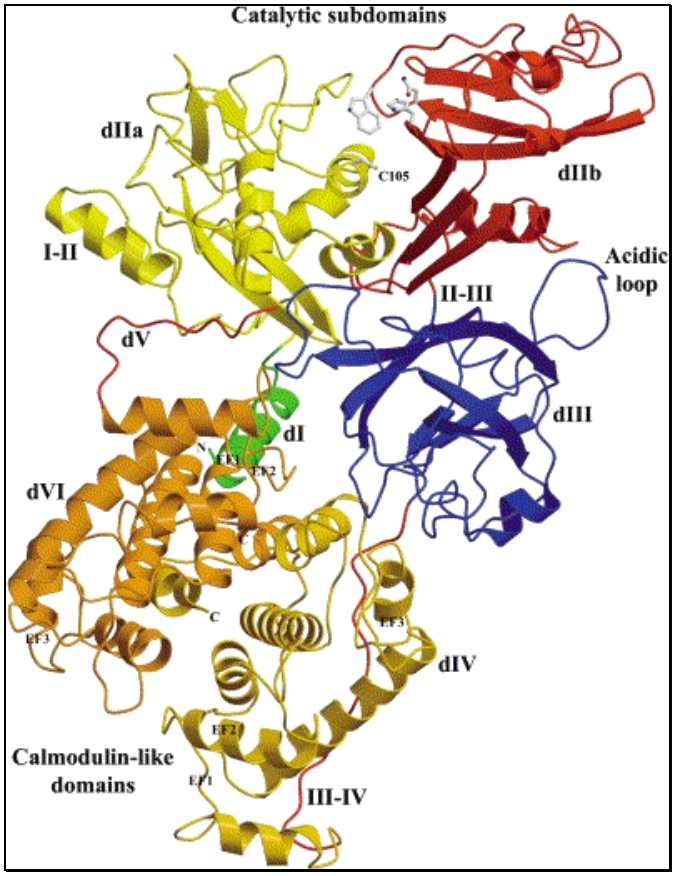

Figure 2.18 *Ribbon structure of the apoform of human m-calpain (Strobl et al. 2000). Domain I shown in green, folds into the surface of the catalytic subdomain IIa (gold). The other barrel like subdomain IIb is in red. The acidic domain III is in blue, domain III-IV linker region (magenta) and the '5EF-hands' domain IV in yellow. Truncated domain V of small subunit is in magenta and the calmodulin binding domain VI in orange. The side chains of catalytic residues C105 (domain IIa), H262 and N268 (both in domain IIb) are also depicted.*

Elucidation of the pathophysiological roles of calpains requires an understanding of their regulation by Ca^{2+} at the molecular level. The crystal structure of the full-length Ca^{2+}-free m-calpain (Strobl et al. 2000) reveals the overall architecture of this enzyme (Fig. 2.18). It also explains the inactivity of the apoform by catalytic domain disruption and indicates several sites

where calcium could bind causing reformation of a papain-like catalytic domain, and additionally reveals modes by which phospholipid membranes could reduce the calcium requirement in vivo. The structure analysis shows that the m-calpain molecule forms a flat oval disc (Fig. 2.18), the upper pole of which is occupied by the two catalytic subdomains domain IIa and domain IIb and lower pole is filled by the calmodulin-like domain pair domain IV-domain VI, respectively. Domain III and the N-terminal domains, domain I and domain V connect the two calmodulin-like domains with both catalytic subdomains. Domain I comprises of a single α-helix anchored in the cavity of domain VI, thereby stabilizing the circular arrangement of the protein. Domain I, considered to being a short prodomain region of the protease, is cleaved off during the initial activation of calpains. Domain II is the cysteine protease domain and contains the catalytic cysteine, histidine and asparagine residues. Domain II, like other cysteine proteases such as cathepsin B, can be further divided into subdomain IIa and IIb, with a substrate-binding cleft in between (Fig 2.18). The catalytic triad residue Cys is on subdomain IIa, whereas His and Asn are part of domain IIb.

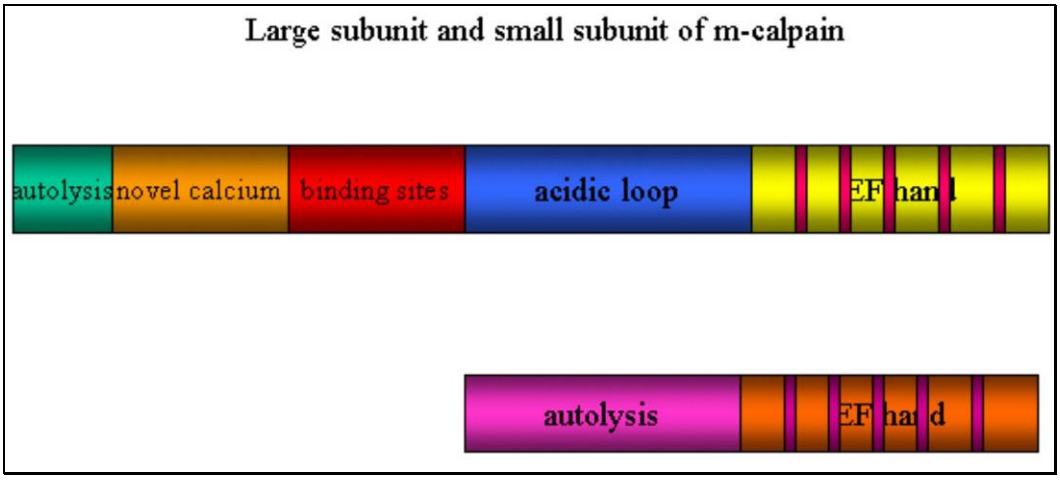

Figure 2.19 *Schematic diagram of the large and small subunit of human m-calpain structure. For details refer text.*

In the absence of calcium, the distance between the catalytic Cys and His is 10 Å, which is too far to be a functional catalytic triad. It is suggested that calcium induced conformational changes draw subdomains IIa and IIb together. Domain III is the solvent exposed “acidic loop”, which carries 10 acidic residues within its 11-residue segment and serves as the linker between the catalytic domain and the calmodulin binding domain IV. It consists of eight strands with a

topology similar to the C2 domains found in various proteins, which are known to bind to calcium and phospholipids. Indeed, the acidic loop within this domain has been suggested to play a role in the calcium promoted activation of calpain. Domain IV and VI are well characterized Ca^{2+}-binding domains, each containing five EF-hand motifs. The small regulatory subunit is composed of a N-terminal glycine-clustering hydrophobic region, domain V (is highly unresolved in the m-calpain crystal structure) and a C-terminal Ca^{2+} binding domain VI. The hydrophobicity of the N-terminal region of domain V has been taken as an indication for its role in membrane anchoring (Khorchid and Ikura 2002; Moldoveanu et al. 2003; Pal et al. 2003). Fig. 2.19 presents an overall view of the domain organization of m-calpain.

Though the structure of apo m-calpain explains the inactive state of the enzyme in the absence of calcium it could not explain the mechanism of activation of the enzyme upon calcium binding. A recent 2.1 Å crystal structure of the Ca^{2+} bound protease core of mini μ-calpain (consisting of only domain I and II) suggests that it binds calcium to two non-EF-hand sites in the protease core, of the enzyme (Fig.2.20) (Moldoveanu et al. 2002). Binding at these regulatory sites aligns the active site cleft and converts the core into an active enzyme. The structure of μ-like calpain crystallized recently is very similar in overall fold to that of m-calpain, but significant differences are observed in the catalytic triad residues of these two isoforms (Strobl et al. 2000; Pal et al. 2003b).

2.4.3. Mechanism of calcium activation

There are at least three different types of Ca^{2+} sites (EF-hand, C2-like domain, and protease domain sites) that act in concert to regulate the biological function of the enzyme. (Moldoveanu et al.2002) suggest a two step mechanism for activation of calpains.

- The first involves the release of constraints imposed by the circular arrangement of the domains, which would essentially involve subtle conformational changes in domain IV and VI upon Ca^{2+} binding, leading to abrogation of the interaction between N- terminal α-helix of domain I and the second EF-hand motif of domain VI. This perhaps promotes conformational changes in domain III and dissociation of the small subunit from the large subunit (Tompa et al. 2001).
- The second step is the realignment of the active site cleft caused by the cooperative binding of Ca^{2+} to domain IIa and IIb.

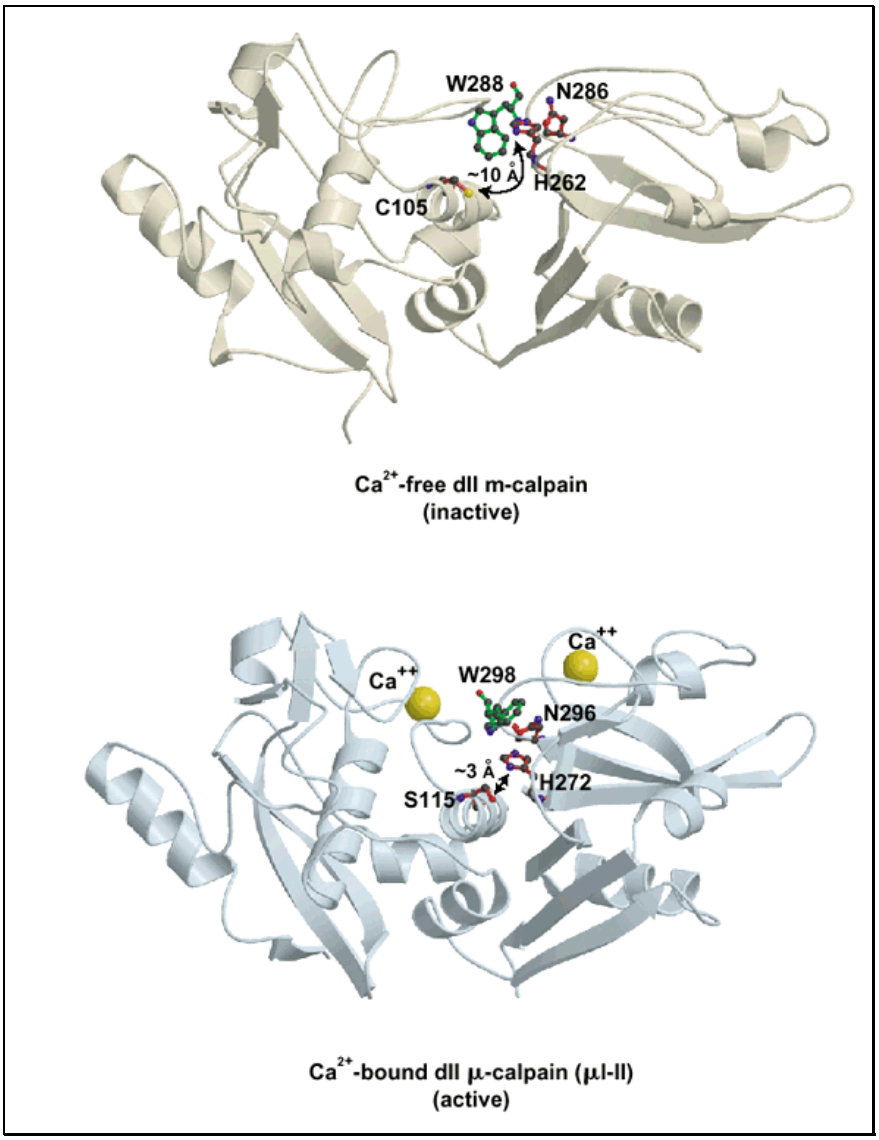

Figure 2.20 *Ribbon structure of the catalytic domain II of μ-calpain showing the structural changes of the inactive and active states of the enzyme. The triad residues are colored in red and the active site Trp in green.*

The two active site domains are present in all members of the calpain superfamily, whereas the flanking domains are varied (Sorimachi and Suzuki 2001). Thus, the cooperative binding of Ca^{2+} to domain I and II demonstrates a new role of Ca^{2+} as a second messenger, which has wide implications in calpain signaling. It suggests a general Ca^{2+} activation mechanism for calpain superfamily members including those that do not contain the small subunit and those that lack EF-hand or C2-like domains in the large subunit. Accordingly, some of the non

heterodimeric calpains might bypass the first activation barrier and could be directly activated by the second mechanism.

2.4.4. Pathological implications of the calpain system

Ca^{2+} signaling by calpains leads to controlled proteolysis but deregulated Ca^{2+} levels result in aberrant proteolysis by calpains, which contributes to tissue damage in heart and brain ischemias as well as neurodegeneration in Alzheimer's disease. Hence calpains are also implicated in various pathophysiological processes, including type-2 diabetes mellitus (Horikawa et al. 2000), muscular dystrophy (Richard et al. 1999) cataractogenesis, inflammation, arthritis, and Alzheimer's and Parkinson's diseases (Vanderklish and Bahr 2000). Furthermore, it is now clear that organ ischemia, trauma and hemorrhage can by increasing the calcium level, lead to activation of calpain, which in turn may trigger the proteolysis of cytoskeletal proteins, cell membrane proteins and regulatory kinases. Indeed, it has been shown experimentally that blockage of calpain-like proteolytic activities with inhibitors can reduce injuries of the brain (Lee et al. 1991; Rami and Krieglstein 1993; Wang et al. 2003; Ziemka-Nalecz et al. 2003), the liver (Kohli et al. 1997) and the heart (Iizuka et al. 1991; Matsumura et al. 2001) caused by ischemia/reperfusion.

2.4.5. Enigma with calpain cleavage

The rules that govern calpain specificity have not yet been determined. Moreover, physiological functions of the calpain system remain unclear despite the major efforts made till date. A number of studies indicated that the calpains have a role in the cell cycle, specifically in the G_1 to S transition (Goll et al. 2003). They are also involved in limited proteolysis of proteins involved in cytoskeletal remodeling, signal transduction, apoptosis and necrosis, embryonic development and long-term potentiation in the central nervous system (Carafoli and Molinari 1998; Ono et al. 1998; Wang 2000). Thus calpains are expected to function as bio-modulators. Calpain mediated degradation of $p21^{KIP1}$, had been reported in preadipocyte cell cycle progression and differentiation (Patel and Lane 2000). However, biological role of calpain in the cell cycle regulation is still poorly understood. Experimental reports published so far indicate that proteolysis by calpains are limited and does not lead to small peptides (Croall and DeMartino 1991; Goll et al. 2003).

In this thesis we attempt to characterize calpain preferred cleavage positions in the insulin-like growth factor binding proteins (IGFBPs) and in the INK4 family protein, $p19^{INK4d}$ which negatively regulate the mammalian cell cycle. In our first study we have chosen to use growth factor binding proteins (IGFBPs) for our calpain study for the following reasons:

- First, proteolysis of IGFBPs is extensively characterized by numerous reports; this is because limited proteolysis of IGFBPs is the major mechanism for the release of IGFs from IGFBP/IGF complexes, generating IGFBP fragments with reduced affinity for IGFs (Binoux 1996; Khandwala et al. 2000) and thereby increasing the concentration of IGFs at the cell surface and allows IGFs to bind and activate the IGF receptor (Bunn and Fowlkes 2003).
- Secondly, IGFBPs are structurally well characterized, they are composed of globular domains linked by large flexible fragments, thus providing model proteins that contain diverse structural elements (Kalus et al. 1998).
- Recently, the presence of specific cell-surface IGFBP receptors has been reported. IGFBP-3 and –5 can enter the cell and bind to several different targets in the cytoplasm. Further more it has been shown that both the proteins can localize in the nucleus and posses nuclear localization sequence (NLS) in their mid-region (Jaques et al. 1997; Li et al. 1997). This raises the possibility that nuclear IGFBP may directly control gene expression.

In the second study, $p19^{INK4d}$ was the model protein because the structure of this protein is known. It is a 165 amino acid protein that comprises ten α-helices assembled sequentially in five ankyrin repeats and it shares structural and biochemical properties of the other three INK4 family proteins (Baumgartner et al. 1998). Moreover, in contrast to the substrate proteins studied so far, it is not composed of globular domains linked by large solvent exposed flexible fragments.

3. NMR structural studies

The major challenge for proteomics is in understanding the function of biological macromolecules like proteins, which requires the knowledge of their spatial arrangement. Multi-dimensional NMR spectroscopy and X-ray crystallography are the two main techniques used to determine the three-dimensional structures. The two techniques complement each other where NMR measurements call for sample molecules capable of existing at high concentration in solution under a near physiological condition and X-ray requires samples capable of forming large single crystals in solid phase. Though NMR has limitation in determining structures of large proteins (max 30 kDa), it finds use in a wide range of structure-function relationships (Shuker et al. 1996), studying unfolded and folded protein dynamics (Dyson and Wright 2004), in distinguishing multiple protein conformations (Muhlhahn et al.1998), also in comparing apo and holo forms of proteins and mapping the binding sites of their cofactors (Wijesinha-Bettoni et al. 2001). The ability of NMR to detect ligands which show a weak affinity towards their substrate, and also its skill in molecular recognition and catalysis (Palmer 2004) have made it an important tool in drug discovery. Moreover NMR can complement X-ray crystallography by identifying protein constructs that are most amenable for crystallography as NMR has the capability to semi-quantitatively identify unstructured regions of the polypeptide chain in an otherwise partially folded protein and to identify proteins that are heterogeneous because of aggregation and other conformational changes (Rehm et al. 2002). Also the same protein sample can be used for crystallographic trial as the NMR measurements do not destroy the sample. Table 4compares the two techniques.

Table 4 *Comparison between NMR and X-ray crystallography*

NMR	X-ray crystallography
Samples in solution phase are used	Samples are in solid phase
Part of the atom involved is the nucleus	Electrons are the components involved
Strong signals are observed for the mobile parts of the structure	Strong signals are observed for the rigid portion of the structure
The final structure is a family of related structures	The final structure is a well refined single structure

Nuclear magnetic resonance spectroscopy makes use of the quantum mechanical property of the nucleus, i.e. the magnetic spin. The nuclei of naturally occurring atomic isotopes that constitute biological molecules either have a nuclear spin at natural abundance (^{1}H, ^{31}P), or naturally less-abundant isotopes (^{13}C, ^{15}N, ^{19}F) which require isotopic labelling. Associated with the magnetic spin of the nucleus is the magnetic spin moment (μ).When such a nucleus is placed in a strong external magnetic field (B_0), the magnetic field of the nucleus tries to align itself along with the external field, however, since the nucleus is also spinning and has an angularmomentum, the torque exerted by the external field will result in the the nuclear magnetic field to precess around the axis of the external field vector with a particular frequency, ω, which is called the Larmor frequency. The rate of this precession is proportional to the external magnetic field strength. NMR spectroscopy depends on the absorption of electromagnetic radiation from the radiowave part of the spectrum causing the nucleus to undergo a transition from a low to high energy spin state. Thus when a strong exciting radio frequency (RF) pulse is applied to the protein sample at right angles to the external magnetic field, the nuclei of the protein molecule precesses back to their equilibrium state and in the process they emit radio frequency radiation that can be measured as free induction decay (FID). Fourier transformation (a mathematical process which convert time domain into frequency domain) of the FID data would produce the NMR frequency spectrum in the form of intensity versus frequency.

The resonant frequency is not only a characteristic of the type of nucleus, but also varies slightly depending on the position of the atom within a molecule (the chemical environment). This occurs due to the magnetic fields of the nearby nuclei on that of the nucleus undergoing transition which modifies the external magnetic field in the vicinity of this nucleus. This subtle variation, on the order of one part in a million (ppm), is called chemical shift and designated as δ, delta. Chemical shift perturbation spectra are very commonly used to probe the structural and functional changes of a molecule after a certain chemical change such as ligand binding. The underlying rationale is that if the system under study has been changed chemically or physically, the NMR peaks would show some changes in the position of the peaks or they would disappear all together due to changed local environment (Pellecchia et al. 2000; Zuiderweg 2002).

One-dimensional (1D) NMR

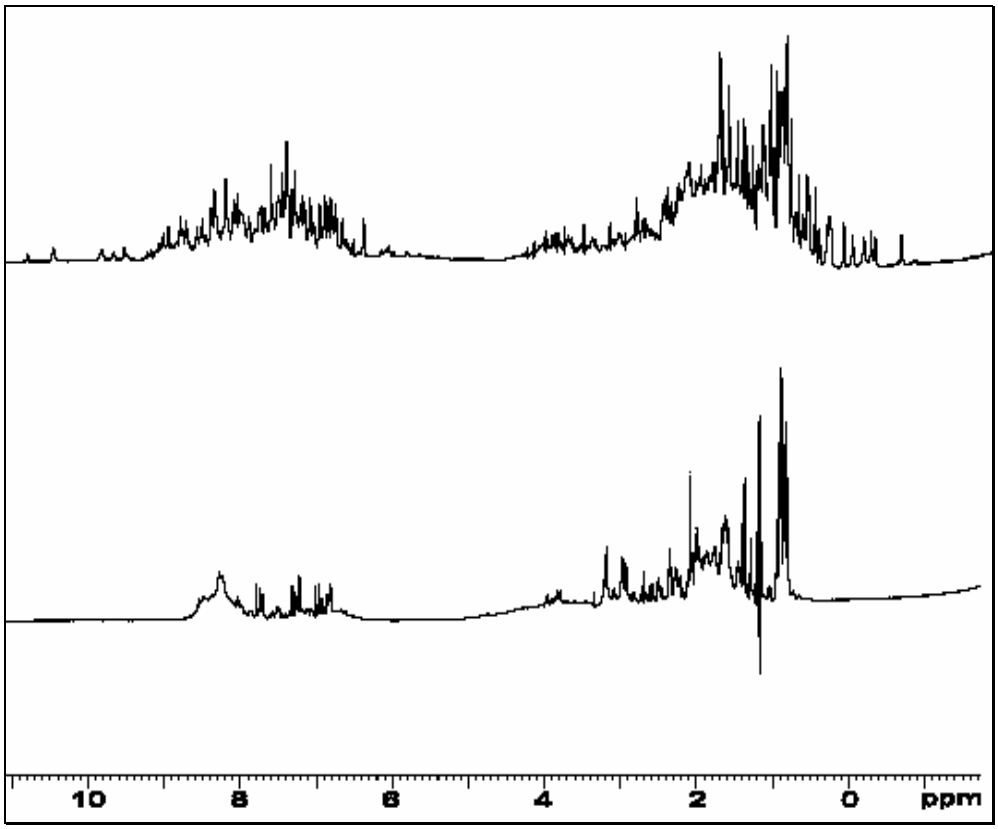

Figure 2.21 *Characterization of protein structures using 1D NMR spectroscopy. The upper panel shows a typical one-dimensional proton NMR spectrum of a folded protein with signal dispersion downfield (left) of 8.5 ppm and upfield (to the right) of 1 ppm. The lower panel shows an unfolded protein showing strong signals appear around 8.3 ppm, the region characteristic for amine groups in random coil conformation. No signal dispersion is visible below approximately 8.5 ppm. Also to the right of the strong methylpeak at 0.8 ppm no further signals show up.*

The 1D NMR spectra of small molecules is structurally informative since resulting resonances are well resolved and arise from individual protons. It is the most basic and simple NMR experiment which can be performed in very short time interval and can provide a great deal of information on the protein folding status (Fig.2.21). Besides it may also provide information on the α-helical or β-strand structures in a protein. The Cα protons in a helix display few resonances in the region between 5 and 6 ppm, while those in a β-sheet resonate in this region (Wishart et al. 1991). 1D spectrum also provides information about purity of the sample any impurity would be readily detected by the sharp peaks it displays. However, 1D spectra of large

bio-molecules such as proteins and nucleic acids yield complex spectra with extensive overlap between individual peaks resulting due to the fact that the differences in chemical shifts are often smaller than the resolving power of the experiment. A 2D NMR spectroscopy overcomes this difficulty by extending measurements of these effects into a second dimension.

Two-dimensional (2D) NMR

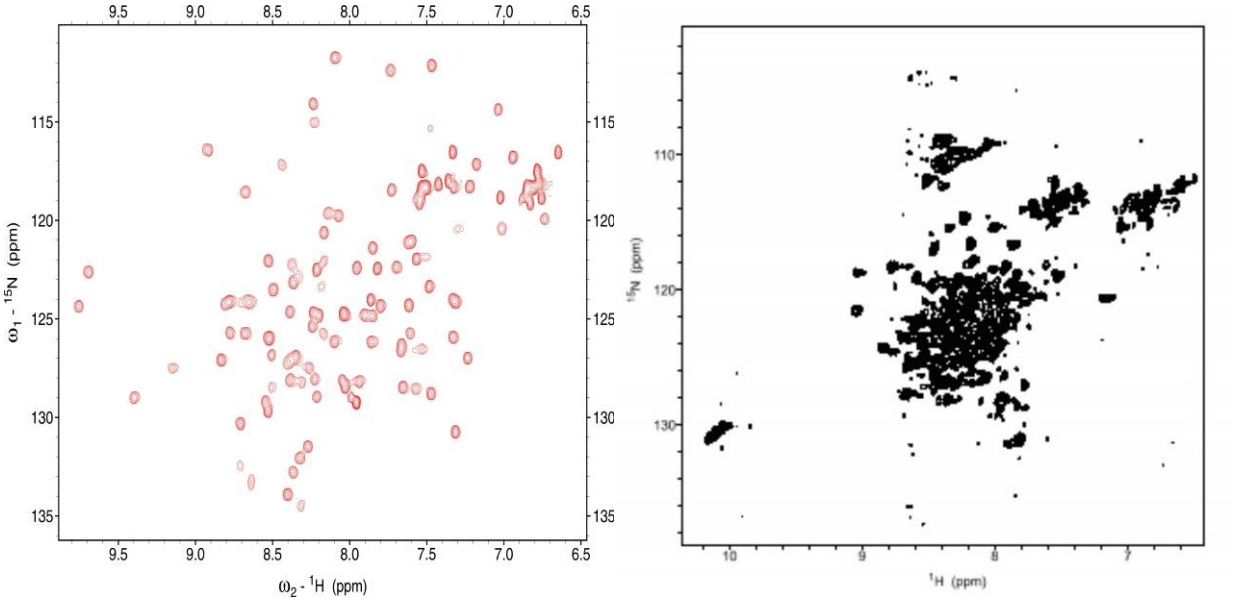

Figure 2.22 *Characterization of protein structures using 2D NMR spectroscopy. The figure shows ^{15}N-HSQC spectra of folded and unfolded proteins. The panel on the left shows spectra of a folded protein (MDM2 residues 1-118) and that on the right is of an unfolded protein. All signals in the right panel cluster around an 8.3 ppm. The broad unresolved signals in the middle of the spectrum indicate either aggregation in the sample or conformational heterogeneity. On the contrary, all the peaks on the left panel show large signal dispersion in both dimensions.*

The 2D NMR experiments provide well resolved spectra and can be used to detect interactions between magnetised protons which are near together in the space and are of two general types; through space or through bond. Through space interactions are called nuclear overhauser effect (NOE) while through bond interactions result in correlation spectroscopy (COSY). Both of these effects are due to interactions between magnetic dipoles in a pair of nuclei which are spatially near to each other and both types of experiment are used in the determination of large bio-molecule structures. NOEs connect pairs of hydrogen atoms separated by less than 0.5 nm. In contrast to COSY, the nuclei involved in NOE correlation can belong to amino acid

residues that may be far apart along the protein sequence but close in space. Another simplest and most powerful technique in 2D NMR is the heteronuclear single-quantum coherence (HSQC) experiment which can used for ligand binding studies. The HSQC shows one peak for every proton bound directly to a nitrogen atom and thus exactly one signal per residue in the protein (apart from proline which is devoid of proton bound nitrogen and some additional side chain signals which can easily be identified). The positions of the peaks are indicative of structured or disordered proteins. In case of an unfolded protein all signals cluster in a characteristic "blob" around a ^{1}H frequency of 8.3 ppm with little signal dispersion in both dimensions. In a spectrum of structured protein, the peaks show large signal dispersion in both dimensions (Fig 2.22). The only extra requirement for the 2D HSQC experiments is that the protein samples should be ^{15}N labelled. Thus NMR has increasingly become important in mapping the ligand binding sites and in calculating the binding constant. A similar approach has been shown in Chapter 5.1of this thesis.

4. Materials and Methods

4.1. Materials

Reagents and chemicals used in the study were of analytical grade and bought from Sigma-Aldrich (Deisenhofen, Germany), Fluka (Buchs, Switzerland), and Merck (Dramstadt, Germany) unless otherwise specified.

Enzymes, antibiotics and other protein and chemicals

- benzonase (Novagen)
- hen egg white lysozyme
- factor Xa (NEB, FRG)
- thrombin (Sigma, FRG)
- ampicillin
- chloramphenicol
- kanamycin

Plasmids and bacterial strains

Plasmids	pET-28 a	IGFBPs,MDM2	Novagen
	pET-30/LIC	MDM2	Novagen
	pGEX-4T 2	MDM2	Amersham
	pQE-40, 60	MDM2	Qiagen
E. coli cloning strains	One shot® TOP10		Invitrogen
	XL blue supercompetent		Stratagene
E. coli protein expression strains	BL21 Star		Invitrogen
	BL21 Star™ (DE3)		Invitrogen
	BL21 Star™ (DE3) pLysS		Invitrogen
	BL21 Star™ (DE3) pLysE		Invitrogen
	BL21 RIL		Stratagene
	M15 (prep 4),SG13 (prep 4)		Qiagen

Kits and reagents

- BD Advantage 2 PCR kit, BD Biosciences.
- QIAquick PCR purification kit, Qiagen.
- QIAprep spin miniprep kit, Qiagen.
- Rapid DNA ligation kit, Roche Applied Science.
- Quick change site-directed mutagenesis kit Stratagene
- Transfection buffer A and B Pharmingen
- IPTG, dATP, dGTP, dTTP, dCTP Peq Labs

Medium for cell growth and stock solutions

All buffers, stock solutions and media, if not mentioned here, were performed exactly like described in Sambrook & Russell (2001).

Minimal Medium (MM) for Uniform Enrichment with ^{15}N		
	Stock solutions	
1	Thiamin	1%
2	Antibiotics	
3	$MgSO_4$	1 M
4	Zn-EDTA solution:	
	EDTA	5 mg/ml
	Zn (Ac)	28.4 mg/ml
5	Trace elements solution:	
	H_3BO_3	2.5 g/l
	$CoCl_2*H_2O$	2.0 g/l
	$CuCl_2$*H2O	1.13 g/l
	$MnCl_2$*2H2O	9.8 g/l
	Na2MoO_4*2H_2O	2.0 g/l
	If difficult to dissolve, pH was lowered with citric acid or HCl.	
6	Glucose, separately autoclaved	5 g/25 ml
	Working solution	
1	Composition for 1l media is given below	
	NaCl	0.5 g
	Trace elements solution	1.3 ml
	Citric acid monohydrate	1 g
	Ferrous citrate (dissolved in 120µl conc. HCl, heated)	36 mg
	KH_2PO_4	4.02 g
	K_2HPO_4 3H_2O	7.82 g
	Zn-EDTA solution	2 ml
	NH_4Cl or 15NH_4Cl	1 g
2	pH was adjusted to 7.0 with NaOH	
3	The mixture was autoclaved	
4	25 ml separately autoclaved glucose was added	
5	Other compounds were added (previously sterile filtered):	
	Thiamin	560 µl
	Antibiotics (half of the usual amount for the LB-medium)	
	$MgSO_4$, 1M	2 ml

Apparatus used

Chromatography equipment, columns and media

- NiNTA-agarose (QIAGEN, FRG);
- ÄKTA explorer 10;
- Peristaltic pump P-1;
- Fraction collector RediFrac;
- ARecorder REC-1;
- UV flow through detector UV-1;
- HiLoad 16/60 Superdex S30pg, S200pg; HiLoad 26/60 Superdex S75pg; HiLoad 10/30 Superdex S75pg; Mono Q HR 5/5, 10/10; Mono S HR 5/5, 10/10; Buthyl Sepharose 4 FF; Q-Sepharose FF; SP-Sepharose FF; Glutathione Sepharose (all Amersham Pharmacia, Freiburg).

Consumables	
Centripreps YM3, YM10	Amicon, (FRG)
Dialysis tubing Spectra/Por MW 3500	Roth, (FRG)
Falcon tubes, 15ml, 50ml	Becton Dickinson (FRG)
Maxi-Prep, Plasmid Isolation Kit	Qiagen, (FRG)
Gel extraction kit	Qiagen, (FRG)
PCR purification kit	Qiagen, (FRG)
NMR-tubes, 5mm	Wilmad, Buena, (USA)
Parafilm	American National, (Canada)
Pipette tips 10µl, 200µl, 1000µl	Gilson, (France)
Plastic disposable pipettes 1ml, 5ml, 25ml	Falcon, (FRG)
Reaction cups 0.4ml, 1.5ml, 2ml	Eppendorf, (FRG)
Sterile filters Millex 0.22µm, 0.45µm	Millipore, (FRG)

Buffers for protein purification under native conditions

- **Lysis buffer:** 50 mM Tris pH 8.0, 300 mM NaCl, 10 mM β-mercaptoethanol, 10 mM imidazole, EDTA-free protease inhibitor cocktail.
- **Ni-NTA wash buffer:** 50 mM Tris, 300 mM NaCl, 10 mM β-mercaptoethanol, 20 mM imidazole, pH 8.0.
- **Ni-NTA elution buffer:** 50 mM Tris, 300 mM NaCl, 10 mM β-mercaptoethanol, 200 mM imidazole, pH 8.0.

Buffers for protein purification under denaturing conditions (Ni-NTA)

- **Lysis buffer A:** 100mM NaH_2PO_4, 10 mM Tris pH: 8.0, 6M guanidinium chloride, 10mM β-mercaptoethanol.
- **Ni-NTA wash buffer B:** 100mM NaH_2PO_4, 10 mM Tris pH: 6.5, 6M guanidinium chloride, 10mM β-mercaptoethanol.
- **Ni-NTA Elution buffer:** 100 mM sodium acetate, pH: 4.0, 6M guanidinium chloride, 10mM β-mercaptoethanol.
- **Dialysis buffer:** 6 M guanidinium chloride, pH 3.0
- **Refolding buffer:** 100 mM Tris, pH 8.0, 200 mM arginine, 1mM EDTA, 2mM reduced glutathione, 2 mM oxidised glutathione, 0.05% NaN_3.

Buffers for GST purification

- **Lysis buffer:** 50 mM Na_2HPO_4 pH 8.0, 250 mM NaCl, 10 mM β-mercaptoethanol, EDTA-free protease inhibitor cocktail.
- **GST-Sepharose wash buffer:** 50 mM Na_2HPO_4 pH 8.0, 250 mM NaCl, and 10 mM β-mercaptoethanol.
- **GST-Sepharose elution buffer:** 50 mM Na_2HPO_4 pH 8.0, 250 mM NaCl, 50 mM glutathione 10 mM β-mercaptoethanol.

Other commonly used buffers for protein purification

- **Phosphate-buffered saline (PBS) buffer:** 10 mM Na_2HPO_4, 2 H_2O, pH 7.3, 1.8 mM KH_2PO_4, 140 mM NaCl, 2.7 mM KCl.

- **Protease acivation buffer:** 2.5 mM $CaCl_2$, 60 mM NaCl, 60 mM KCl, 50 mM Tris, pH 8.0, 0.05% NaN_3.
- **Ion exchange buffer:** 0 M buffer pH 7.2; 8 mM KH_2PO_4, 16 mMNa_2HPO_4, 0.05% NaN_3 and for salt buffer 1 M salt is added to the above constituents.

4.2. Molecular biology techniques

All employed molecular biology protocols, if not mentioned here, were used exactly as described in Sambrook and Russell (2001).

4.2.1. Molecular cloning

Plasmid constructs produced during this study were cloned with the aid of polymerase chain reaction (PCR), followed by restriction digestion and ligation. The standard PCR protocol followed is summarized in table

Standard protocol for polymerase chain reaction					
Reaction composition	Amount (µl)	Thermal cycling parameters			
Sense primer (10 pm)	1.5	Segment	Cycles	Temperature (˚c)	Time
Anti sense primer. (10 pm)	1.5	1	1	95	1 min
Template DNA (100-150 ng)	2.0	2	20-30	95	1 min
				50-55	30 sec
				68-72	1 min/kb
dNTPs (10 mM)	1 0	3	1	72	4 min
pfu DNA polymerase	1.0	4	1	4	Hold
10xpfu buffer	5.0				
Sterile ddH_2O	38				

All PCR reaction mixtures were prepared in sterile thin wall PCR tubes and PCR was performed using the master cycler (Eppendorf). The amplified PCR products were analyzed by agarose gel electrophoresis [1% agarose dissolved in TBE buffer containing ethidiumbromide (10

µg/ml)]. Desired PCR amplified products were purified by QIAquick PCR purification kit following the manufacturer's instructions. Restriction digestion of purified PCR products and desired vector was then carried out using the specific restriction endonucleases in amounts recommended by manufacturers (NEB) at 37°C in a 50 µl reaction for a couple of hours. Treating with 5 units of calf intestinal phosphatase at 37°C for one hour then dephosphorylated the restriction digested vectors. All reactions were stopped by heating at 65/85°C for 20 min. Desired digested products were then agarose gel purified using QIAquick gel extraction kit following the manufacturers instructions. Ligation reactions were then set up using T4 DNA ligase, following the standard protocols at vector to insert ratio of 1:3 to 1:5 and were usually kept overnight. 1 to 2 µl of this mixture was then used for transformation into TOP10 *E.coli* cells using electroporation.

4.2.2. Competent cells preparation

- Bacteria were streaked on an LB agar plate, and incubated at 37°C overnight.
- 50 ml of LB medium in a 250 ml flask were inoculated with a single colony from the LB plate and incubated at 37°C with shaking (200 rpm) overnight.
- 1 L of LB medium in a 3 L flask was inoculated with the 50ml overnight culture. The culture was grown in shaking (200 rpm) incubator at 37°C until the OD600 was between 0.5 – 0.6 (approximately 2 hrs).
- The culture was transferred to the two chilled, sterile 500ml centrifuge bottles and incubated on ice for 30 min. Thereafter centrifugation followed at 2000 G for 15 min at 0 – 4°C.
- Supernatant was decanted, and bottles put back on ice. The cell pellet in each bottle was resuspended in approximately 500 ml of cold (0 – 4°C) sterile water, and subsequently centrifuged like before.
- The cells in each bottle were washed again with 250 ml of cold sterile water, and centrifuged.
- The cell pellet in each bottle was then resuspended in 20 ml cold sterile 10 % glycerol and transferred to a chilled, sterile, 50 ml centrifuge tube. Centrifugation followed at 4000 G for 15 min at 0 – 4°C.
- The 10 % glycerol was decanted and pellet resuspended for the second time in 1ml cold sterile 10 % glycerol.

- Using a pre-chilled pipette the cell suspension was aliquoted (40 µl) to pre-chilled 5ml tubes and frozen immediately in liquid nitrogen. The aliquots were kept at –80°C ready for use.

4.2.3. Site directed mutagenesis

Quick-change® site-directed mutagenesis kit was used to introduce single amino acid substitutions, deletion and addition mutations at desired sites in the plasmid containing gene of interest. Gene encoding a supercoiled double stranded DNA carrying a gene of interest was used as a template and complementary oligonucleotide primers containing the desired mutations were used for PCR following manufacturer's instructions. The extension of mutagenic primers generated mutated covalently closed and nicked plasmids. Following PCR, the product was treated with 1 µl of Dpn I at 37°C for few hours. The Dpn I endonuclease was used as it is specific to methylated and hemimethylated DNA which is not found in the newly synthesized daughter strands and hence helps to digest the non mutated parental strands and select mutated DNA. After digestion 1-2 µl of this DNA was used for transformation.

4.2.4. Transformation

Electrocompetent *E. coli* cells were used to amplify hetrologous genes and over-express hetrologous proteins. In this study 50-100 ng of plasmid DNA was gently mixed together with the 40 µl aliquot of electrocompetent cells and placed between the electrodes of a 0.1 cm electroporation cuvette (Biorad, FRG). The cuvette was then put into the electroporator (Stratagene, FRG), and a pulse of 1660 V was applied. The value of the time constant was observed (usually 4-5 ms). The mixture was then washed out from between the electrodes with 1ml of the sterile prewarmed (37 °C) LB medium (without antibiotics), and transferred to a sterile 1.5ml tube for shaking (800 rpm) at 37 °C. After 1 hr 50 to 100 µl of culture was streaked on a LB agar plate containing the appropriate antibiotic.

4.2.5. Protein expression in *E. coli*

- **Small scale test expression of proteins**

Once the clones were obtained and transformed into expression strains small scale test expression were done to identify the optimal condition optimal conditions for hetrologous protein

production. 5 ml LB containing the appropriate antibiotic was inoculated with a fresh single bacterial colony and incubated overnight at 37 °C with vigorous shaking (280 rpm) in a 100 ml flask. Pre-warmed 50ml LB medium in 250-500 ml flask was inoculated with 1ml of the overnight culture, supplemented with appropriate antibiotic, and incubated at 37 °C with shaking (180 rpm) until the OD600 reached the 0.6-0.8 value. Induction by IPTG addition followed upto 1 mM IPTG concentration was usually used. The cells were then grown for another 2-6 hrs or overnight depending on temperature (15-37 °C).1ml of sample was then taken at regular intervals, the cells were pelleted and lysed by sonification and loaded on a SDS-PAGE gel and visualized by coomasie blue staining to see levels protein induction.

4.2.6. SDS-polyacrylamide gel electrophoresis

SDS-polyacrylamide gel electrophoresis (SDS-PAGE) under denaturing and reducing conditions were used to separate proteins based on mass. Mass of desired proteins worked on during this study and the effectiveness of protein purification scheme were analyzed by this method. Protein samples to resolve on SDS-PAGE were prepared by addition of 5x sample buffer (10% SDS, 10 mM β-mercaptoethanol, 250 mM tris-HCl pH 6.8, 50% glycerol and 0.5% bromophenol blue) to the final concentration of 1x followed by incubation for 3 min at 98°C. 10-20 µl of this sample was then loaded on the gel. For the present study, 10-15 % Tricine gels were used since the proteins to be detected was of small size. Applying a constant current of 125 V always performed electrophoretic separations.

SDS-PAGE reagents and buffer

- Separation buffer: 1 M Tris pH 8.8, 0.3% SDS
- Stacking buffer: 1 M Tris pH 6.8, 0.3% SDS
- Separation acrylamide: 48 % acrylamide, 1.5 % bis-acrylamide
- Stacking acrylamide: 30 % acrylamide, 0.8 % bis-acrylamide
- Anode buffer (+): 200 mM Tris, pH 8.9
- Cathode buffer (-): 100 mM Tris, pH 8.25, 100 mM Tricine, 0.1 % SDS

4.2.7. Protein purification methods

Recombinant proteins were purified to homogeneity using various chromatographic techniques like affinity chromatography, Ion exchange chromatography and gel filtration

chromatography. Native proteins were obtained after removal of the affinity tag by proteolytic digestion and subsequent separation of an untagged protein from the affinity tag. *E. coli* expressed and purified native proteins were characterised by subjecting to immunoblotting and N-terminal amino acid analysis. Folding status and the secondary structural content of proteins were monitored by NMR.

4.3. NMR sample preparation

For the NMR experiments the protein solutions were concentrated with a Centricon or Amicon to the volume of 450 µl and 50 µl D_2O (99.9%) was added to the sample. The sample concentration ranged from 0.2 to 0.8 mM. All NMR spectra were acquired at 300 K on a Bruker DRX-600 spectrometer. ^{1}H-^{15}N-HSQC spectra (Mori et al. 1995) were recorded with 128 increments in the indirect ^{15}N dimension with a number of scans varying from 4 to 1024 depending on the concentration of individual samples. Measurement times ranged thus from 2 to 24 hours. Processing and analysis of the spectra was performed using the programs XWIN NMR (Bruker) and Sparky, respectively.

4.4. ITC experimental setup

For the ITC experiments the proteins were dialysed in the ITC buffer (25 mM Tris, pH 8.00, 250 mM, NaCl, 10 mM β-mercaptoethanol, 2.5% glycerol and 1% DMSO) and used at a concentration of 50 to 60 µM. All Inhibitors were dissolved in 1% DMSO and made to a final concentration of 1 mM. ITC run conditions are given below:

Run parameters:

Injections: 30-40

Volume: 5 µl

Duration: 10 sec

Interval: 420 sec

Temperature: 25˚C

All runs were set up with a protein to inhibitor ratio of 1:10 to 1:20. ITC results were analysed with the program Microcal Origin.

4.5. MDM2 expression, refolding and purification

The recombinant human MDM2 protein was obtained from an *E. coli* BL21 expression system and contained the first 118 N-terminal residues of human MDM2 cloned in a pQE-40 vector, C-terminally extended by an additional serine residue. Protein expression was performed in shaking cultures at 300 r.p.m. at 37°C. The cultures were induced with 1 mM IPTG at the cell density of $O.D_{600}$ = 0.65. Cells were harvested by centrifugation after 3 h of induction. Inclusion bodies were solubilized in 6 M guanidine hydrochloride at physiological pH. Refolding was performed for overnight at room temperature. Refolded human MDM2 was applied to hydrophobic interaction chromatography. Finally concentrated protein was further purified by size exclusion chromatography using the HiLoad 26/60 Superdex 75 pg gel filtration column. The uniformly labeled ^{15}N isotopically enriched protein samples were prepared by growing the bacteria in minimal media containing $^{15}NH_4Cl$.

NMR spectra and ligand binding for MDM2

NMR measurements consisted of monitoring changes in chemical shifts and line widths of the backbone amide resonances of uniformly ^{15}N-enriched MDM2 samples in a series of HSQC spectra as a function of a ligand concentration. The chalcone derivatives were lyophilized and finally dissolved in DMSO. No shifts were observed in the presence of 1% DMSO (the maximum concentration of DMSO in all NMR experiments after addition of inhibitors). All chalcone-MDM2 complexes showed a continuous movement of several NMR peaks upon addition of increasing amounts of inhibitors. From these experiments, the spectra of MDM2 could be assigned unambiguously. The complexes of human MDM2 and the chalcones were prepared by mixing the protein and the ligand in the NMR tube. Typically, NMR spectra were recorded 15 min after mixing at room temperature. An initial screening of all compounds used in this study was performed with a 10-fold molar excess of boronic or cyano chalcones to human MDM2. All subsequent titrations were carried out until no further shifts were observed in the spectra. Typically, the concentration of human MDM2 was 0.1 mM and the final concentration of the chalcone ligand was 50 mM in each titration. All K_D values obtained by NMR spectroscopy were based on at least eight data points. From the independently determined K_D values, one ligand-binding site for these chalcone derivatives per MDM2 was calculated taking into account the

molar ratio of ligand to protein in the NMR experiments. Quantitative analysis of induced chemical shifts was performed on the basis of spectra obtained at saturating conditions of each chalcone derivative.

Ligand binding was detected by acquiring ^{15}N-HSQC spectra. All NMR spectra were acquired at 300 K on Bruker DRX-600 spectrometer. Typically, NMR samples contained up to 0.1 mM of protein in 50 mM KH_2PO_4, 50 mMNa_2HPO_4, and 150 mM NaCl, pH 7.4, 5 mM DTT, 0.02 % NaN_3 and protease inhibitors. The quality of the spectra for MDM2 with and without inhibitors was reduced by aggregation, especially at concentrations higher than 0.7 mM at pH 7.3 and 300 K. To avoid aggregation, all experiments were carried out at lower concentration of around 0.1 mM. Before measuring, the sample was centrifuged in order to sediment aggregates and other macroscopic particles. 450 µl of the protein solution was mixed with 50 µl of D_2O (5%) and transferred to an NMR sample tube. The stock solutions of compounds were 100 mM in DMSO-d_6. As a control experiment, we first titrated the free MDM2 against DMSO-d_6 and recorded their respective HSQC's. pH was maintained constant during the whole titration. The binding was monitored by observation of the changes/shifts in the ^{15}N HSQC spectrum, as a function of ligand concentration.

4.6. IGFBPs expression, refolding and purification

To purify the protein as a His-tag fusion protein the IGFBPs cDNA was cloned into pET-28 (a) vector (Qiagen, Hilden, Germany) with appropriate restriction sites in frame to a His-tag. Standard procedures were adopted for the construction of the vector pET-28 (a) with the desired insert, which was expressed as a fusion protein in *E. coli* strain of BL21 (DE 3) under kanamycin selection. Expression was performed in shaking cultures at 300 r.p.m. at 37 °C. The cultures were induced with 1 mM IPTG at the cell density of $O.D_{600}$ = 0.85. Cells were harvested by centrifugation after 3 h of induction. The cell pellets were resuspended in the lysis buffer and kept for 1 h shaking. To obtain complete lysis, the cells were sonicated using the macro tip where pulsed, high frequency sound waves are used to agitate and lyse cells. To prevent excessive heating, ultrasonic treatment was applied in multiple short bursts to the sample immersed in ice bath. The sonication was done for 2 minutes at duty cycle 50% and output control 7. First treating the cells with the lysozyme and then sonicating the extract performed the sonication/lysozyme treatment. All of the extracts were clarified by centrifugation for 60 minutes at 60,000 x g at 4

°C. The supernatants were recovered and then analyzed for total protein by the Bradford protein assay. The supernatent was loaded onto the Ni-NTA column and protein elution was performed by the pH gradient method (Qiagen, Hilden, Germany). The fractions containing protein were pooled and β-mercaptoethanol was added at a concentration of 10 mM. The final volume was concentrated to approximately 2 ml by ultrafiltration and then dialysed against 6 M guanidinium chloride. The protein solution was then diluted into the refolding buffer. After 24 hrs of refolding at 4°C, the protein solution was again concentrated by ultrafiltration and dialysed against phosphate buffer and loaded onto an anion exchange column (Mono S) in which the proteins were bound to the column material in 25 mM phosphate buffer, 25 mM NaCl, pH 7.2, and bound proteins were fractionated by a linear gradient of 25-700 mM NaCl over 20 column volumes. The fractions containing the protein were pooled and a size exclusion chromatography was performed on a Superdex 75 column.

His tag cleavage using thrombin: The protein was dialysed in thrombin cleavage buffer and thrombin was added at a concentration of 1 µl/mg of protein. This sample was left at room temperature for 72 hrs with gentle shaking. Finally Histag cleaved protein of interest was separated on the size exclusion chromatography column.

5. Results and Discussion

5.1. Novel boronic and cyano chalcone derivatives as inhibitors of the p53-MDM2 pathway

Our previous biochemical experiments with chalcone derivatives show that these compounds can disrupt the MDM2/p53 protein complex, releasing p53 both from the p53/MDM2 and DNA-bound p53/MDM2 complexes (Stoll et al. 2001). The present study was focussed on chalcone derivatives that could bind to MDM2 and are selectively toxic to the MDM2 over-expressing breast cancer cells (Kumar et al. 2003). A series of novel boronic and cyano-chalcones have been synthesized, which were shown to be 5-10 folds more toxic to human breast cancer cell lines as compared to normal breast epithelial cell lines (Kumar et al. 2003). Our study shows NMR evidence for binding of these novel chalcones in and near the tryptophan-binding pocket of the p53 binding cleft of human MDM2 and propose three-dimensional models consistent with these data. Since an X-ray structure of MDM2 in complex with p53 peptide (Kussie et al. 1996) is available, we were able to examine in detail how these chalcone derivatives should mimic the p53 binding site. The analysis also shows that the compounds fit into one of the sites of the p53-binding pocket of MDM2. These compounds represent a novel lead compound for further p53-MDM2 inhibitor design.

5.1.1. Expression and purification of N-terminal domain of MDM2

For performing the inhibitor binding studies, the N-terminal of the MDM2 protein was required. Various N-terminal constructs were designed in both pET and pQE series of expression vectors. The best working construct i.e. the one with highest expression of stable and biologically active protein was chosen. This construct consisted of residues 1-118 in the pQE vector. Promising results were also obtained with a larger construct, which contained residues 1-180 in the pET 30 LIC vector. In the case of the longer N-terminal construct in pET 30 LIC, protein expression was quite high and was obtained in the soluble fraction. Since the His-tag was the fusion partner, clear cell lysates were loaded on the Ni-NTA column and affinity chromatography was performed. Results are shown in Fig 5.1 and 5.2. Further purification, using the anion exchange and Superdex 75 size exclusion columns, resulted in a well purified protein and in the

yields were suitable for structural studies. Next step was to remove the long fusion tag of 4 kDa, which was in the N-terminus of the protein. A factor Xa protease site was introduced in the gene and the proteolysis was performed as described by the manufacturer (NEB). The protein was further purified by gel filtration chromatography (Fig. 5.3). 1D-NMR studies were then performed to check the folding status of the protein. The results showed that the protein was partially unfolded and thus not suitable for inhibitor binding studies (Fig. 5.4).

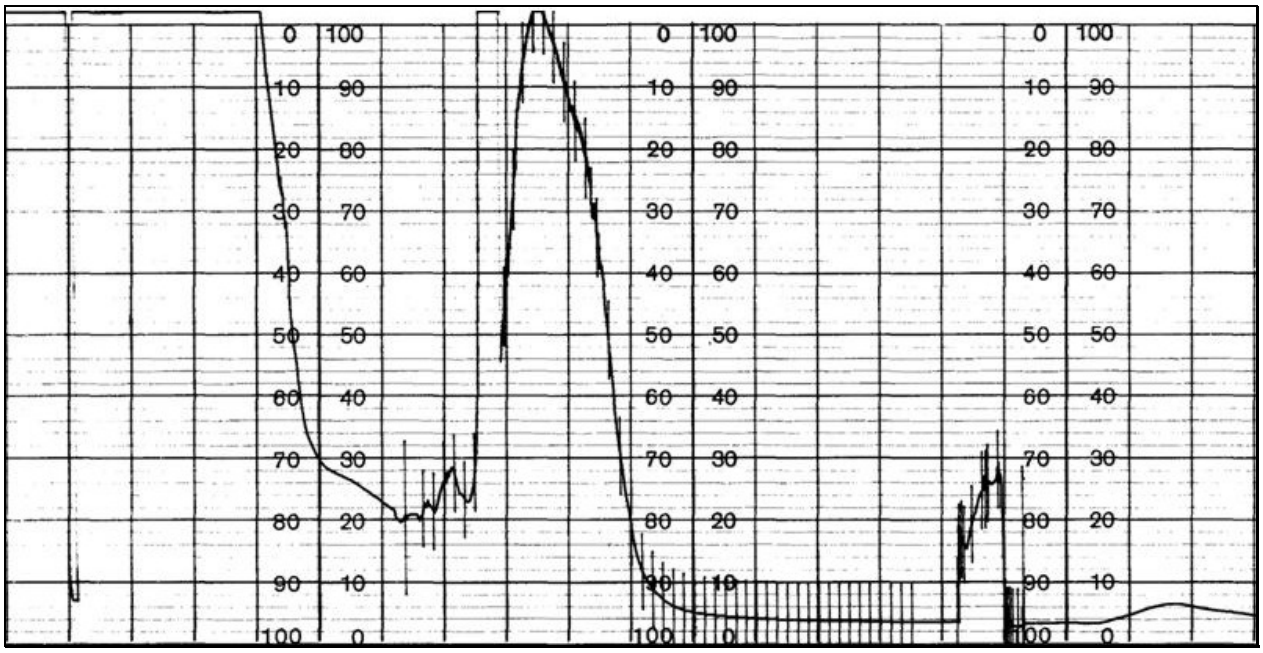

Figure 5.1 *Affinity chromatography performed with the linear imidazole gradient. The chromatogram shows the elution profile of N-terminal MDM2 (1-180) purified as a histag fusion protein.*

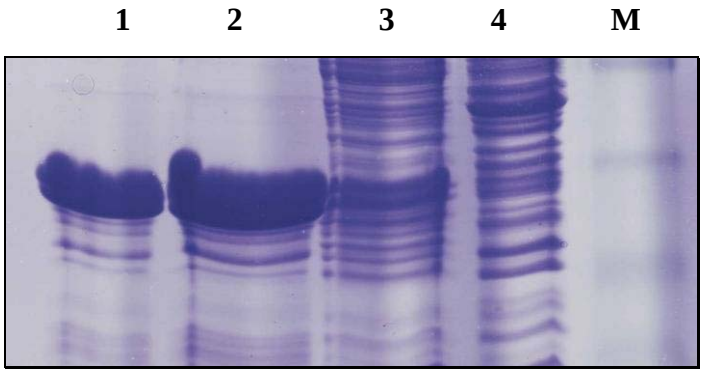

Figure 5.2 *SDS-gel electrophoresis of the affinity chromatography fractions. Lane M denotes the prestained protein marker. Lanes 1 and 2 show the eluted Histag fusion MDM2, lane 3 denotes the impurities obtained in wash buffer and lane 4 shows the flow-through.*

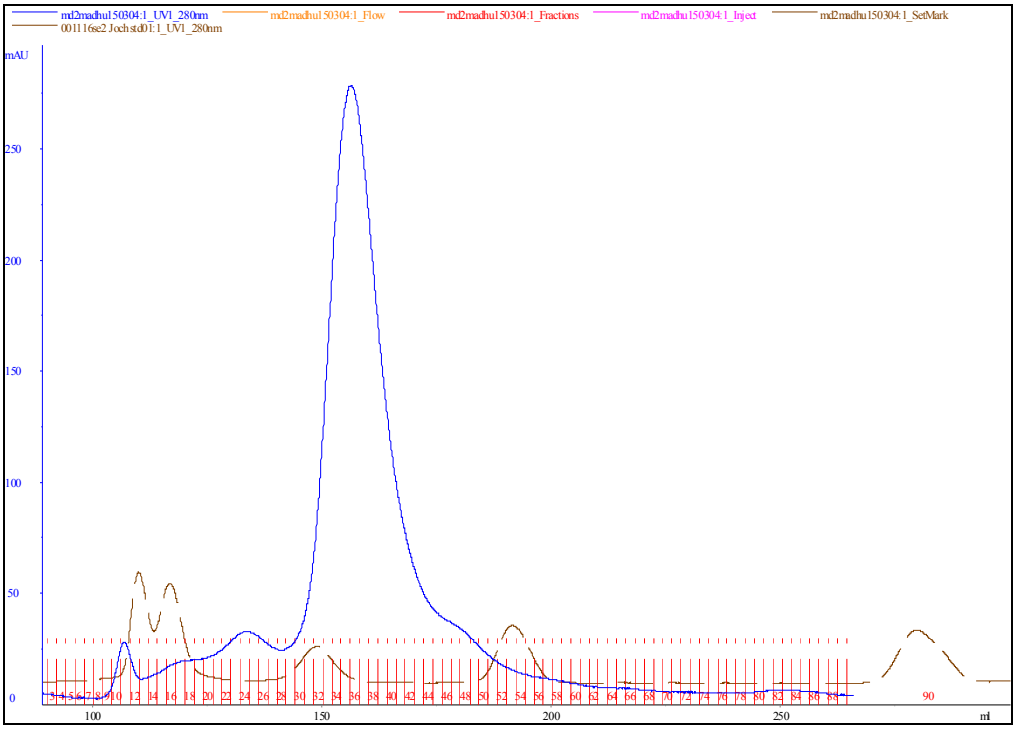

Figure 5.3 *Size exclusion chromatography of N-terminal MDM2. The chromatogram shows at UV 280 nm, the protein peak (blue) obtained is at around 30 kDa when compared with the standard chromatogram (brown).*

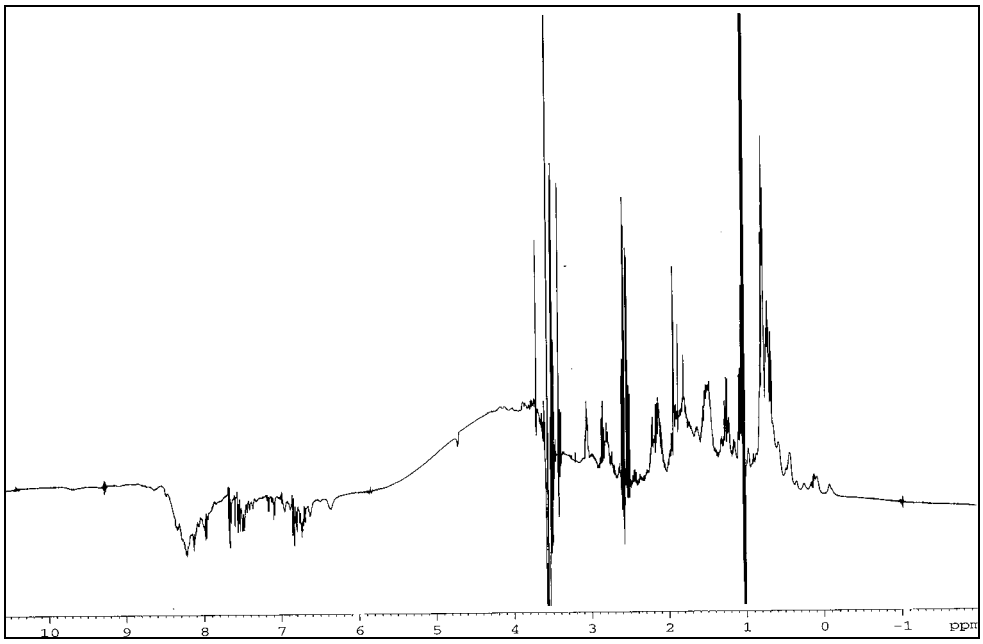

Figure 5.4 *1D NMR spectra of the N-terminal domain (1-180). The spectrum shows a partially folded protein.*

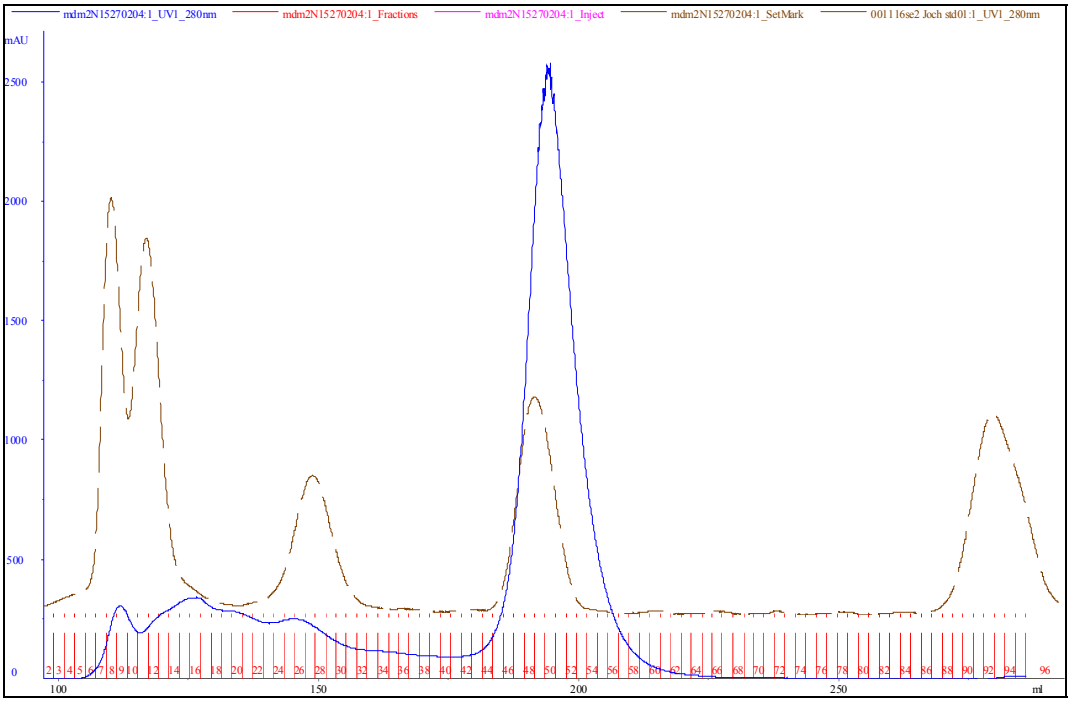

Figure 5.5 *Construct 1-118 N-terminal MDM2 elution chromatogram after Superdex column.*

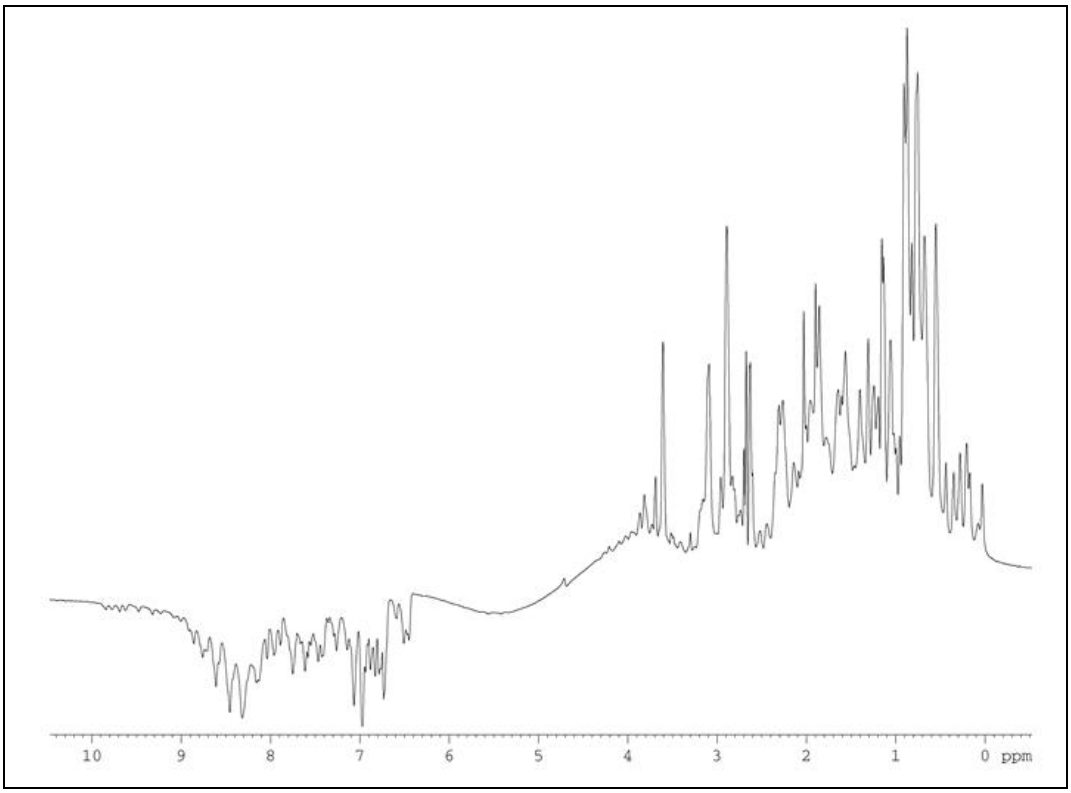

Figure 5.6 *1D NMR spectra of 1-118 showing large signal dispersion beyond 8.3 ppm and also in the aliphatic region.*

The second construct was truncated from the C-terminal by about 60 residues and composed of residues 1-118 of N terminal MDM2. The 13 kDa MDM2 construct (1-118) was expressed as inclusion bodies and was initially purified using denaturing conditions and then refolded. Finally the protein was further purified using the Superdex 75 column where the running buffer was PBS (Fig. 5.5). 1D NMR studies showed the protein to be folded (Fig. 5.6). Binding studies by NMR for possible inhibitors of p53-MDM2 interaction were carried out with this N-terminal construct.

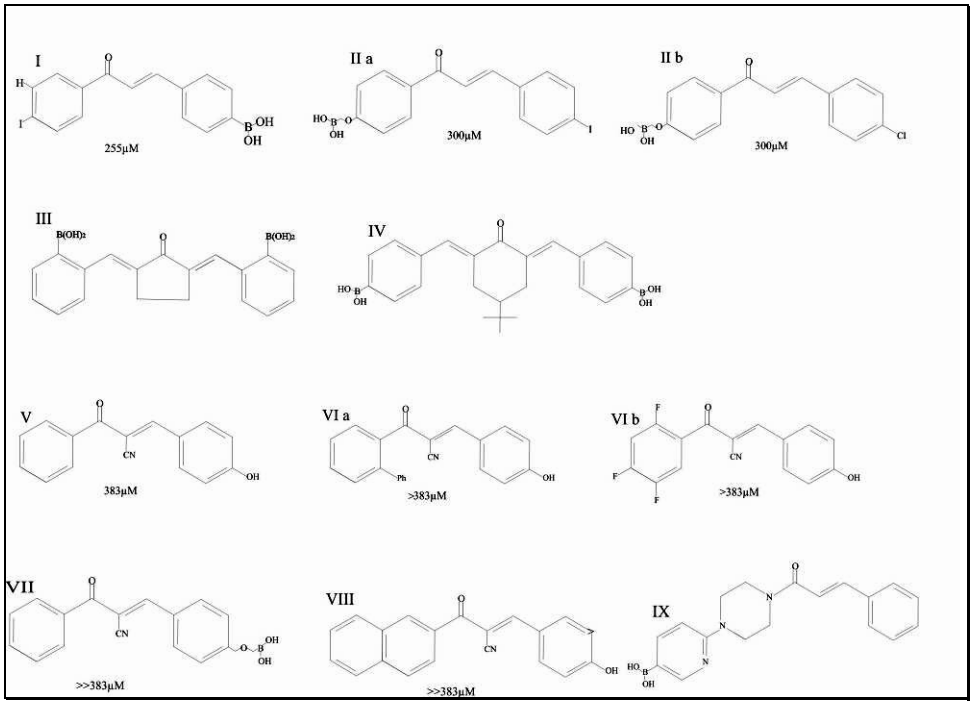

Figure 5.7 *Chalcone derivatives used for MDM2 binding. Inhibition of p53-MDM2 interaction measured by NMR titration experiments with the respective K_D values are shown next to the compounds.*

5.1.2. NMR spectroscopy

Determination of binding sites of lead chalcone compounds was carried out using ^{15}N-HSQC NMR spectroscopy of the ^{15}N isotopically enriched N-terminal (1-118) domain of human MDM2. A nearly complete assignment (Stoll et al. 2001) of the backbone ^{1}H and ^{15}N NMR resonances is available for the uncomplexed MDM2 (apo-MDM2). The N-terminal MDM2 domain produced well-resolved NMR spectra and spectral quality remained high upon complexation with chalcone derivatives. Small but significant chemical shifts were observed in the p53 binding site of human MDM2 on complexation with boronic and cyano derivatives of

chalcones. Chemical shift perturbations of ^{15}N labeled human-MDM2 upon complexation with these compounds were used to verify the binding of the compounds and to determine the ratio of concentration of MDM2 to inhibitors required to ensure saturation. A list of the chalcone derivatives used in our study is shown in (Fig. 5.7).

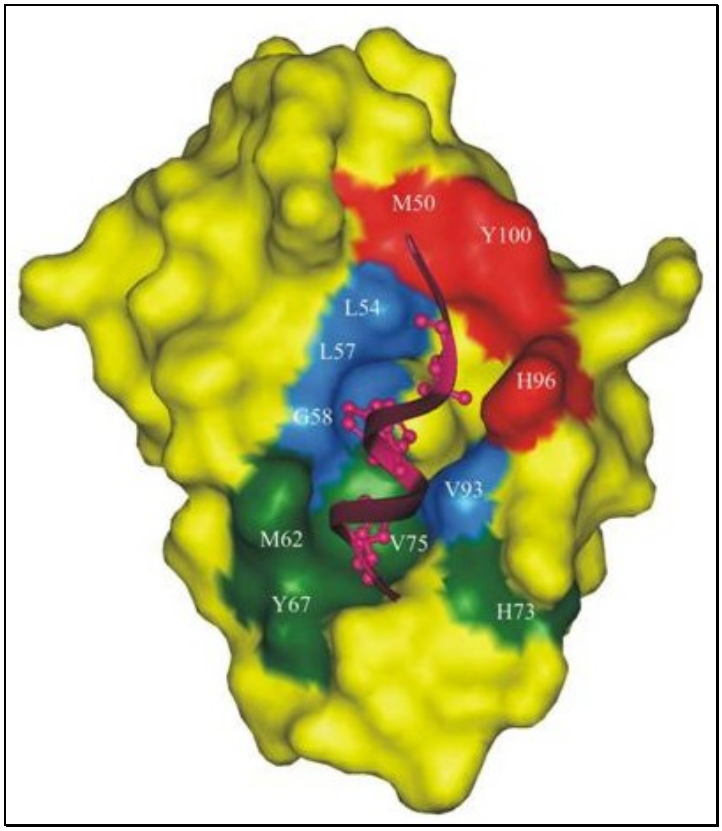

Figure.5.8 *Binding mode of p53 peptide in the hydrophobic core of MDM2 protein.The p53 peptide shown in purple ribbon is superimposed on the MDM2 binding surface. The side chain residues of p53, F19, W23, and L26, which bind to MDM2 are shown as pink sticks. The MDM2 residues, which constitute the leucine, tryptophan, and phenylalanine binding, are coloured in red, blue and green respectively. The MDM2 residues, which bind to p53, are labelled. The atomic radius was set to the Van der Waals value and the solvent radius to 1.4 Å generated from the 1YCR data set (Kussie et al. 1996).*

5.1.3. General structural features of the MDM2 binding p53 peptide and the chalcone derivatives

The crystal structures of N-terminal domains of human and *Xenopus* MDM2 in complex with p53 peptide (Kussie et al 1996) show that The hydrophobic surfaces of MDM2 and p53 are sterically complementary at the interface. The binding surface of p53 is dominated by a triad of

p53 amino acids phenylalanine 19 (F19), tryptophan 23 (W23) and leucine 26 (L26) which contribute to a great extent to the interaction and consequently to the binding energy of the p53 peptides and define the corresponding phenylalanine, tryptophan and leucine subpockets for the p53/MDM2 interaction that bind along the MDM2 cleft (Fig. 5.8).

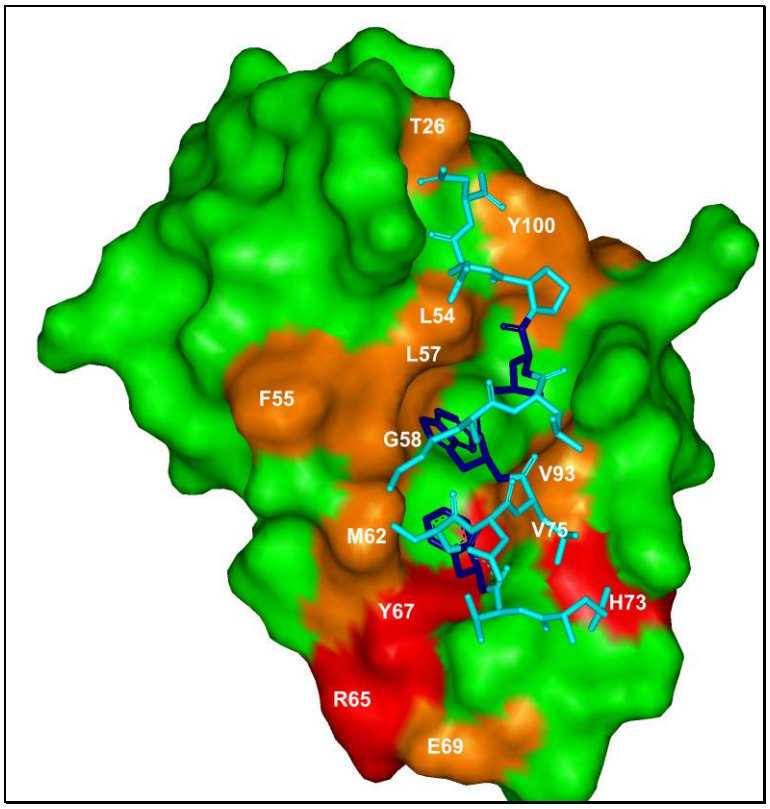

Figure 5.9 *Residues that show significant chemical shifts on complexation with the p53 peptide. p53 peptide, comprising residues 15 to 29, binds to an elongated hydrophobic cleft of the MDM2 domain. The p53 peptide is shown in stick model in cyan, F19, W23, L26 of p53 are indicated in dark blue. The MDM2 protein surface is indicated in green. The MDM2 residues, which show significant chemical shifts, are marked as red patches followed by brown, which are relatively weak shifts.*

In this classification, the leucine pocket is defined by V53, Y100 and T101 the tryptophan pocket is defined by L54, L57, G58, Y60, F91, S92 and V93 the phenylalanine pocket is defined by M62, R65, Y67, E69, H73, I74, V75 and V93. The NMR ^{15}N-^{1}H NOE experiment indicated that the folded core of the MDM2 domain in solution extends from T26 to N111 which is in agreement with the crystal structure. Transfer Nuclear Overhauser enhancement studies of p53 derived peptides show that these fragments do not have a stably folded structure in solution

(Blommers et al. 1997). These measurements indicate that the p53-peptides adopt a helical conformation upon binding to MDM2 (Fig. 5.9).

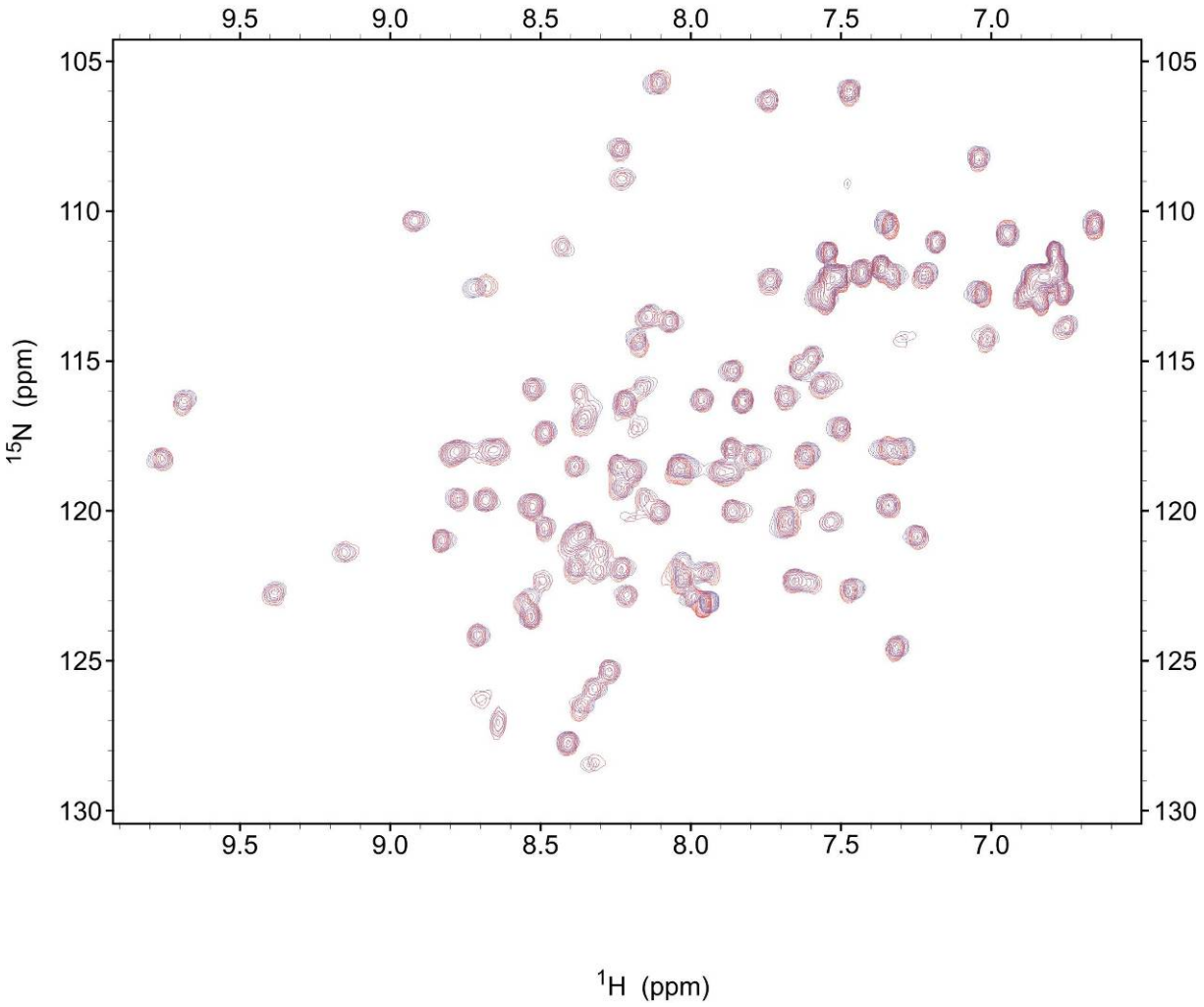

Figure 5.10 *MDM2 titrated with increasing concentrations of DMSO-d_6.Cross peaks of free MDM2 are shown by the red peaks and the final titration results are superimposed as purple peaks.*

5.1.4. Detailed examination of binding residues exhibited by the boronic and cyano chalcones

A full set of MDM2/p53 interface residues comprises M50, L54, L57, G58, I61, M62, Y67, H73, V75, F91, V93, H96, I99, and Y100 of MDM2 (Kussie et al 1996). The ^{1}H-^{15}N NMR resonances of these residues were all shifted upon addition of the p53 peptide. Additionally, large shifts are observed for β strand residues T26, L27, V28, R29, L107, and V108 and for residues

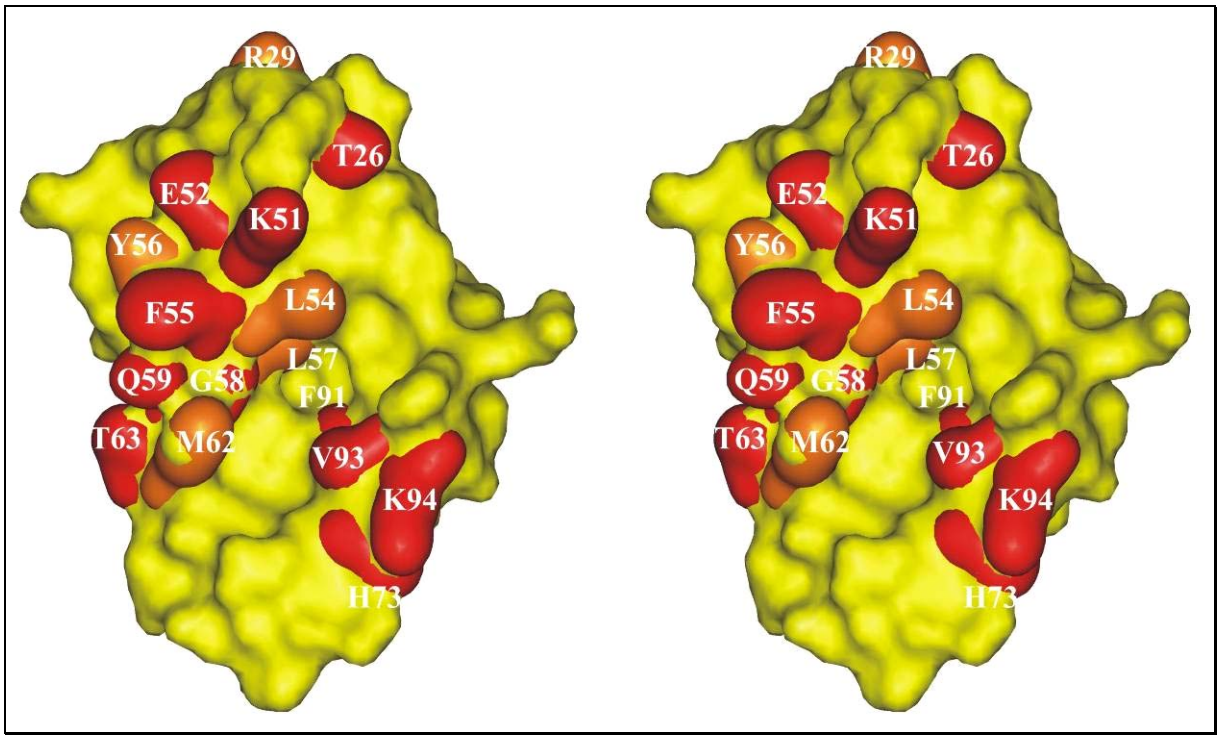

Figure 5.11 *MDM2 residues which show significant induced NMR chemical shifts on complexation with boronic chalcones. Contact surface of human MDM2 (residues 25-109) is obtained from 1YCR data set (Kussie et al 1996). The MDM2 surface is shown in yellow. The residues shown in red depict strong vectorial shifts and those shown in orange are weak signals which are within the vectorial shift range of 0.08-0.12ppm.*

L34, L37, and K64 (Fig. 5.9). Titration for the MDM2-p53 peptide complex was carried out as a control experiment. Although almost all amino acids of the apo-MDM2 exhibit changes in chemical shifts upon complexation with the p53 peptide, the largest chemical shifts were observed in the region of the three binding subpockets of p53 on MDM2. Shifts observed for amides outside the binding regions may be caused by secondary effects, such as allostery or change in mobility upon binding, and do not necessarily indicate direct binding of the p53 peptide to MDM2. Such possible secondary effects (e.g., residues L34, L37, and K64) must be considered when analyzing ligand binding to allosteric proteins**.**

The interactions that boronic chalcones and cyano chalcones make with MDM2 are predominantly hydrophobic in nature. Boronic chalcones demonstrated largest shifts at the residues of T26, L34, K51, E52, V53, F55, L57, G58, Q59, T63, H73, I74, F91, S92, V93, K94,

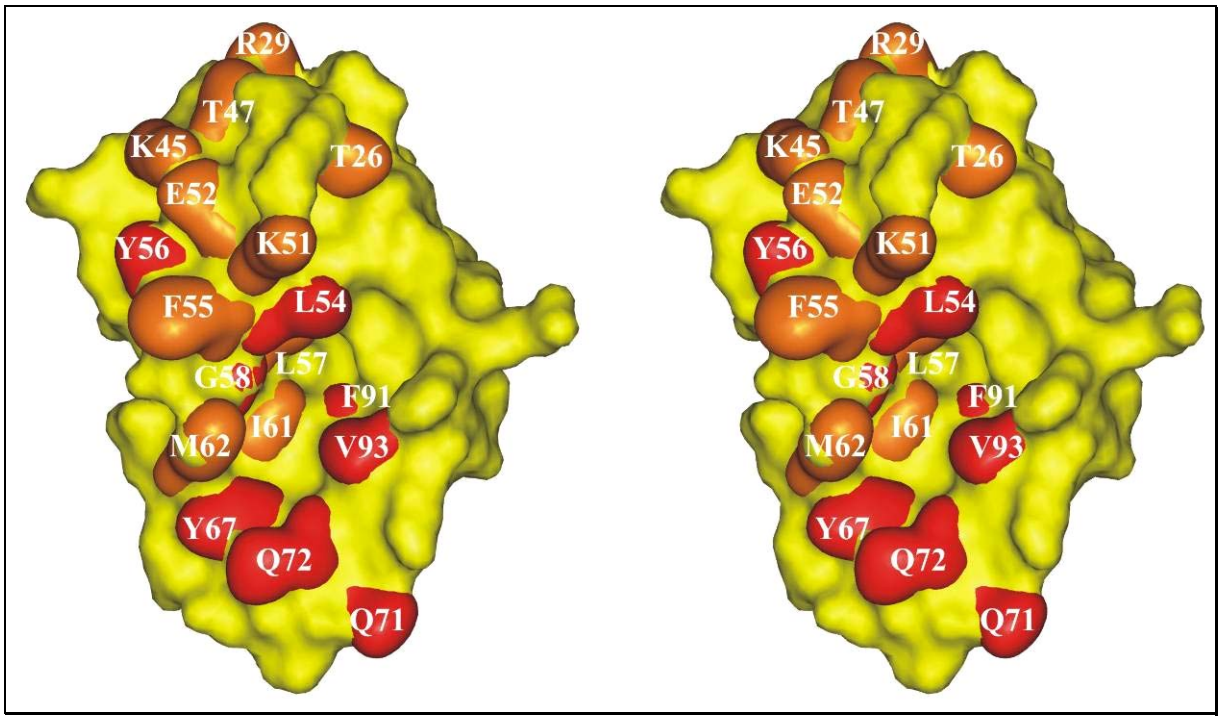

Figure 5.12 *Binding sites of cyano chalcones on the MDM2 surface. Residues which show significant chemical shifts upon complexation with cyano chalcones are coloured red and the ones which bind within a range of 0.08-0.12 ppm are shown in orange. Contact surface of human MDM2 (residues 25-109) is obtained from 1YCR data set (Kussie et al 1996).*

V109 and some weak signals were also observed, these being V28, R29, L54, L57, Y56, M62, V108 (Fig. 5.11).The shift pattern is consistent with the binding in the tryptophan-binding pocket of MDM2. The K_D values determined by NMR spectroscopy lie within the range of 255 µM in the case of compound I. Compound I showed the strongest shifts followed by boronic chalcones II a and II b, the K_D value of which is 300 µM. For the cyano chalcones, the strongest shifts were observed at residues L54, Y56, G58, Y67, Q71, Q72, F91, and V93. Weak binding was shown for T26, V28, R29, K45, T47, K51, E52, F55, L57, I61, M62, and S92 (Fig. 5.12).

The overall shift perturbation for cyano chalconesis slightly different from those of boronic chalcones as besides tryptophan binding pocket, induces chemical shifts are also observed in the phenylalanine binding site, the residues being M62, Y67, V93, but the K_D values obtained by NMR are higher as compared to boronic chalcones (383 µM for compound II). Compound III induces aggregation of the protein and compounds IV and IX lead to denaturation. The shifts obtained for these compounds cannot reliably be used for inhibitor interaction assay

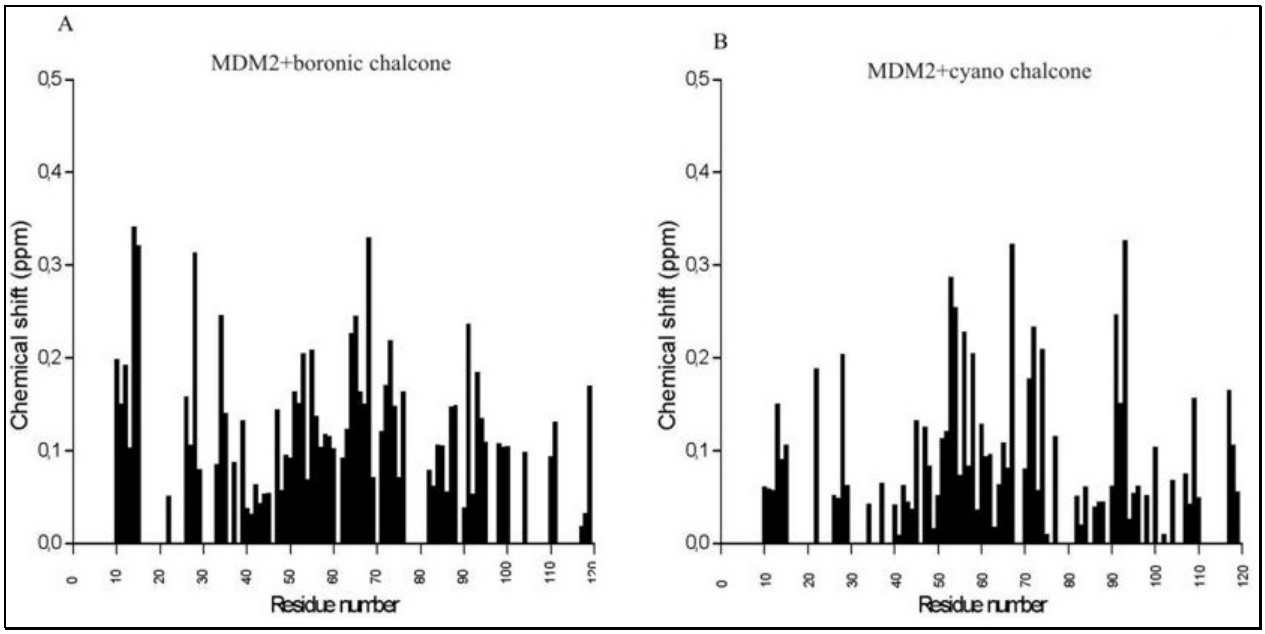

Figure 5.13 *Plots of induced differences in the NMR chemical shifts versus the amino acid sequence. (A) MDM2 with boronic chalcone I. (B) MDM2 when bound to a cyano chalcone V*

since these inhibitors induce precipitation of the MDM2 protein. Moreover induction of protein aggregation is usually considered as a non-specific effect of compounds and hence an indicator of low therapeutic potential. Fig. 5.13 shows the plots of the induced NMR chemical shift perturbations observed on binding of these chalcones to MDM2. Thus these chalcone derivatives bind mainly to the tryptophan pocket of the p53-binding site of MDM2 as in both boronic and cyano derivatives the strongest shifts are observed for the tryptophan pocket, e.g. residues G58, S92, F91, and V93.

5.1.5. Comparision between boronic and cyano chalcones and the p53 peptide ligand

According to the crystal structure obtained from (Kussie et al. 1996) the p53/MDM2 interface residues of MDM2 in the α-helix regions are defined as M50, L54, L57, G58, I61, M62, Y67, H73, V75, F91, V93, H96, I99, Y100 and in the β-strand, T26, L27, V28, R29, L34, L37, K64, L107, V108. Here in the case of boronic chalcones residues from the α-helix that bind to the tryptophan pocket of p53 are G58, H73, S92 and the ones that bind to the phenylalanine pocket are H73, V93. The only residue that fits into the leucine pocket is V53. The other β-strand residues that show chemical shift differences are L34, T26 and V108. The overall NMR shift

perturbation pattern in the case of cyano compounds is similar to that observed for the boronic chalcones (Fig. 5.14 and Fig. 5.15) G58, H73 and S92 show binding in both the chalcone derivatives.

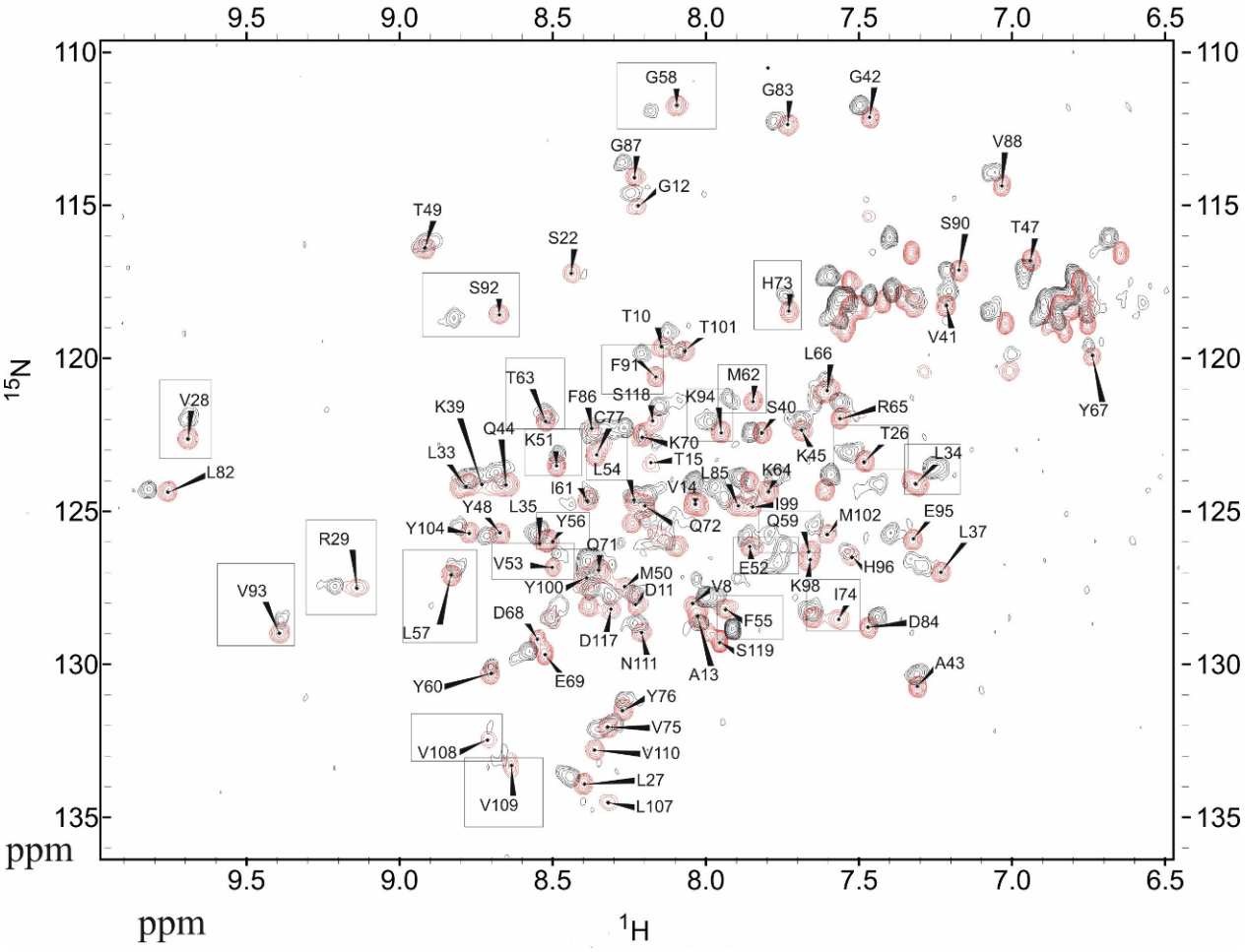

Figure 5.14 *A 2D ^{1}H-^{15}N HSQC spectrum of human MDM2 titrated with increasing concentrations of boronic chalcone I. Crosspeaks for apo-MDM2 are marked in red and the black peaks denote final complexation of MDM2 with boronic chalcone. The residues that show significant chemical are marked in boxes.*

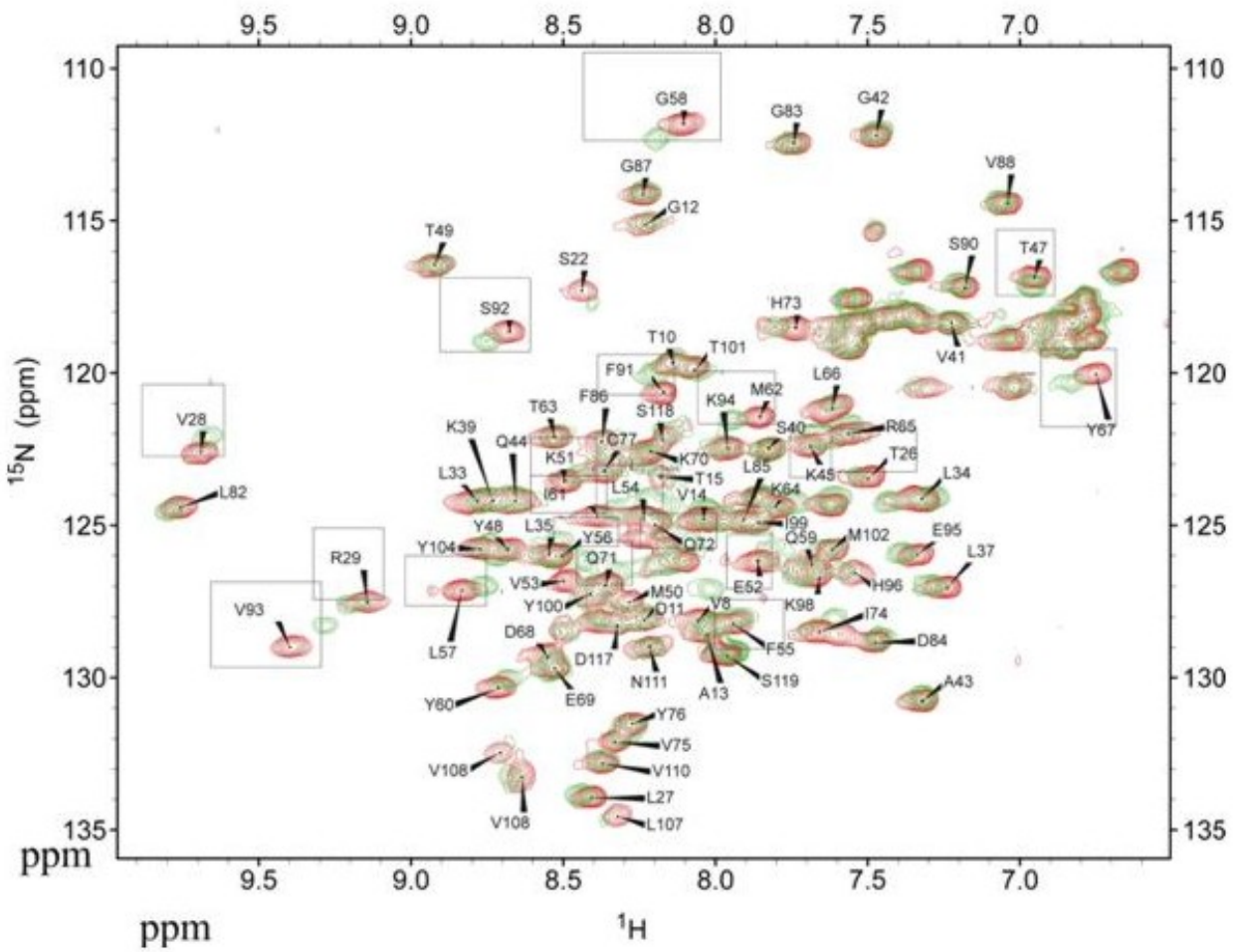

Figure 5.15 *A 2D ^{1}H-^{15}N HSQC spectrum of human MDM2 titrated with increasing concentrations of cyano chalcone V.Crosspeaks for apo-MDM2 are marked in red and the green peaks denote final complexation of MDM2 with cyano chalcone. The residues, which show largest chemical shifts, are marked in boxes*

For cyano compounds, the tryptophan binding pocket involves G58, F91 and L54 all being in the α-helical region and the other phenylalanine site which shows a stronger binding when compared with boronic chalcones, are bound by M62, Y67 and V93. The β-strand residues showing shifts are V28 and R29. The remaining residues that show perturbation on complexation with cyano compounds belong to the α-helix of MDM2 protein. The tryptophan pocket is successfully bound in the case of chalcone derivatives leaving behind only partially occupied leucine and phenylalanine sites.

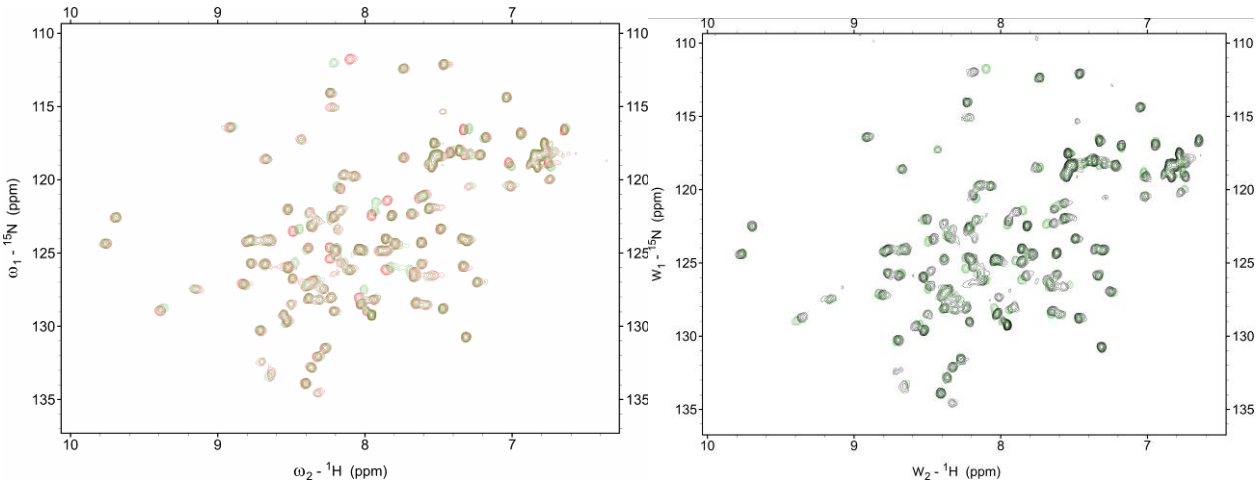

Figure 5.16 *A 2D ^{1}H-^{15}N HSQC spectrum of human MDM2 titrated with increasing concentrations of cyano chalcone VI a shown on the left panel. Crosspeaks for apo-MDM2 are marked in red and the green peaks denote final complexation. The panel on the right denotes titrations done with cyano chalcone VI b. Reference peaks of free MDM2 are shown in black and the ones in green show the chemical shifts obtained on final complexation.*

Titrations were also performed with compounds VI a and VI b but they showed no binding. (Fig. 5.16) as there were hardly any chemical shifts which could be detected.

5.1.6. CONCLUSIONS

We conclude that boronic and cyano chalcones bind to the tryptophan-binding pocket of the p53-binding site of MDM2 and cyano chalcones also show binding in the phenylalanine pocket. These chalcone derivatives act as antagonists of the p53/MDM2 interaction; however, these compounds do not fully occupy the p53/MDM2 binding cleft, which might explain their micro molar affinities. Since these antitumor compounds are more toxic to cancer cells than to normal cells they still could offer a starting point for structure-based drug design for cancer therapeutics.

Another class of nonpeptide small molecular compound used in our experiments as possible inhibitor was sulphonamide. The chemical structure has been shown in Fig. 5.17. This compound was obtained from the chemistry and synthesis branch of National Cancer Institute. Galatin and Abraham have reported that this compound inhibits the physical interaction of

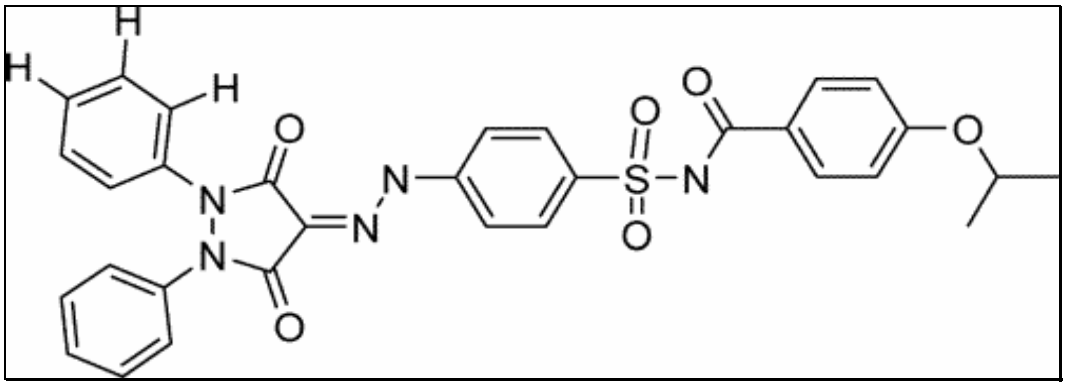

Figure 5.17 *Sulfonamide compound used in our study (NCI)*

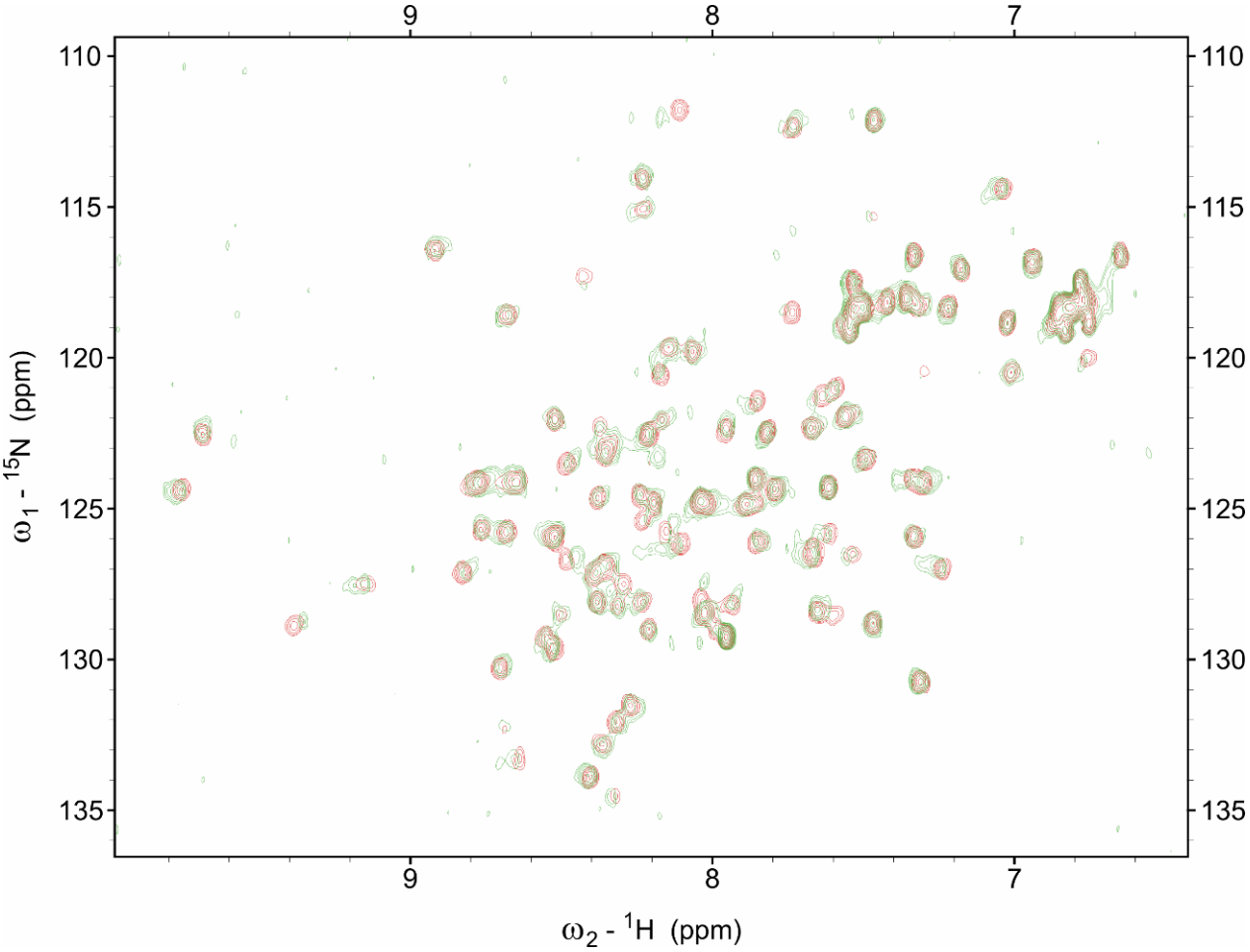

Figure 5.18 *2D HSQC showing titrations experiments with sulphonamide.*

recombinant p53 and MDM2 in vitro and increases p53-dependent transcription in an MDM2 overexpressing cell line (Galatin and Abraham 2004). We performed titration experiments with sulphonamide and our MDM2 construct in order to find the binding sites. The titration conditions were same as in the case of chalcones. But the 2D HSQC results show a very weak binding.

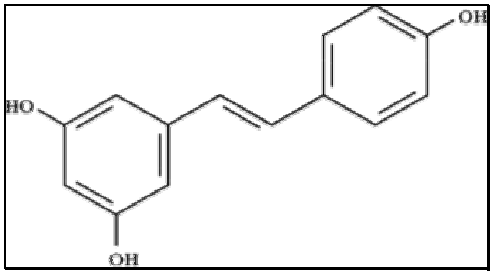

Resveratol

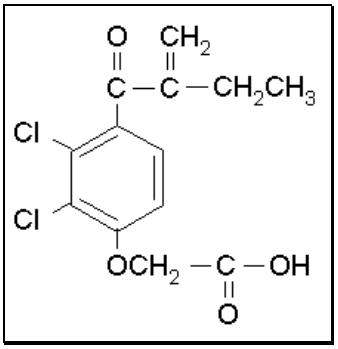

Ethacrynic acid

Binding tests with this domain of MDM2 was also tried out with other possible inhibitors, like resveratol and ethacrynic acid. Resveratrol, 3, 5, 4'-trihydroxystilbene, which occurs naturally in grapes, is an effective inhibitor of cell growth in general, triggers partial arrest of G1/S transition in prostate cancer cell lines and induces apoptosis (Hsieh et al.1999). Titration results show no binding (Fig. 5.19).

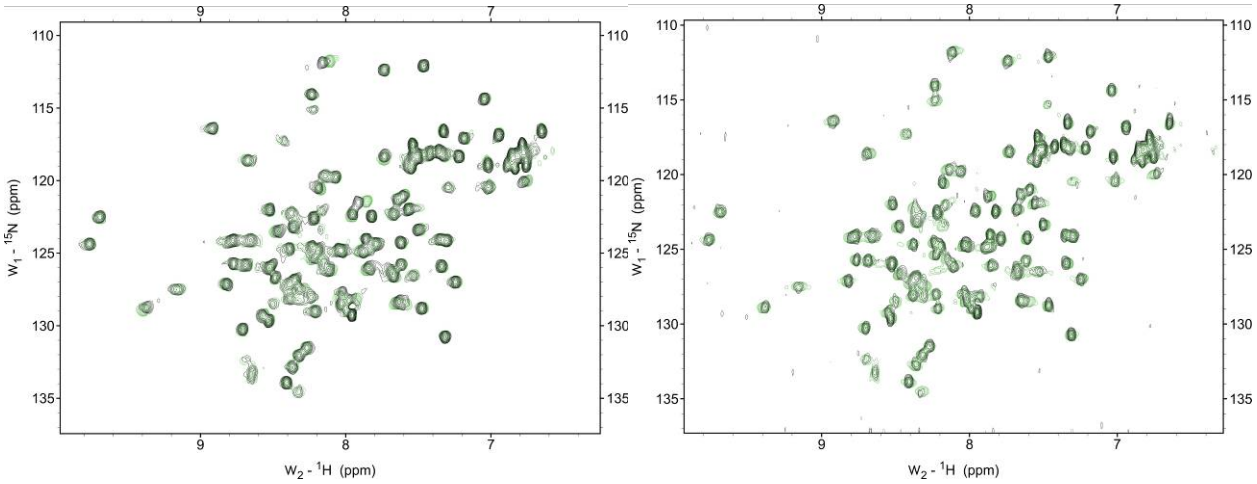

Figure 5.19 *600 MHz 2D ^{1}H-^{15}N HSQC spectrums of human MDM2 titrated with increasing concentrations of ehtacrynic acid (left panel) and with resveratol (right panel). Crosspeaks for apo-MDM2 are marked in black and the green peaks denote final complexation of MDM2*

5.2. Preliminary investigations of full length and C-terminal MDM2 constructs

The human *Mdm2* gene, of the full length MDM2 protein was cloned in frame to 6xHis-tag into pET-28 (a) vector (Novagen) using the standard PCR based cloning techniques as described in the methods (Chapter 4). Protein expression in *E. coli* is a convenient, economical and rapid method for obtaining high yields of protein. Since, the pET-28 (a) expression vector is a low copy number vector, BL21 Star strains were chosen to express MDM2 gene under T7-promoter.

5.2.1. Pilot scale test expression of full-length MDM2 construct

To check the expression level of the full-length construct small-scale experiments were performed. For protein expression *E. coli* cells were grown in LB medium under suitable antibiotic selection at 37º C to an O.D of 0.7 followed by 3 hrs induction at 37º C with 1mM IPTG, as BL21 Star cells require IPTG to induce expression of the T7 RNA polymerase from the *lac*UV5 promoter. Samples for SDS PAGE analysis were taken after every hour of induction. Samples for electrophoresis were prepared by centrifuging cells and dissolving the pellet in 40µl of the 1x SDS PAGE sample-loading buffer (Material and Methods) and heated for 3 minutes. Results showed a very poor expression and hence to find out the most favourable protein expression conditions, a series of expression tests were carried out. Since the expression level was extremely poor hence, it was considered that the protein could be toxic for the cells. Host cells were then changed to BL21 (DE3) pLysS and BL21 (DE3) pLysE (Invitrogen) strains, which produce T7 lysozyme to reduce basal expression of heterologous genes and are recommended for expressing toxic proteins. Similar expression tests as mentioned above were performed in these cells, but results showed no improvement in protein expression. After various failed attempts to express full length MDM2 protein, attempts to express smaller constructs of the *Mdm2* were tried.

5.2.2. Determination of solubility of different MDM2 constructs

Various *Mdm2* gene constructs were PCR amplified and cloned into different expression vectors and their expression levels and solubilities were tested. The results obtained are shown in Table 5. For these tests the *E. coli* cells were grown and cultured as mentioned earlier. They were

harvested by centrifugation and resuspended in lysis buffer (Material and Methods). After sonication and further high speed centrifugation, 20 µl the supernatent was dissolved in 20 µl of sample buffer (material and methods) and heated for 3 min. The cell pellet was dissolved in denaturing buffer (Material and Methods) and SDS PAGE sample was prepared as above.

Figure 5.20 *Schematic representation of different MDM2 constructs made.*

There are various factors that influence protein expression and solubility a few important ones are:

- the expression vector,
- host cell,
- growth/induction conditions,
- the nutrient medium supplied,
- temperature at which the culture is grown.

Changing one or more of these factors can dramatically influence the protein expression and solubility levels. The various conditions used for optimizing protein expression and solubility of the protein are summarized in Table 6. As the protein was intended for structural studies, a high expression and biologically active form of the protein was desired. Of the many factors mentioned above, expression host is considered to be one prime aspect for protein expression and hence expresson was tried using the pQE vectors (Qiagen), which combine a powerful phage T5 promoter (recognized by *E. coli* RNA polymerase) with a double lac operator repression module to provide tightly regulated, high-level expression of recombinant proteins in *E. coli*. Basal level expression is effectively blocked in the presence of high levels of lac repressor and the stability of cytotoxic constructs is thus enhanced. Moreover the vector has an N-terminal 6xHis-tagged

Table 5 *showing expression test under various conditions*

Tags and vectors	Constructs (residues)	Expression	Solubility
His-tag; pET-28a	1-491, full length	very low	------
His-tag; pET-30 Xa/LIC	1-491, full length	low	-------
His-tag; pET-30 Xa/LIC	64-491	very low	-------
His-tag; pET-30 Xa/LIC	268-491, C-terminal	good	Insoluble
His-tag; pET-30 Xa/LIC	268-321, pRb binding region	average	Insoluble
GST-tag; pGEX 4T-2	1-491, full length	low	-------
GST-tag; pGEX 4T-2	1-400	average	-------
GST-tag; pGEX 4T-2	1-200, E2F binding domain	average	-------
GST-tag; pGEX 4T-2	268-321, pRb binding region	average	Soluble
His-tag; pQE-60	268-491,C-terminal	low	----------
His-tag; pQE-60	268-321	low	----------

and DHFR gene. DHFR-fusion proteins are recommended for expression of poorly expressed proteins as it increases the stability of the target protein translation. Since it was known that GST tag aids in fusion protein solubility, pGEX vectors under the powerful T5 promoters were also tried. Hence, *Mdm2* gene was also cloned in these vectors. Results are shown in Table 5.

In many cases overexpression of foreign proteins (eucaryotic) in *E. coli* results in insoluble inclusion bodies. Since many proteins can be successfully folded from inclusion bodies,

and as protein production in the form of inclusion bodies has a number of merits, recovery of folded and biologically active protein from inclusion body material was tried. Nevertheless, different proteins may require different conditions for renaturing; hence various refolding buffers from Hampton were tried. For detail information on protein folding refer Rudolph et al, (Rudolph and Lilie 1996).

Table 6 *showing different conditions that were tried for expression.*

Conditions	Temperature of incubation	O.D at induction	Post induction time	IPTG concentration
Control	37º C	0.8	3-4 hrs	1.0 mM
1	37º C	0.6	3-4 hrs	1.0 mM
2	37º C	1.0	3-4 hrs	1.0 mM
3	37º C	0.8	3-4 hrs	0.5 mM
4	37º C	0.8	3-4 hrs	0.1 mM
5	32º C	0.8	3-4 hrs	1.0 mM
6	26º C	0.8	5-6 hrs	1.0 mM
7	15º C	0.8	Over night	1.0 mM

5.2.3. Expression and purification of the C-terminal domain of MDM2

An attempt was made to express the C terminal domain of MDM2 for pRb binding. The C-terminal construct comprising residues 268-491 was cloned into pET 30 LIC vector. It showed good protein expression and further purification studies were performed with this construct. Most of the expressed protein was found to be in the inclusion bodies. Hence the protein was initially purified under denaturing conditions. Affinity purification was performed using the Ni-NTA column as the fusion partner was 6x His-tag. The protein was eluted using a linear pH gradient as shown in (Fig. 5.21). The results obtained were further confirmed by performing Western blot using C-terminal specific MDM2 monoclonal antibody (Fig. 5.22). Attempts were made to refold the protein using different refolding buffers. Further purification was performed using the anion exchange column, Mono Q, as the p. I. of the protein (4.5) was

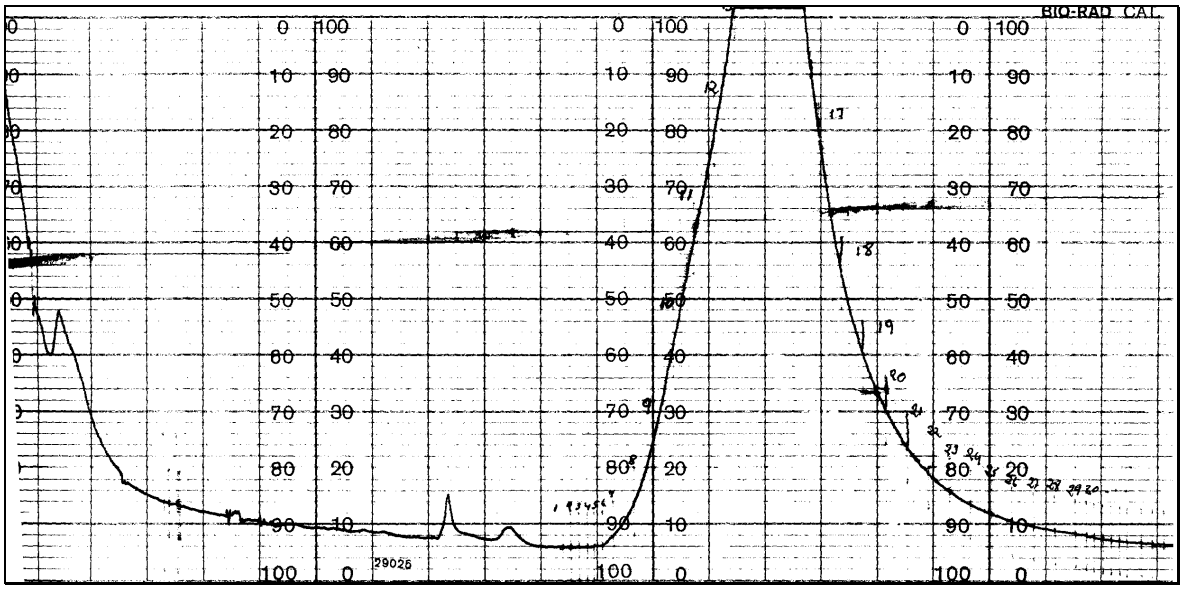

Figure 5.21 *Affinity chromatography performed with linear pH gradient. The chromatogram shows the elution profile of C-terminal MDM2 (268-491) purified as a His-tag fusion protein.*

Western blot **Affinity chormatography**

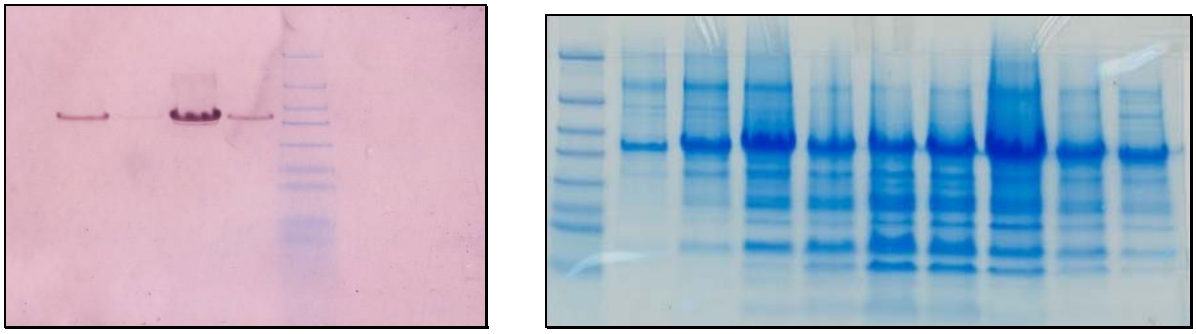

Figure 5.22 *The panel on the left Western blot analysis and SDS-PAGE analysis of the His-tag fusion protein after affinity purification is shown on right.*

less than the pH (7.3). The final protein purification was performed on the superdex 75 column, where running buffer was PBS (Material and Methods). Fig. 5.23 show the SDS-PAGE analysis results after ion exchange and gel filtration respectively. The gel filtration (Fig. 5.24) results showed that the protein was highly aggregated as the peak was obtained at around 600 kDa when compared with the standard curve at UV 280 nm. This can be explained by the fact that this domain is composed of the acidic region, the ring finger domain and the zinc finger regions along with 14 cysteines. Though zinc was added during the cell growth but no significant changes were

Ion Exchange **Gel filtration**

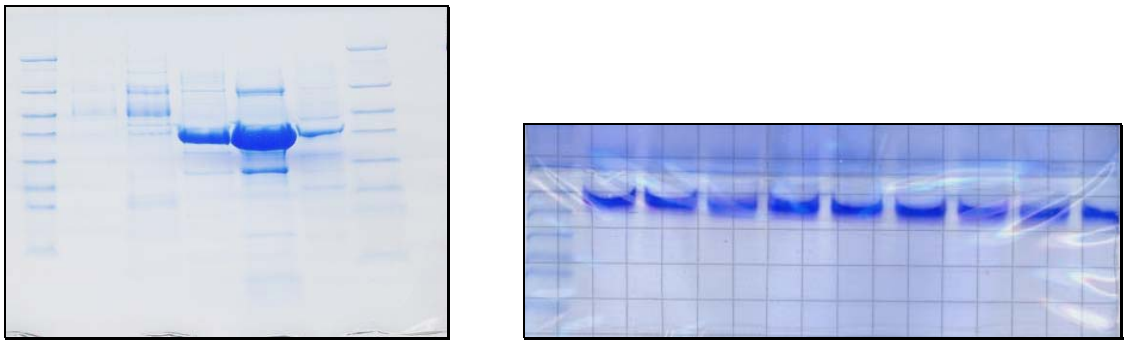

Figure 5.23 *SDS-PAGE analysis of the C terminal domain after ion excahange and size exclusion chromatography columns.*

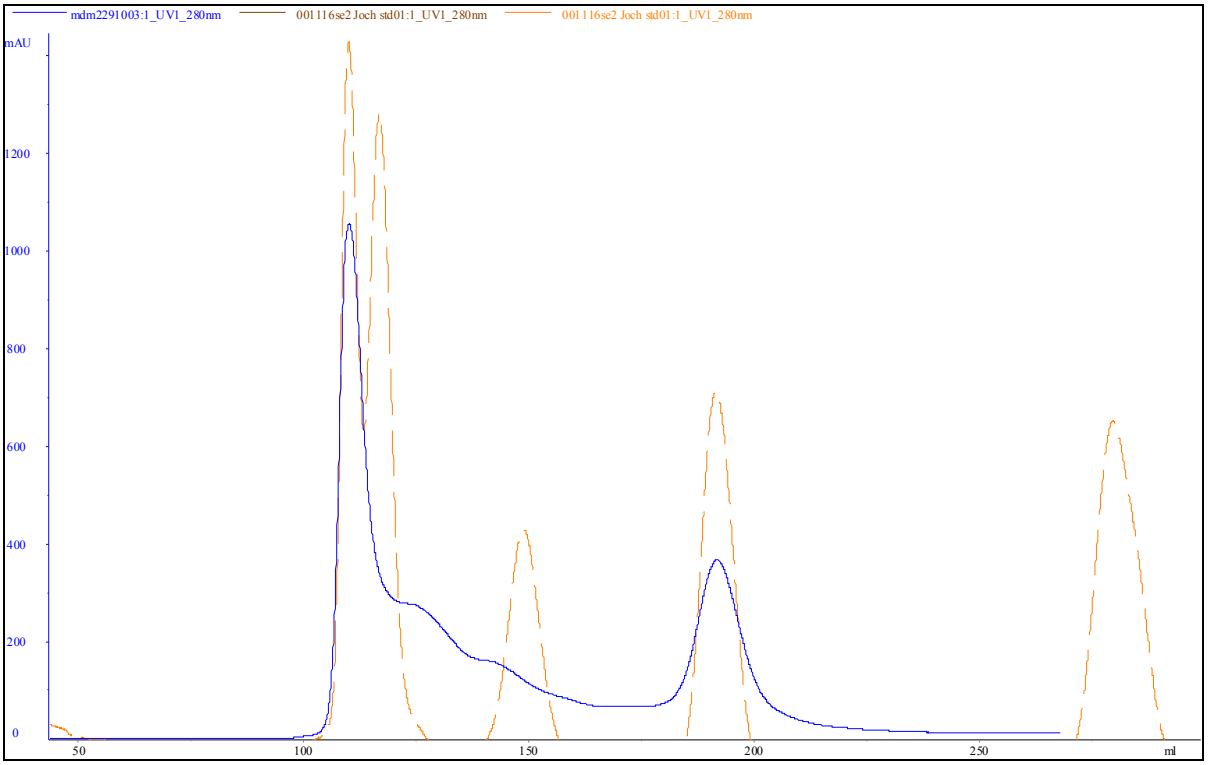

Figure 5.24 *Elution profile of the aggregated C-terminal construct.*

observed in the aggregation pattern. This region interacts with various other proteins including pRb and the absence of these partner proteins could lead to the observed aggregation. Still the protein was concentrated down for taking a 1D NMR spectrum (Fig 5.25). The spectrum shows

poor signal dispersion at the aliphatic region (between +1.0 and -1.0 ppm) and at a region from 8.3 to 11 ppm, which clearly indicated that the major portion of the protein was unfolded.

Literature studies showed that residues 272-321 were essential for MDM2 to bind to pRb. Hence, residues 268-321 was cloned in the above mentioned (Table 5) vectors of which the pET 30 LIC construct showed some positive results, although the expression was low and the protein was insoluble. Further purification was carried out under denaturing (Material and Methods) conditions but since the yields were extremely low even from a 10 L culture hence, this construct was discarded. Finally an attempt was made to co-express MDM2 and pRb so as to get a folded binary complex of these proteins

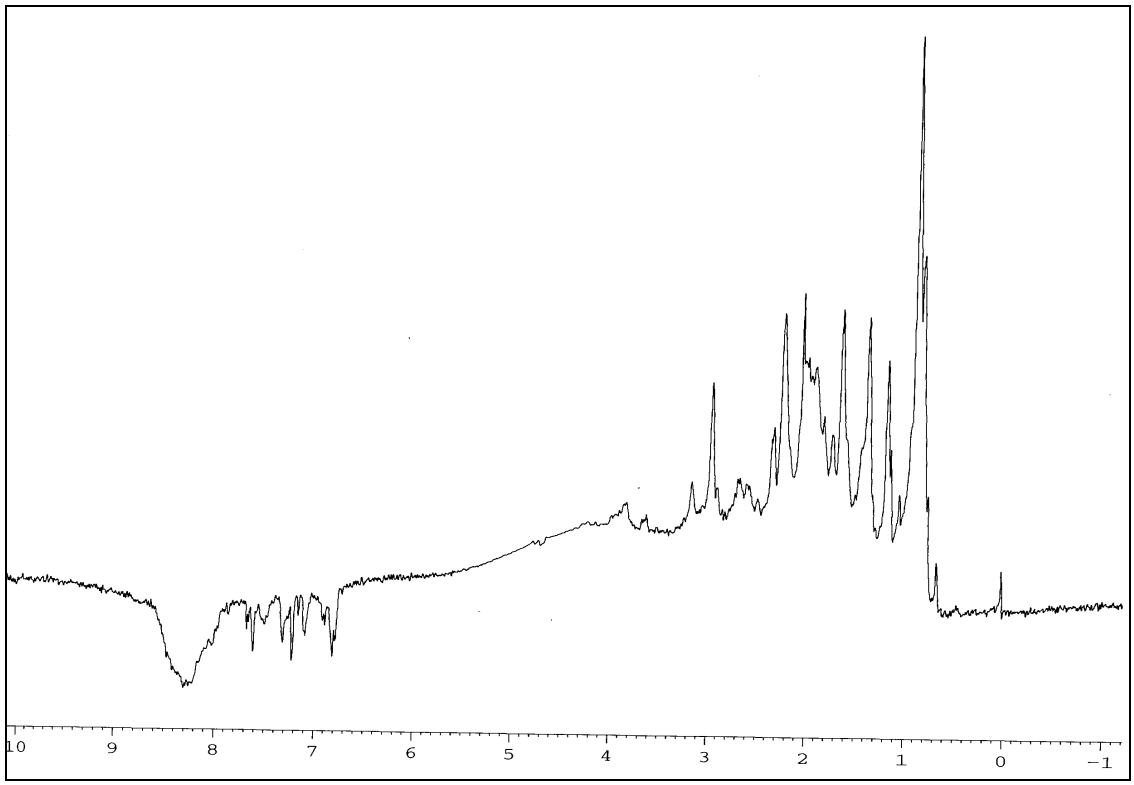

Figure 5.25 *1D NMR of the C-terminal domain of MDM2. Details in text.*

5.2.4. Co-expression tests on MDM2-pRb in *E. coli*

The next part of the study involved the application of a dual vector co-expression system for the overproduction of another tumor suppressor protein pRb and MDM2 in *E. coli*. Structural analysis of protein complexes largely depend on reconstituting the binary protein complexes from

separately prepared recombinant proteins where such a reconstitution often involves refolding of one or more of the protein components of the complex. The co-expression system has an edge in such cases since it allows for the direct preparation of binary protein complexes. Moreover, co-expression often achieves optimal yield, solubility, and activity and may protect individual subunits of the protein from degradation.

To facilitate these studies we chose the duet vectors, pACYCDuet-1 and pETDuet-1 (Novagen). Each vector carried two expression units each controlled by a T7*lac* promoter for high-level protein expression. Each promoter is followed by a ribosome binding site and multiple cloning site (MCS) region. For a convenient two vector co-expression system it is essential that the vectors for have the following characteristics:

- Both vectors are compatible with a T7-promoter/T7-polymerase protein expression system.
- Each vector has a different antibiotic resistance gene for selection.
- The two vectors have compatible origins of replication to prevent segregation and ultimate loss of one plasmid in culture.
- Both vectors have useful multiple cloning sites that are compatible with each other and facilitate the shuttling of DNA constructs between the two vectors.

The chosen vectors met all the above criteria. Co-expression system was utilized to promote the optimal protein conformation for complex formation immediately after expression. The PCR cloning was performed as mentioned in Chapter 4, but here care was taken about the multiple cloning sites and especially the restriction sites chosen, when cloning in the same vector.

Expression of proteins in *E. coli*

Colonies were picked from plates containing fresh co-transformed cells and grown in LB media under kanamycin and chloramphenicol or kanamycin and ampicillin selection at different temperatures of (37°C, 25°C, 15°C) for the MDM2-pRB complexes. At the absorbance of 0.8 at $O.D._{600}$, the cultures were induced with 1 mM IPTG and were incubated for 3-14 h depending on temperature conditions. During induction, zinc acetate and magnesium chloride were added to the cultures for better folding. Cells were harvested and checked for the solubility conditions. Western blot (Fig 5.26) was carried out with the appropriate MDM2 and pRb antibodies for construct 4.

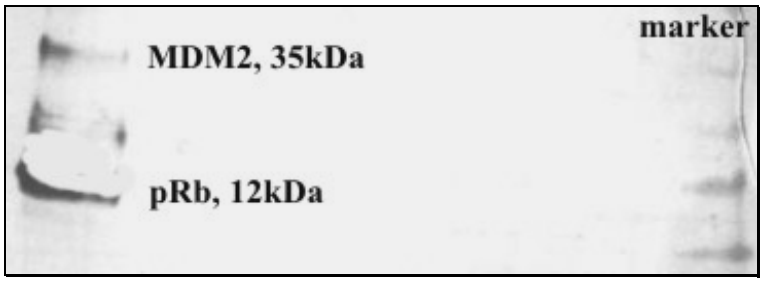

Figure 5.26 *MDM2 and pRb co-expression test in E. coli. The individual constructs were cloned in pACYDuet-1 and transformed into BL21 Star DE3. Cultures were grown at low temperature and harvested after 14 h. The cell pellet were analysed by SDS-PAGE and Western blot analysis.*

Table 7 showing the co-expression constructs

	Constructs	**Vectors**	**Expression**	***E. coli* strains**
1	MDM2 (268-491) in MCS1	pETDuet-1	none	BL21 Star DE3
	pRb (792-928) in MCS 2	pACYCDuet-1		
2	pRb (645-928) in MCS 1	pACYCDuet-1	none	BL21 Star DE3
	MDM2 (268-491)	pET 30 LIC		
Cloned in the same vector				
3	MDM2 (268-400) in MCS 1 and pRb (792-928) in MCS 2	pACYCDuet-1	poor	BL21 Star DE3
4	pRb (792-928) in MCS 1 and MDM2 (268-400) in MCS 2	pETDuet-1	low	BL21 Star DE3

For obtaining good expression under the co-expression system, both recombinant proteins should express well in bacteria. The overall expression levels of recombinant proteins during co-expression typically reduce to one half to one fourth of that of the single recombinant protein expression levels. Since expression for constructs 1 and 2 was almost negligible, as nothing could

be observed in the SDS-PAGE gels, it was assumed that such extremely low expression levels could be due to unequal plasmid copy number, hence a third construct was made where the MDM2 and pRb were cloned in the same plasmid as shown in Table 7. But still the expression levels were low. Attempts were also then made to express the protein in baculovirus expression system.

5.2.5. Expression tests in the baculovirus expression system

Since most of the *E. coli* constructs of MDM2 stated above resulted in protein aggregation or very poor protein expression it was assumed that maybe expression in insect cells would be of help. Baculovirus expression vector system (BEVS) is used to generate large quantities of recombinant protein that maintain many post-translational modifications (N- and O-linked glycosylation, phosphorylation, acylation, amidation, carboxymethylation, isoprenylation, signal peptide cleavage and proteolytic cleavage) and functional activity. The system is based on the ability of the baculovirus to infect and multiply in cultured insect cells. A variety of insect cell lines are susceptible to infection with the AcNPV baculovirus. The cell lines used here were the *Sf9* cells, originally established from ovarian tissues of *Spodoptera frugiperda* larvae. The protocols were followed as described in O'Reilly et al. (1994). The full length MDM2 gene was cloned in the baculo gold pBlueBacHis2 vector (BD Biosciences) in between the restriction sites BamHI and EcoRI. The *Sf9* cells were grown to a count of 2 million/ml and infected with 10 ml of the high viral titer (0.05×10^{-3}/ml) for 1liter culture. 1ml samples for SDS PAGE were taken after 0, 24, 37, 49, 54 h post infection. Results showed no improvement in protein expression.

5.3. Studies undertaken on different IGFBPs' constructs

In order to commence structural investigations on IGFBPs, large quantities of well folded, functionally active protein is the basic need but the intrinsic properties of IGFBPs, such as 30% of the protein being intrinsically unstructured, having one of the most disulfide rich folded domains, and rapid aggregation of IGFs have made these proteins difficult for structural studies. The various IGFBPs (IGFBP-3, -4, -5, -6) gene were constructed in pET-28 (a) vector (Novagen) as shown in Fig. 5.27 using the standard PCR based cloning techniques as described in the methods (Chapter 4). The protein expression was performed in BL21 Star DE3 strains. The different constructs expressed are assembled in a tabular form in Table 8. Mutants were also

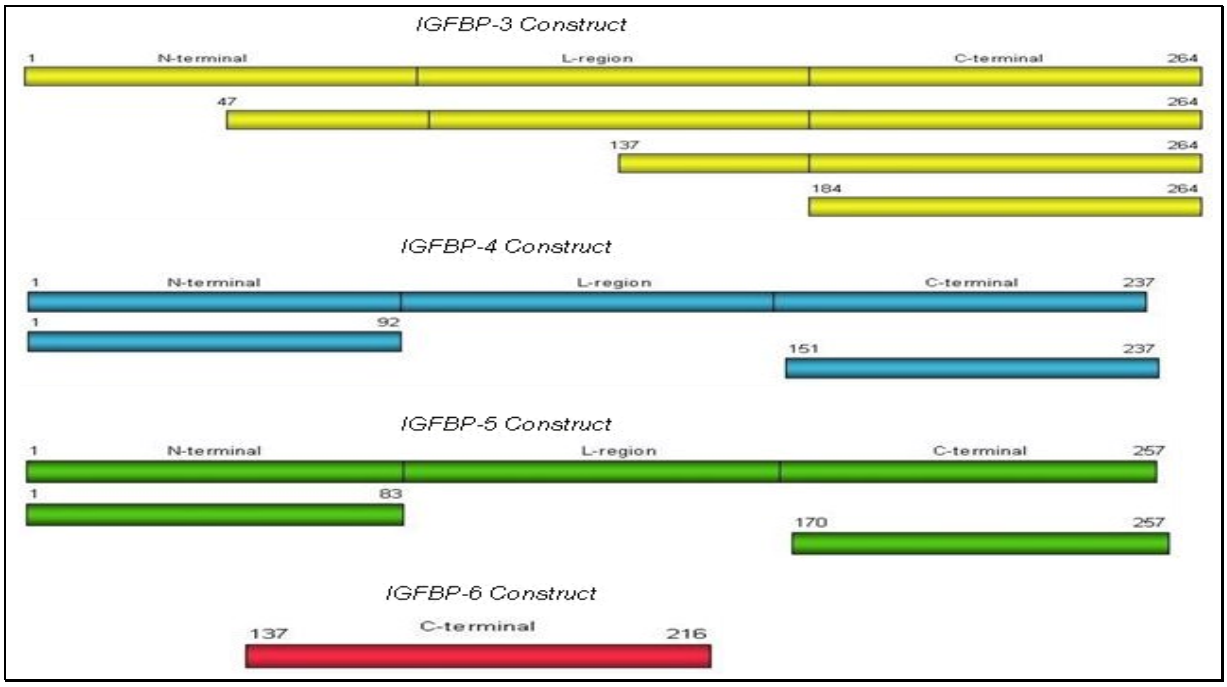

Figure 5.27 *Schematic representation of different MDM2 constructs made.*

Table 8 *Different IGFBP constructs made*

	Residues	**Expression**	**Solubility**
IGFBP-3	47-264	High	Insoluble
IGFBP-3 longer C terminal	137-264	High	Insoluble
IGFBP-3 C terminal	184-264	Very low	Insoluble
IGFBP-4 (full)	3-237	High	Insoluble
IGFBP-5 (mini)	40-92	High	Insoluble
IGFBP-5 (mini) Mutant	40-92 (L73>M)	High	Insoluble
IGFBP-5 (mini) Mutant	40-92 (L73>Y)	High	Insoluble
IGFBP-6 C terminal	137-216	High	Insoluble

constructed are also shown in table 8. The proteins were expressed as inclusion bodies and functionally active protein were obtained on refolding the denatured form in a refolding buffer at a dilution of 1:50. Figs. 5.28-5.31 show the various steps of the IGFBP protein purification (the procedure is explained in detail in Material and Methods). The purified proteins then were used for various structural and biochemical studies including X-ray crystallography, NMR, ITC and proteolytic studies to give better insights to the binding of IGFs to IGFBPs and to understand the control of IGFBPs by proteases.

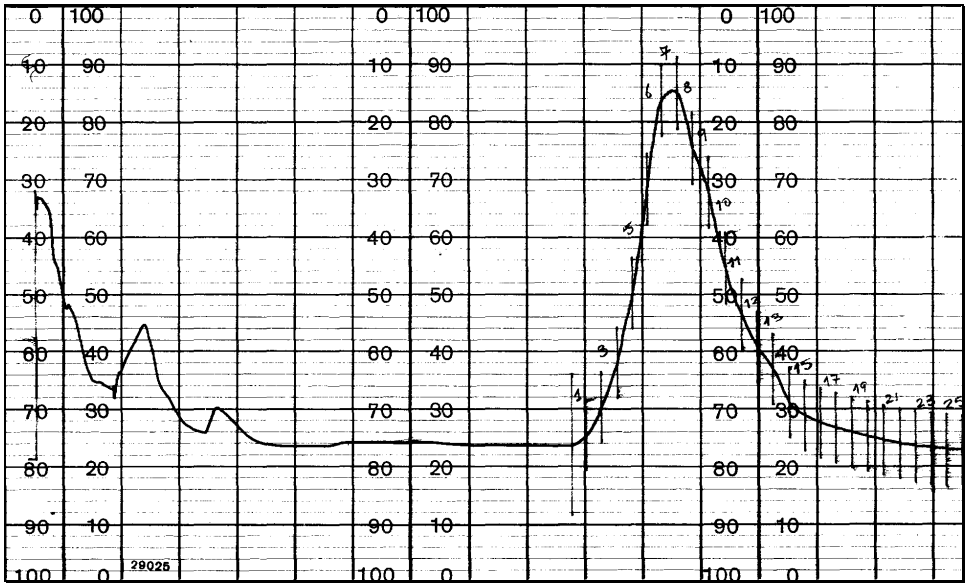

Figure 5.28 *Affinity chromatography performed with a linear pH gradient. Since the protein was purified from inclusion bodies, the affinity chromatography was performed under denaturing conditions of 6M guanidinium chloride. The Ni-NTA binding was also performed in 6 M lysis buffer.The chromatogram shows the elution profile of IGFBP-4 purified as a His-tag fusion protein.*

Affinity Chromatography

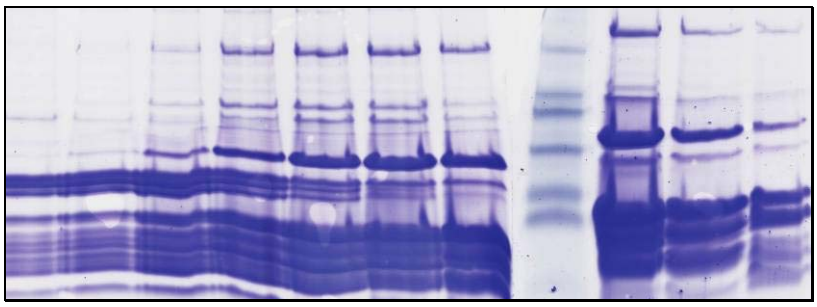

Figure 5.29 *SDS-PAGE showing affinity purified His-tag fused IGFBP-4.*

Ion exchange chromatography **Size exclusion chromatography**

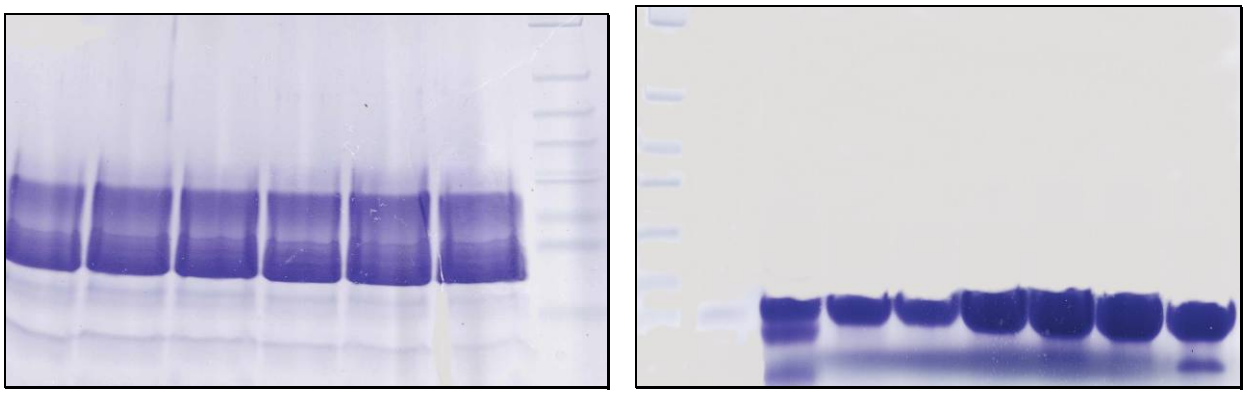

Figure 5.30 *Gel electrophoresis results of the mini-IGFBP-5 after ion exchange chromatography. The right panel shows SDS-PAGE after gelfiltration of mini IGFBP-5 mutant in Superdex 75 column.*

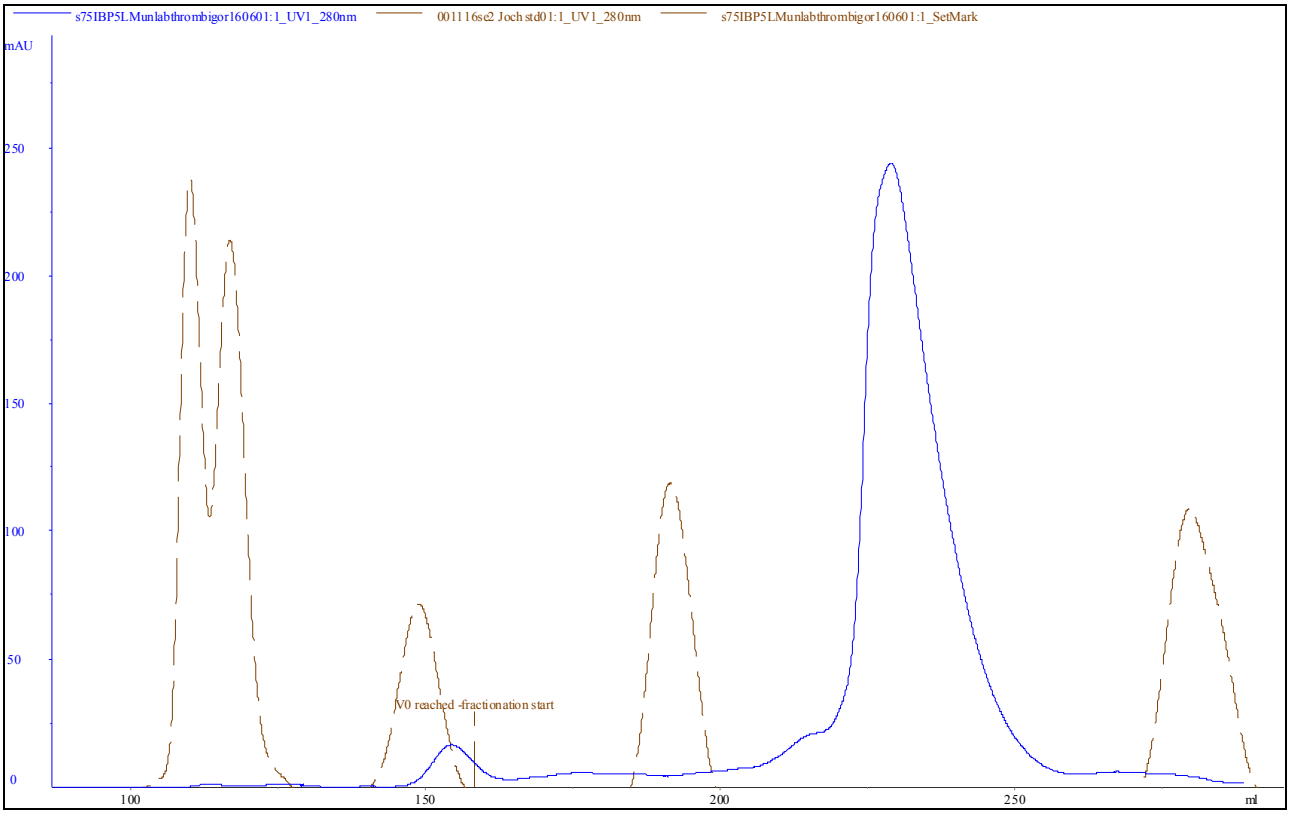

Figure 5.31 *Elution profile of mini IGFBP-5 mutant (L>M) after size exclusion chromatography.The brown peaks are the standard protein weight elution peaks and the blue peaks obtained is of mini IGFBP-5 mutant.*

5.3.1. Molecular architecture of IGFBPs

The two well-defined domains of IGFBPs, amino-and carboxy-terminal, form together a high-affinity IGF binding site, but their relative contribution to the binding affinity varies among one-dimensional ^{1}H NMR spectra of the full length IGFBP-4 and –5 and their isolated N- and C-domains. Inspection of such spectra yields semi-quantitative information on the extent of folding in partially structured proteins or their domains (Rehm et al. 2002). The spectra of full-length IGFBP-3, -4, and -5 exhibit a substantial peak at 8.3 ppm and some signals downfield close to the noise level. The appearance of intensities at chemical shifts near ~8.3 ppm is an indicator for a disordered protein, as this is a region characteristic of backbone amides in random coil IGFBPs. To gain a more detailed understanding of the IGFBPs domain organization and structural requirements for binding to IGFs, the inter- and intra-domain arrangement and the extent of folding within domains of IGFBP-4, -5 and –6 was studied by NMR. Also the structure of the complex of the N-terminal domain of IGFBP-4 (NBP-4, residues, 1-92) and IGF-I was determined. This structure underscores a critical role of the first amino-terminal residues of IGFBPs for IGF signaling. Whereas the IGFBPs anchor IGF primarily using residues 40-50, residues 1-6 prevent access of the IGF-I receptor to IGF-I through steric hindrance.

5.3.1.1. Domain organization of IGFBPs and the determination of exact domain boundaries

Distinct regions of amino acid sequence homology suggest that all IGFBPs consist of three domains of approximately equal lengths. The amino- and carboxyl-termini domains are highly conserved and contain 16-18 spatially conserved cysteine residues. Figure 5.32 shows configuration (Wuthrich et al. 1984). On the other hand large signal dispersion beyond 8.3 ppm proves a protein to be folded. Due to the different chemical environment and thus the varying shielding effects the resonances of the single protons will be distributed over a wide range of frequencies. A typical intensity pattern of a folded protein can be observed in spectra of the N-terminal domain of IGFBP-4 (residues 1-92) and IGFBP-5 (residues 1-83). The spectra of the C-terminal fragments, CBP-4 (151-232) and CBP-5 (170-247) indicate that there are some unstructured regions located also in the C-terminal fragments. Based on these spectra we concluded that the whole central variable domain of IGFBP-4 and -5 is in a random coil conformation. The amide region of a 1D spectrum of the full length IGFBP-3 obtained from

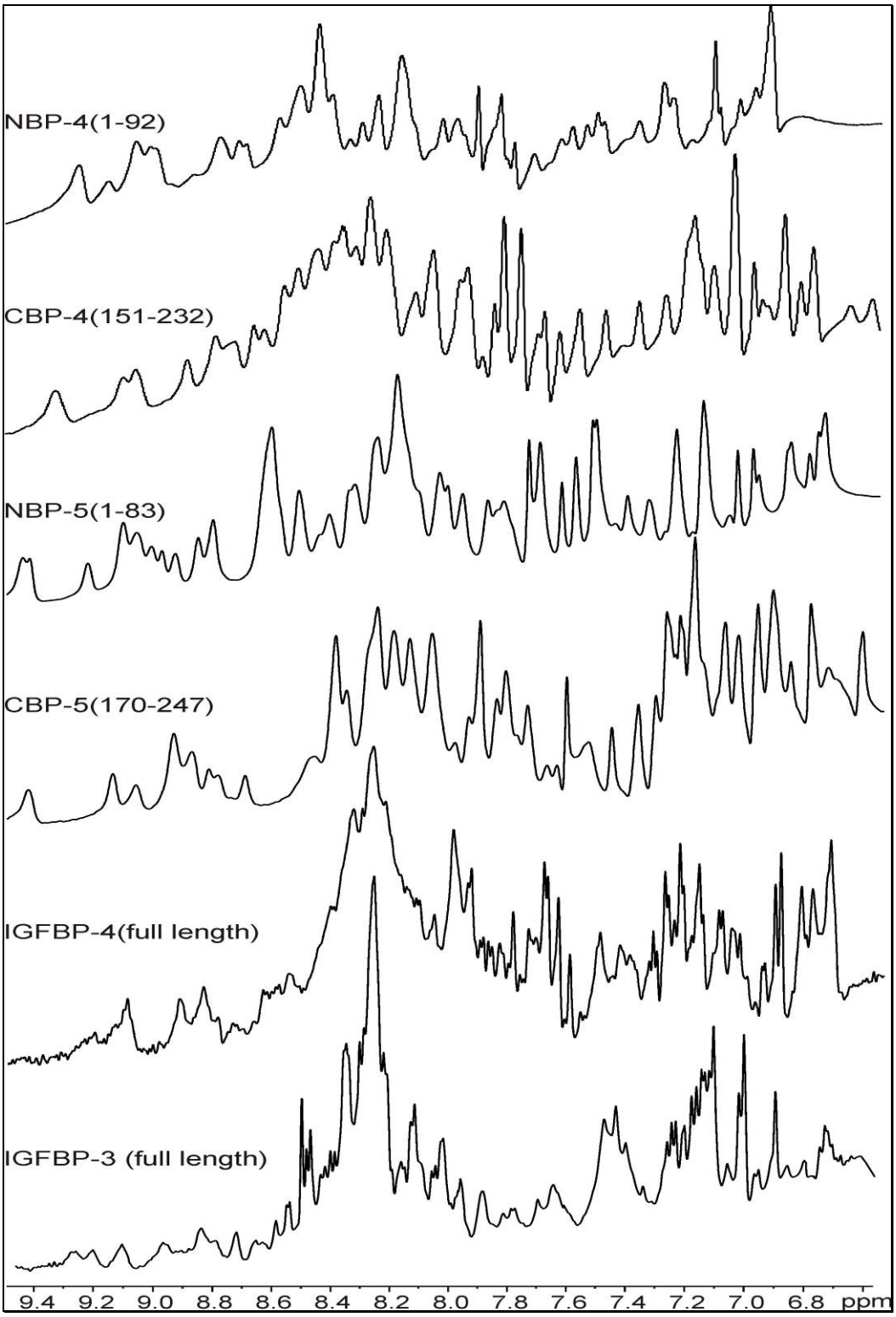

Figure 5.32 *The amide region of ^{1}H NMR spectra of the isolated domains and intact recombinant IGFBP-4 and –5. The spectrum of the human cell culture derived IGFBP-3 is included as a reference for the native protein (bottom).*

human cell cultures is also shown to compare its extent of folding to that of the artificially refolded proteins. Thus the properties of IGFBPs are the same whether expressed in *E. coli* or in the mammalian expression system.

The N-terminal domain, NBP-4, can be divided into two subdomains: the fragment from residues Asp1-Cys39 and the segment Met44-Glu90. The latter can exist autonomously and corresponds approximately to the mini-IGFBP-5 described by Kalus et al. (1998). The two subdomains are connected by a short stretch of amino acids: Ala, Leu, Gly, Leu, and Gly. The NMR ^{15}N relaxation measurements of molecular motions in uncomplexed (^{15}N-Gly, ^{15}N-Leu)-labeled NBP-4 showed only one peak below the threshold level of 0.6, indicating that the linker stretch is rigid. The one peak can be assigned with high probability to Gly56 present in a loop known from mini-NBP-5 NMR studies to be flexible.

5.3.1.2. Optimization of the C-terminal construct of IGFBP-4

1D NMR experiments revealed that the COOH-terminal fragments of IGFBP-4, -5 contained disordered polypeptide fragments. Such flexible sections of proteins are known to inhibit crystallization or result in crystals of low quality. Assuming that the disordered regions are most likely to occur within the longest stretches of amino acids between cysteines of disulfide bridges, we designed four deletion mutants. The deletions spanned different lengths of polypeptide chains and were localized either between Cys153 and Cys183: CBP-4Δ(Gln168-Asp174) and CBP-4Δ(Ser167-Ile178), or Cys207 and Cys228: CBP-4Δ(Leu216-Lys223) and CBP-4Δ(Gly213-Glu225). The four mutants did no exhibit any improvement in the extent of folding over the wild type proteins, as determined by ^{15}N–HSQC spectra of the ^{15}N-labeled mutant proteins. On the contrary, determinants of unstructured regions were more pronounced, more so in the case of both longer deletion mutants**.** The inability of these constructs to form stable IGF-I/NBP-4/del-CBP-4 ternary complexes, as demonstrated by analytical gel filtration chromatography of the protein mixture indicated that either the global fold was disrupted by these deletions or/and residues important for IGF-I-binding were removed.

5.3.1.3. Binding among domains of IGFBP-4 and IGF as studied with isothermal titration calorimetry and NMR

ITC measurements showed that the amino- and carboxyl-terminal domains of IGFBPs

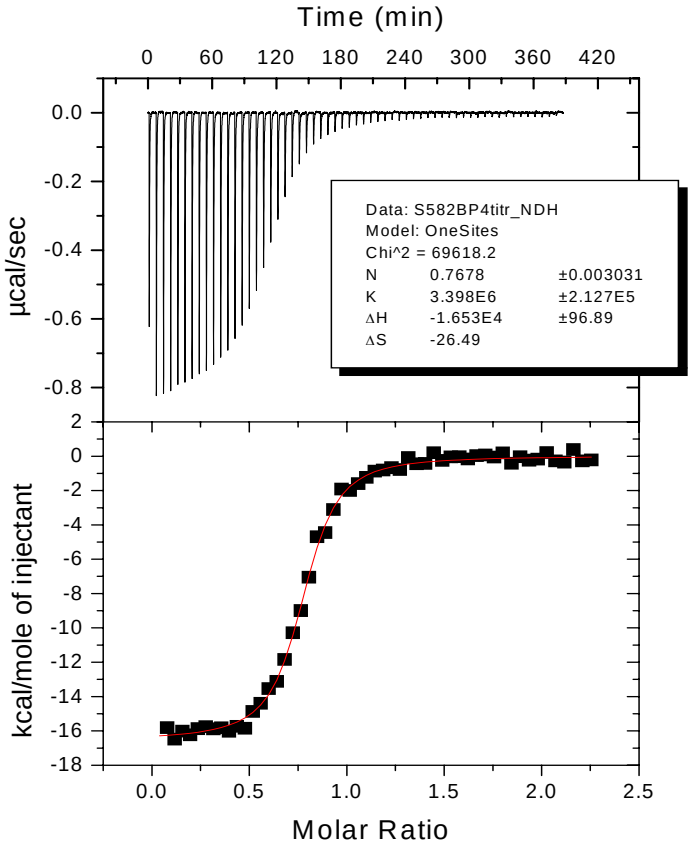

Figure 5.33 *ITC data shows N-terminal (1-82) IGFBP4 in complex with IGF. The K_D calculated to be 294±19.*

cooperate to form a high affinity IGF-I complex: a 3-6 times tighter binding to IGF is observed in the presence of the C-terminal domain. Fig. 5.33 shows the results of N.terminal IGFBP-4 titaration with IGF-I. No direct binding between CBP-4 and NBP-4 (and CBP-4 and IGF-I) could be detected. In order to exclude any interaction that could be weak (Rehm et al. 2002), these interactions were tested by NMR using ^{15}N labeled CBP-4 or NBP-4. Addition of CBP-4 did not cause any changes in the ^{15}N–HSQC spectrum of ^{15}N labeled NBP-4, proving no interaction. In a similar manner, addition of IGF-I to ^{15}N-CBP-4 had no effect on the ^{15}N HSQC. Ligand binding–induced folding of partially unstructured proteins and peptides is an often-observed phenomenon. The experiments described above did not reveal such a behavior for CBP-4: no cross peaks emerged from the ^{1}H 8.3-ppm spectral region after NBP-4/IGF-I addition. Similarly, 1-D spectra of full-length IGFBP-4/IGF-I complex do not show any improvement in terms of folding over free IGFBP-4. These experiments show that neither carboxyl-terminal unstructured regions nor

the linker domain are influenced by the complex formation, and the overall folding pattern of IGFBP-4 is unaffected by IGF-I binding.

5.3.1.4. Fine-tuning of the "Thumb"

Extreme-amino terminal residues of IGFBPs had been neglected in all carried to date mutagenesis studies aiming at delineation of the proteins' structure/function relationships (Clemmons, 2001). To assess contribution of the "thumb" region of IGFBP (which are the hydrophobic residues Ala 3 and Ile 4 of the N-terminus) to its IGF-I binding activity, we have produced a number of N-terminal mutants of NBP-4 and compared their IGF-I binding activity using isothermal titration calorimetry (Table 9). The differences in the K_D values among the constructs, although not substantial, show that the extra contacts made by the "thumb" residues do influence the strength of IGF-I binding.

Table 9. List of NBP-4 constructs, their sequences and IGF-I binding constants

Name	N-terminal sequence	Kd [nM]
NBP-4(1-82)	**D E A I H C**	294±19
NBP-4(3-82)	**A I H C**	865±78
NBP-4(6-82)	**G C**	3350±590
BP1-NBP-4	**A P W H C**	544±45
BP3-NBP4	**G A S S G G L G P V V H C**	268±14

5.3.1.5. Characterization of the thumbs' microenvironment in the IGFBP/IGF-I complex using fluorescence spectroscopy

The mutant BP1-NBP-4 was constructed, with the N-terminal residues Ala, Ile and Trp mimicking the thumb region of IGFBP-1, in order to investigate its influence on the IGF-I binding action. Incorporation of the tryptophan residue within the thumb enabled us also to monitor changes in its microenvironment related to the complex formation with IGF-I and CBP-4. Extreme variability of the emission of the indole fluorophore, depending on polarity and mobility of its environment, makes tryptophan fluorescence a sensitive tool in protein analysis.

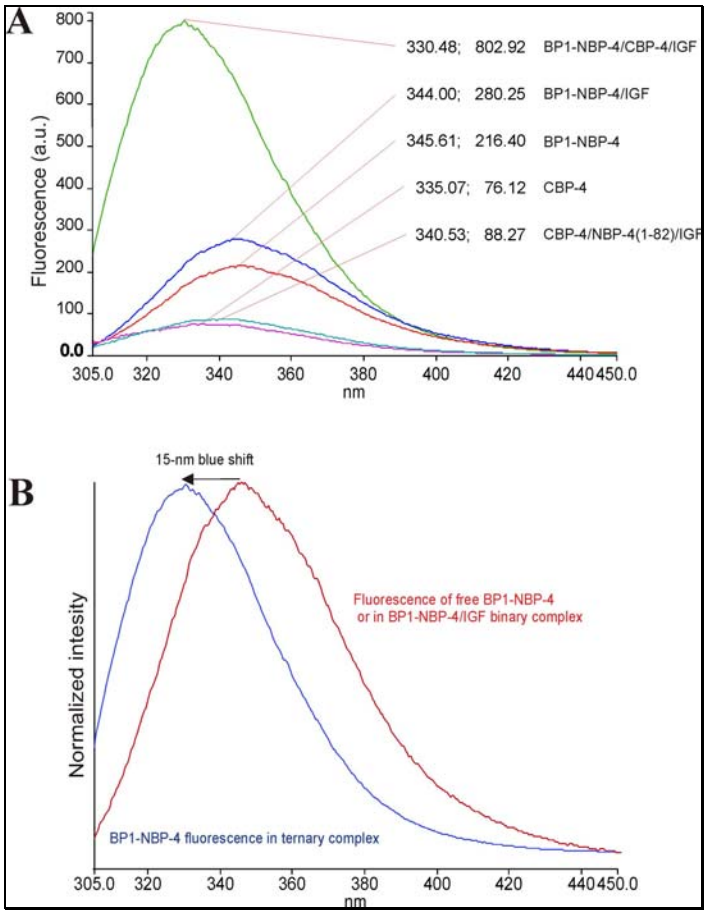

Figure 5.34 *Fluorescence spectra of the tryptophan residue of N- and C- terminal IGFBP-4.*

The position of the maximum of the fluorescence spectrum of tryptophan residues in proteins varies from 307 to 350 nm. According to the model of discrete states of (Burstein et al. 1973) there are five most probable spectral forms of tryptophan residues: Spectral forms A and S correspond to the emission of the indole chromophore in the extremely nonpolar environment inside the protein globule. Spectral form I corresponds to the emission of the chromophore in the somewhat polar but rigid environment inside the protein globule, forming a 2:1 exciplex (complex in an excited state) with two neighboring polar moieties. The fluorescence spectrum of class I has a maximum at about 330 nm, width of ca. 50 nm. Spectrum of class II corresponds to the emission of tryptophan at the protein surface, in contact with bound water and other polar groups. The position of the maximum is at ca. 340 nm and the width is ca. 55 nm. Spectral form III is characteristic for the indole chromophore at the protein surface in contact with free water molecules. The spectrum of class III, with its maximum at about 350 nm and width of ca. 60 nm,

nearly coincides with the spectrum of free tryptophan. Tryptophan residues of spectral class III very seldom occur in the native proteins, but are typical for unfolded states.

The fluorescence spectrum of Trp 3 in BP1-NBP-4, with its maximum at 345 nm and width of about 57 nm, falls between spectral classes II and III. Trp3 can be therefore categorized as a solvent-exposed residue, in contact with bound as well as free water molecules. Binding of IGF does not change spectral characteristics of Trp 3 (Fig 5.34 A). The slight increase in fluorescence intensity can be explained either by resonance energy transfer from IGF tyrosine residues or by partial shielding of the indole from water molecules. Trp 206 of CBP-4, with its emission peak at 340 nm, shows properties of an indole moiety at the protein surface. The observed low intensity of fluorescence emission can be explained by quenching by side chains of amino acid residues present in the microenvironment of Trp 206. Sulfur atoms of disulfide bonds are known as effective quenchers of tryptophan fluorescence. Cys 205 and Cys 207 are close neighbors of Trp 206 in the backbone. Nonetheless, as the side chains of two neighbor residues are oriented in opposite directions from the backbone, the distances between the sulfur atoms of disulfide bond Cys 205-Cys 194 and Cys 207-Cys 228 and the indole ring of Trp 206 are too large to influence tryptophane fluorescence (>5 Å). Other potential Trp206 fluorescence quenchers are Gln 139 and His 141.Binding of NBP4 (1-82)/IGF-I complex shifts the Trp206 emission peak maximum ca. 5 nm into the shorter wave region, further quenching can be observed (Fig. 5.32 A). We assume therefore that contribution of C-terminal Trp206 to the fluorescence of the BP1-NBP-4/CBP-4/IGF-I ternary complex is negligible due to the significant quenching of its fluorescence observed in the NBP4(1-82)/CBP-4/IGF-I complex. The fluorescence spectrum of BP1-NBP-4/CBP-4/IGF-I is corrected for the Trp206 fluorescence in the NBP4 (1-82)/CBP-4/IGF-I ternary complex. When CBP-4 joins the BP1-NBP4/IGF-I binary complex, drastic changes in the emission properties of Trp3 are observed. There is a 3-fold increase in fluorescence intensity accompanied by a 15 nm blue shift of the peak maximum. The spectrum is a model class I spectrum, with maximum at 330 nm and width 50 nm (Fig. 5.34 B), and is characteristic for a buried residue. Tryptophan fluorescence is susceptible to the quenching by water that leads to decrease in quantum yield when tryptophan becomes exposed to an aqueous environment. The increase in fluorescence of Trp3 upon CBP-4 binding can be attributed to the burying of the residue in a water-free microenvironment.

5.3.1.6. Discussion

On the basis of 1D NMR spectra of the full length IGFBP-4 and –5 and their N- and C-domains we can conclude that their whole central variable domain is in a random coil conformation, while the first ca. 90 amino acids from the N-terminus form a folded structure. The spectra of the C-terminal fragments indicate presence of disordered regions also within the carboxyl-domains. Addition of IGF and formation of binary complex has no influence on the folding extent either in the linker region or in the C-domain alone.

The amino-terminal third of IGFBP-4 can be further divided into two subdomains: the fragment from residues Asp 1-Cys 39 and the segment Met 44-Glu 90, joined by a short, glycine rich linker. Each of the subdomains has its own system of disulfide bridges reinforcing their folds and theoretically assuring autonomous existence. Thus according to these findings the N-terminal domain can be viewed as a globular base, corresponding to miniBP-5 that contains the primary IGF binding site, with an extended, inflexible "palm" completed with a hydrophobic "thumb" (Ala 3, Ile 4) attached to it. The thumb interacts with IGF residues Phe 23, Tyr 24 and Phe 25 upon complex formation. The palm, even though it is noticeably flat, is rigid. This is assured by the presence of four disulphide bonds arranged in one plane, in a ladder-like manner. The palm is unable to move or rotate significantly in respect to the base due to the H-bonding inter-subdomain interactions.

The high degree of rigidity characterizing the N-terminal domain of IGFBP may be of significance when the competition with IGF-IR for IGF binding is concerned. Previous studies revealed that Phe 23, Tyr 24 and Ph e25 of IGF-I and corresponding Phe 26, Ty 27 and Phe 28 of IGF-II are important for binding to insulin and IGF-type I receptors (Cascieri et al. 1988; Bayne et al. 1990; Bach et al. 1993; Cascieri and Bayne 1993; Hodgson et al. 1996; Hashimoto et al. 1997). To displace the hydrophobic thumb that covers the primary IGF-IR binding site of IGF-I (Phe 23-Phe 25), the receptor has to lift the rest of the N-terminal domain, which is bound on the opposite side of the IGF-I molecule, and does not prevent receptor binding on its own (Kalus et al. 1998). Thus, the thumb does not have to significantly contribute to the overall binding affinity of IGFBPs for IGFs. This mechanism is expected to be shared by all IGFBPs given the conserved arrangement of the N-terminal cysteine residues and the consensus presence of 2 hydrophobic residues at positions –2 and –3 with respect to the first N-terminal Cys residue.

The experiment utilizing Trp3 of BP1-NBP-4 as an intrinsic fluorescence probe shows that upon C-terminal domain binding to the NBP-4/IGF-I binary complex, microenvironment of the tryptophan significantly changes its character. Formation of the IGFBP/IGF-I complex leads to the enclosure of the thumb residues into a rigid, water free core. To exclude water from the Trp3 microenvironment, the interacting molecules must show high degree of surface complementarity in the immediate vicinity of the thumb. The experiments prove that the two domains of IGFBP cooperate to block the primary IGF-IR binding site of IGF-I: the thumb is pressed firmly into the Phe23-Tyr24-Phe25 pocket with the aid of the palm, while C-terminal domain reinforces the interaction with the hydrophobic path, covering it further.

Knowledge of the novel structural determinants of the IGF binding places at our disposal a means (makes more feasible) to regulate the actions of the IGFs. This can be done either by site-directed mutagenesis, producing IGFBPs of modified binding affinity, or design of novel, low molecular weight ligands.

5.3.2. Pattern of proteolytic cleavage of IGFBPs by μ-calpain

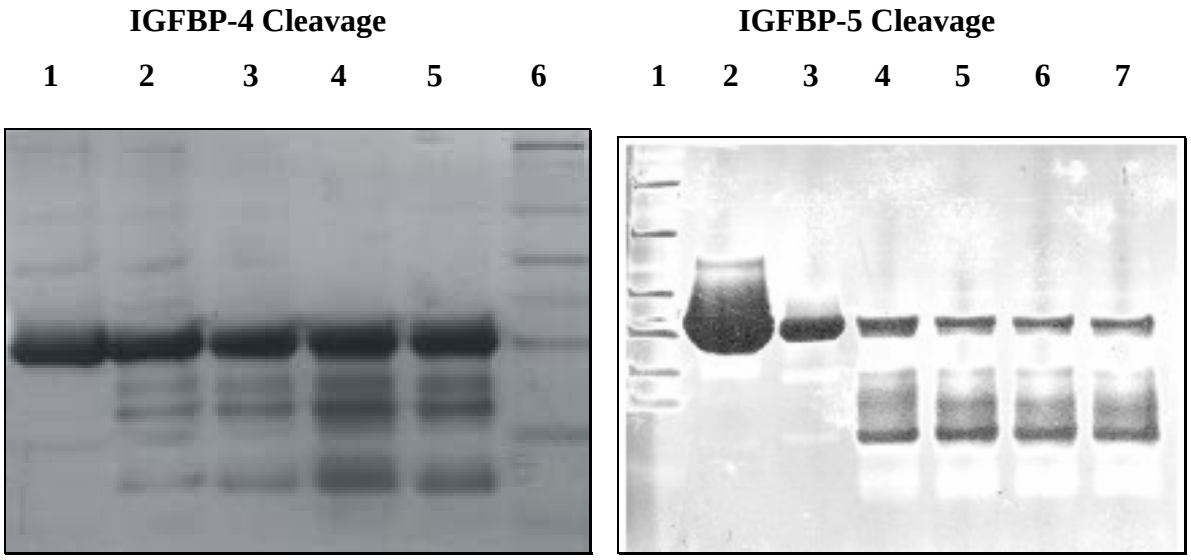

Figure 5.35 *The panel on the left shows SDS-PAGE analysis of IGFBP-4 proteolysis by μ-calpain. Lane 1 contains aliquots of the undigested protein as the control. Lanes 2-5 contain aliquots of the digestion reaction of IGFBP-4 cleavage at different calpain concentrations (20 nM, 50 nM, 100 nM, and 250 nM) in the calpain reaction buffer. Lane 6 shows the prestained molecular weight protein marker (kDa).Panel on right depicts SDS-PAGE analysis of IGFBP-5 digested by μ-calpain. Lane 1 shows the prestained marker. Lane 2 consists of the undigested IGFBP-5 protein. Lanes 3-7 show IGFBP-5 cleavage at different time*

intervals of 0 min, 30 min, 1 h, 2 h, 4h, respectively, at a constant calpain concentration of 20 nM in the calpain reaction buffer. IGFBP-4 is a 28 kDa protein and IGFBP-5 is 28.5 kDa in molecular weight.

The SDS-PAGE analysis of the in vitro assay clearly showed that there were calpain cleavage sites in both IGFBP-4 and IGFBP-5 and both proteins were rapidly cleaved into smaller fragments (Fig. 5.35). For 1000 nM of IGFBPs as little as 20 nM of μ-calpain was sufficient to induce cleavage and further increase in concentrations of the protease up to 250 nM did not result in any change in the cleavage pattern. Also there was no change observed with increasing time: cleavage patterns obtained within the first 30 min,. were the same as those obtained after 4 h. This was expected as calpain is an autolytic enzyme (Li et al. 2002) and autolyses within the first 30 min. which results in the protease activation but increased time interval does not result in any extra cleavage sites which shows calpain mediated proteolysis is limited. The protein stability assays showed that the proteins were stable and did not degrade at room temperature for up to 48 h, as shown in Fig. 5.36.

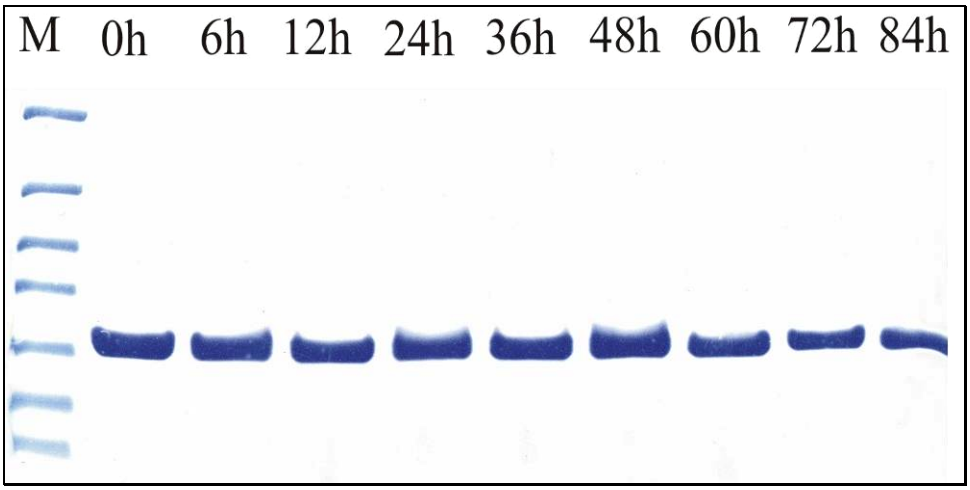

Figure 5.36 *IGFBP stability gel showing the protein at different time intervals. Lane M shows the prestained molecular weight protein marker (kDa) and the remaining lanes contain aliquots of the protein at different time intervals. The protein remains stable even after 3 days.*

5.3.2.1. Calpastatin inhibitory assay

Fig. 5.37 shows the results of the inhibitory assay of the endogenous proteinous inhibitor of calpains, calpastatin. Calpastatin efficiently blocked the cleavage of both IGFBP-4 and

IGFBP-5 as no cleavage fragments of the proteins were observed. Domain I of calpastatin was chosen for the pupose as it posses the best ability to inhibit μ or m-calpain as compared to other domains. This result clearly indicated that the cleavage pattern observed was entirely due to calpain and not to any other contaminating protease. Also no cleavage was observed in the absence of calcium, in agreement with the fact that calcium is necessary to induce the autocatalytic activity of calpain, which results in the formation of the functional catalytic domain. Fig. 5.37 (right panel) shows the Western blot analysis of IGFBP cleavage products after digestion with μ-calpain.

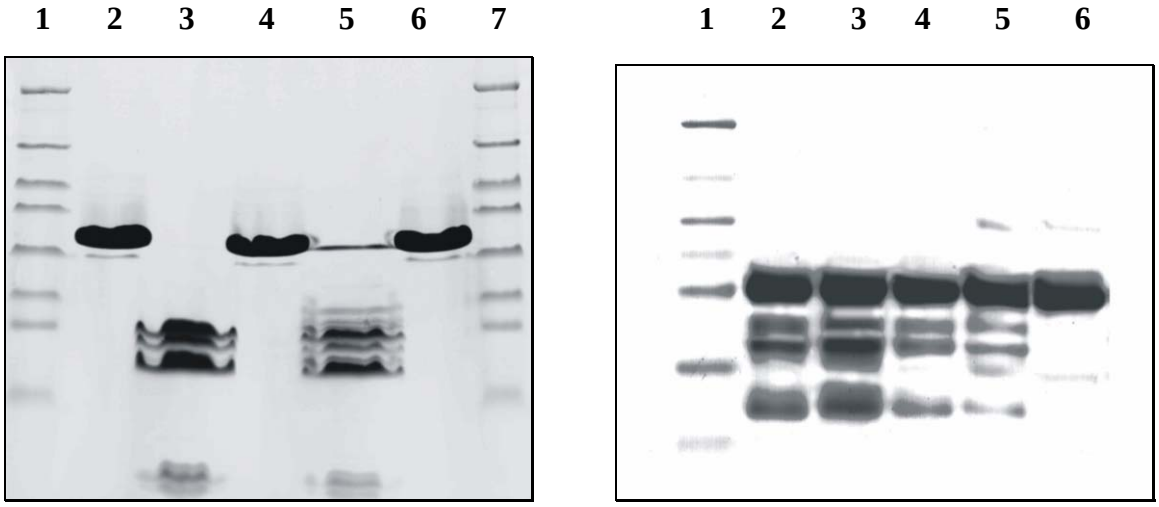

Figure 5.37 *Panel on the left shows calpastatin inhibitory and Ca^{2+}-dependent protease assay.Lane 1 and 7 show the molecular weight protein marker. Lane 2 shows IGFBP protein the protease, μ-calpain and calpastatin in the absence of Ca^{2+} where no cleavage occurs. Lanes 3 and 5 contain aliquots of IGFBP-4 and IGFBP-5 respectively digested with μ-calpain in the absence of calpastatin and supplemented with 1mM of Ca^{2+}. Lanes 4 and 6 show the inhibition of the IGFBP-4 and 5 cleavages by μ-calpain in the presence of calpastatin at molar concentrations of 1: 1 with calpain. The right hand panel shows Western blot of IGFBP fragments generated by μ-calpain protease cleavage. IGFBP digested with calpain was resolved on SDS-PAGE and transferred onto the nitrocellulose membrane. Cleaved fragments of IGFBP were detected by immunoassaying with IGFBP polyclonal antibodies. Lane 1 shows the prestained marker. Lanes 2-5 highlight the cleavage products of IGFBP. Lane 6 consists of the undigested IGFBP protein as control.*

5.3.2.2. NH_2-terminal sequencing

Characterization of the cleavage sites was accomplished by subjecting the proteolytic products to the NH_2-terminal sequencing by Edman degradation. The amino acid sequences

obtained for IGFBP-4 were: GSSHH, A_3IHC, M_{73}HGQG, A_{87}IQESL, A_{123}KIR, and G_{139}APR. Exact molecular weights of the isolated fragments were determined by MALDI-MS. Similarly for IGFBP-5, the amino acid sequences obtained from the N-terminal sequencing were S_3FVH, C_8EPCD, Q_{142}SKFV and A_{153}HPRI. The results of the generated fragments from the PVDF analysis and the reverse phase HPLC were mapped onto the IGFBP-4 and IGFBP-5 sequences and all the theoretically possible cleavage fragments for both IGFBPs were simulated.

5.3.2.3. Mass spectrometry

Mass spectrometry showed that fragments of the following sizes were generated for IGFBP-4: 14.75 kDa, 13.10 kDa, 11.01 kDa, and 10.90 kDa, 4.10 kDa, 2.45 kDa (Fig. 5.38 A). For IGFBP-5, fragments of 15.69 kDa, 16.81 kDa, 12.70 kDa and 11.60 kDa were obtained (Fig. 5.38 B). These mass spectrometry results, together with the results from N-terminal sequencing, identified cleavage sites at amino-acid positions 2, 86, 122, and 138 in IGFBP-4 (Fig. 5.38). Hence in IGFBP-4 calpain appears to act on the bond between Glu 2 and Ala 3 generating fragment of approximately 2.45 kDa, which corresponds to the 20 His-tag residues along with the first three residues of the amino terminus of the protein. The other three major cleavage sites were found in the weakly conserved regions of the protein at Glu 86 and Ala 87 generating a fragment of approximately 11.01 kDa and 16.0 kDa, but another small fragment of 4.10 kDa was observed in mass spectrometry instead of the large 16.0 kDa fragment. This discrepancy arose because this larger fragment was further cleaved at another major internal cleavage site, Phe 122 and Ala 123 which generated fragments of 4.10 kDa and 13.10 kDa. The last major site was the bond between Asp 138 and Gly 139, which resulted in fragment of 10.90 kDa. The NH_2-terminal sequencing of IGFBP-4 yielded another weak cleavage site at the bond between Leu 72 and Met 73 which corresponds to the N-terminal region of the protein but mass spectroscopy did not show any such fragment with the corresponding molecular weights. Hence this site was not considered as a major cleavage site. In IGFBP-5, we identified cleavage sites at residues 2, 141, and 152, as shown in Fig. 5.38 and 5.39. Three major cleavage sites were observed: the first site is between the residues Gly 2 and Ser 3 located at the very beginning of the protein at the amino terminus. NH_2-terminal sequencing of IGFBP-5 also showed another very close site between His 7 and Cys 8, but this was probably due to degradation of the N-terminus following initial cleavage, as no corresponding fragment was seen in mass spectra. The other two cleavage sites are located in the weakly conserved domain of the protein similar to IGFBP-4 but not at the same residues. The

first, located between Thr 141 and Gln 142, results in fragment of 15.69 kDa and 12.70 kDa, and the second between Thr 152 and Ala 153, thus generating fragments of 16.81 kDa and 11.61 kDa.

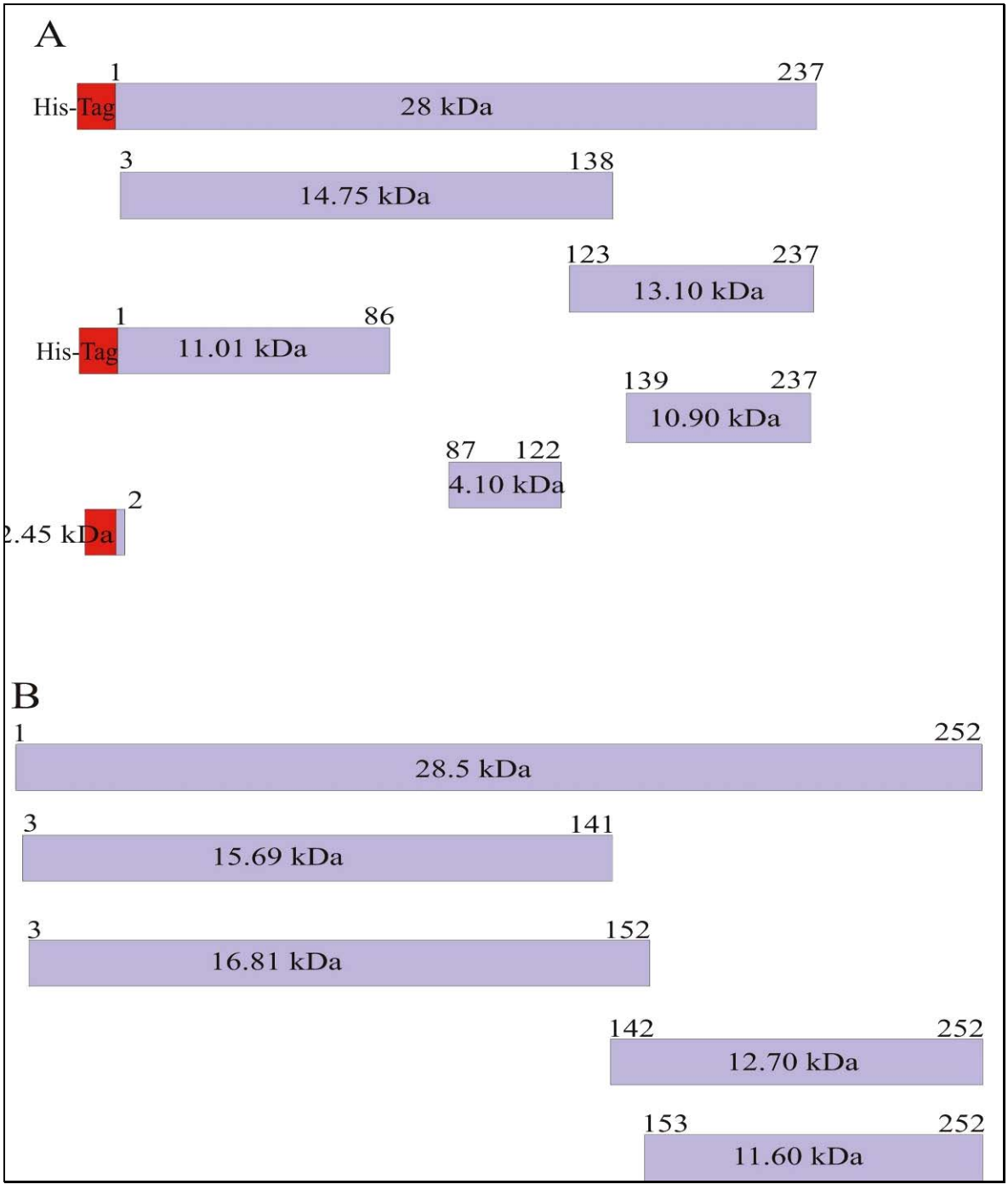

Figure 5.38 A. *Schematic representation of the fragments generated by calpain cleavage.* ***A****, Fragments for IGFBP-4 and,* ***B****, IGFBP-5.*

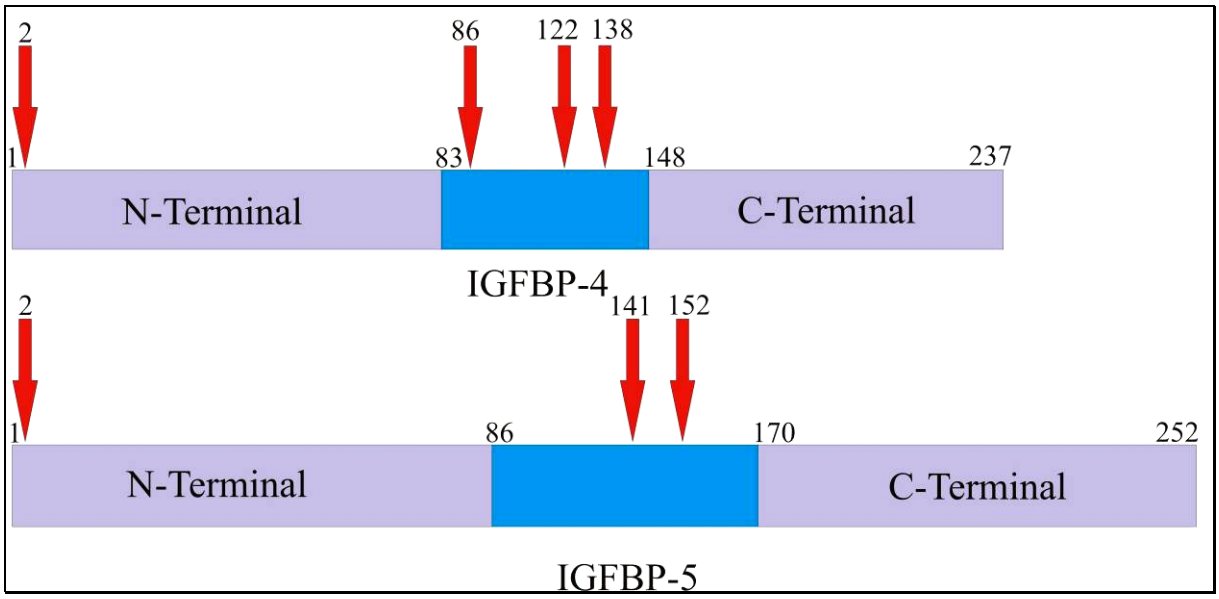

Figure 5.39 *Summary of the location of the principal calpain cleavage sites in IGFBP-4 and IGFBP-5.*

5.3.2.4. ^{1}H NMR spectra of IGFBP-5

Fig. 5.40 shows one-dimensional ^{1}H NMR spectra of IGFBP-5. Inspection of such spectra yields semi-quantitative information on the extent of folding in partially structured proteins or their domains (Rehm et al. 2002). The upper panel shows the spectrum of the full- length IGFBP-5; this spectrum exhibits a large peak at 8.3 ppm and some signals downfield (that is shifted to higher ppm values) close to the noise level. The appearance of intensities at chemical shifts near ~8.3 ppm is an indicator for a disordered protein, as this is a region characteristic of backbone amides in random coil configuration (Kalus et al. 1997; Rehm et al. 2002). On the other hand large signal dispersion beyond 8.3 ppm proves a protein to be folded. Due to the different chemical environment and thus the varying shielding effects the resonances of the single protons will be distributed over a wide range of frequencies. A typical intensity pattern of a folded protein is shown in the lower panel, which shows the spectrum of the N-terminal fragment IGFBP-5. The spectrum of the C-terminal fragment indicates that there are some unstructured regions located also in the C-terminal fragment (Fig.5.40, middle). Based on these spectra we can conclude that the central variable domain of IGFBP-5 is in a random coil conformation. Nearly identical estimates were obtained from NMR on IGFBP-3 and IGFBP-4.

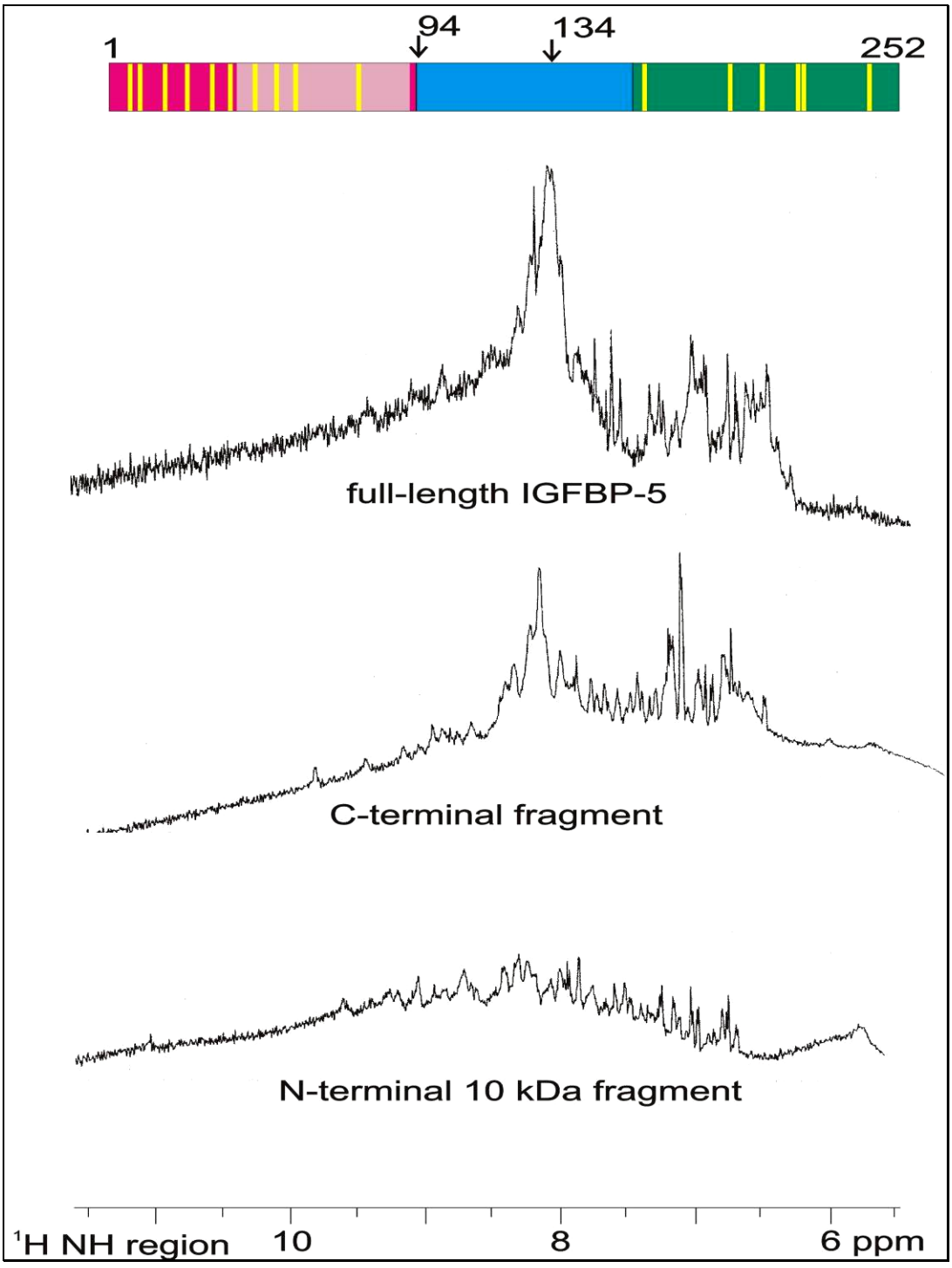

Figure 5.40 *The amide region of one-dimensional spectra of the recombinant human IGFBP-5: the upper, middle and lower panels show the full-length protein, a C-terminal fragment of 112 (residues 135-246) and a N-terminal fragment of 94 residues, respectively. The fragments were created by limited proteolysis with endoproteinase Asp-N. A schematic domain structure of IGFBP-5 consist of the N-terminal domain (purple), a central domain (blue) and the C-domain (green). Yellow sticks mark cysteines*

5.3.2.5. Discussion

The IGFBP family comprises six proteins (IGFBP-1 to 6) that bind to IGFs with high affinity and a group of IGFBP-related proteins (IGFBP-rP 1-9) which bind IGFs with lower affinity (Clemmons et al. 2001; Khandwala et al. 2000). A key conserved structural feature among the six IGFBPs is a high number of cysteines (16-20 cysteines), clustered at the N-terminus (12 cysteines) and also, but to a lesser extent, at the C-terminus. IGFBP-1 to 6 share a high degree of similarity in their primary protein structure (identities around 30-40%), with highest conservation at the N- and C-terminal regions (Figure 5.39 and Figure 5.40). It has been shown that these regions participate in the binding to IGFs (Baxter 2000; Payet et al. 2003; Shand et al. 2003). The structure of the N-terminal domain of IGFBP-5 discloses a rigid, globular structure that consists of a centrally located three-stranded antiparallel β-sheet (Zeslawski et al. 2001). This is in contrast to the central, weakly conserved domain in IGFBPs for which the NMR spectra presented here indicate a highly flexible, unstructured conformation (Fig. 5.40). This domain is also the site of proteolytic activity in IGFBPs (Fig. 5.39). Our data indicate that there are four major calpain cleavage sites in IGFBP-4 and three in IGFBP-5 (Figure 5.37) all located in this region of the protein except for the first cleavage sites in the N-terminal domain of both the proteins. Comparison to the cleavage pattern of IGFBP-5 with endoproteinase Asp-N reveals that endoproteinase Asp-N cleaves in a generally similar manner to calpain (i.e. in the central domain of the protein), the specific bonds were however different (Kalus et al. 1998). Endoproteinase Asp-N cleaves IGFBP-5 into three distinct fragments, the N- terminal fragment, containing residues 1-94, the C terminal fragment with residues 135-246 and a central 4 kDa fragment that spans residues 95-134 (Kalus et al. 1998). This is a common pattern of cleavage as most of the endoproteinases cleave in the non-homologous region of the protein.

Fig. 5.39 and Table 10 show locations of cleavage sites on IGFBPs found in the present study and those compiled from the literature for other proteases. All IGFBPs, except IGFBP-6, are highly sensitive to proteolysis (resistance of IGFBP-6 may be due to the absence of hydrophobic residues like tyrosine, tryptophan or phenylalanine and very small variable domain and also the low number of basic amino acid residues).

Generally for all IGFBPs two to three major proteolytic cleavage sites always occur at the beginning and towards the end of the variable domain (Fig. 5.41). Calpain follows this rule too though we also observe cleavage sites at the second residue of the N-terminal domain of both

IGFBP-4 and -5. The conserved N-terminal regions of IGFBPs are resistant to proteolytic attack, and degradation of C-terminal regions has been observed only for IGFBP-3 (for plasmin, PSA, cathepsin D, and thrombin) and IGFBP-5 (thrombin) in *in-vitro* studies. Fig. 5.39 also includes our *in-vitro* proteolysis of the recombinant human IGFBP-5 (residues 158-247) with thrombin. This fragment shows two extra cleavage sites compared to proteolysis of a full-length IGFPB-5 at physiological concentrations of thrombin (Zheng et al. 1998). A corresponding C-terminal region of IGFBP-4 (residues171-252) was completely resistant to thrombin proteolysis.

Location of protease cleavage sites in IGFBPs

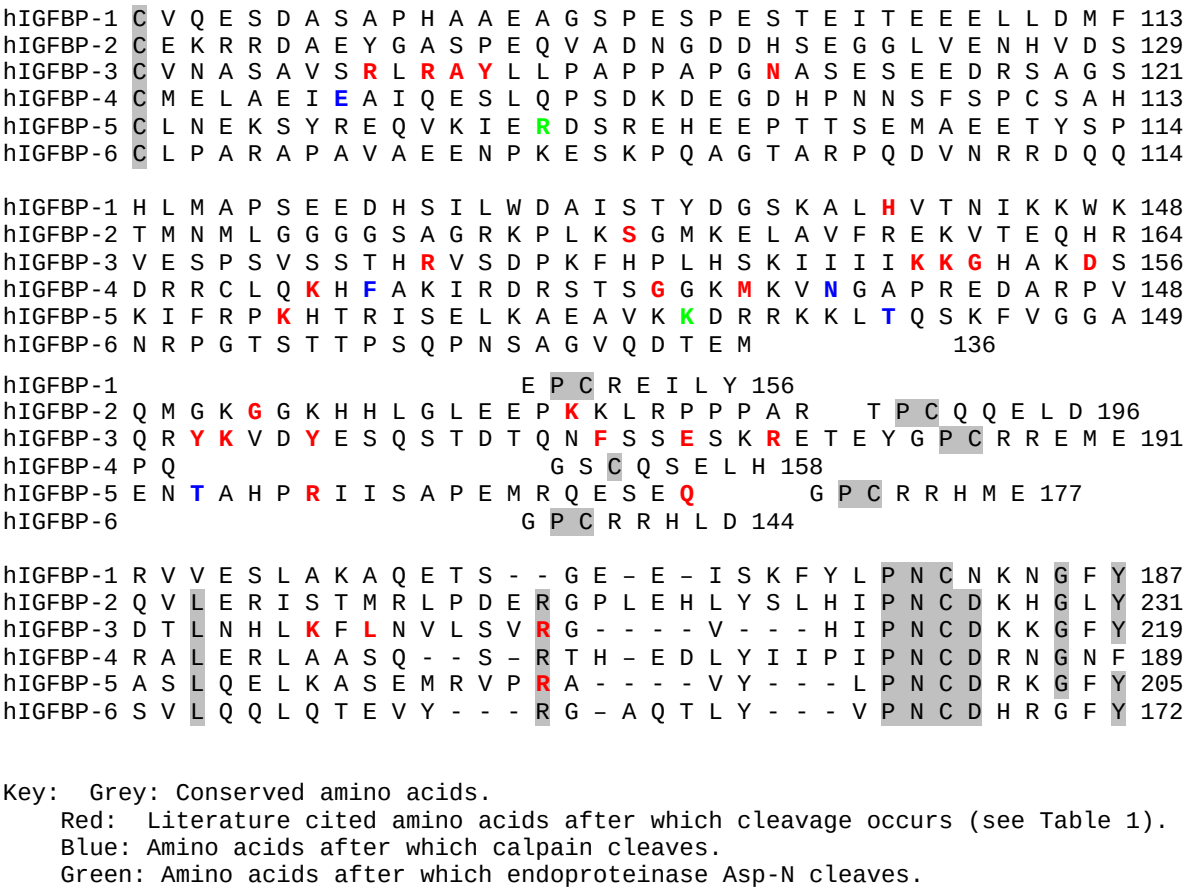

Figure 5.41 *The sequence alignment of all the IGFBPs non-conserved regions highlighting all the protease cleavage sites in these proteins reported until now, amino acids labelled in blue show the calpain cleavage site. Cleavage occurs after the marked amino acid, Table 10 lists the proteases involved*

Since IGFBP-3 and IGFBP-5 show structural similarities and both are synthesized by cell types derived from the mesenchyma, calpain is expected to cleave IGFBP-3 in the same fashion

Table 10 *Proteolytic cleavage sites in IGFBPs*

	Proteases (Types of origin)	Cleavage sites (P1 residue)	Reference
IGFBP-1	Stromelysin-3	140	(Manes et al. 1997)
IGFBP-2	Fetal rat liver cell line	147	(Wang et al. 1988)
	Human milk	169, 181	(Ho and Baxter 1997)
IGFBP-3	Plasmin	95, 97, 149, 150, 151	(Lalou et al. 1997)
		155, 160, 198, 220	(Booth et al. 1996)
	PSA	97, 132, 159, 173, 179	(Fielder et al. 1994)
	Human serum	97, 148, 149, 150,154	(Booth et al. 1996)
	MMP-1	99	(Fowlkes et al. 1994)
	MMP-2 (human fibroblasts)	99	(Fowlkes et al. 1994)
	MMP-3	99, 109, 176.	(Fowlkes et al. 1994)
	Cathepsin D	98, 159, 163, 200	(Claussen et al. 1997)
	Thrombin	97, 206	(Booth et al. 1996)
	MCF-7 cell line	97	(Salahifar et al. 2000)
IGFBP-4	Rat neuronal cells	90, 120, 132.	(Chernausek et al. 1995)
	Human Fibroblasts	135	(Conover et al. 1995)
	Cathepsin D	135	(Claussen et al. 1997)
	Calpain (human erythrocytes)	3, 86, 122, 138	This work
IGFBP-5	Human osteoblasts	169	(Andress and Birnbaum 1991)
	Porcine aortic smooth muscle cells	137, 138	(Imai et al. 1997)
	Thrombin	120, 156, 192.	(Zwad et al. 2002)
	PAPP-A	143, 144	(Laursen et al. 2001)
	Calpain (human erythrocytes)	2, 140, 151	This work
	Asp-N	94, 134	(Kalus et.al. 1998)

Table 11. Calpain cleavage sequences. Cleavage occurs after third residue

Protein	Cleavage site	Cleavage sequence
IGFBP-4 (this work)	2	GDEAIH
	86	EIEAIG
	122	KHFAKI
	138	KVNGAP
IGFBP-5 (this work)	2	SLGSFV
	141	KLTQSK
	152	ENTAHP
Crystallin (Shih et al. 1998)		
βB1	12	ATAAVN
	15	GPPPGP
βA3	11	ELESLP
	17	TTKMAQ
βB2	8	QTQAGK
βB3	5	EQHSTP
	10	PEQAAA
Calpain (autolysis)(Brown and	9	KLAKDR
Crawford 1993)	19	GLGSHE

as it cleaves IGFBP-5. There is evidence that calpain-like cysteine protease is a key regulatory component required for passage through G_1 phase of the cell cycle in eukaryotes (Mellgren 1997) and as IGFBP-3 can traverse into the nucleus calpain might also regulate the IGF-independent functions of IGFBP-3 (Baxter et al. 2000).

There are a limited number of reports on subsite specificity of calpains and these have been reviewed (Croall and DeMartino 1991)and more recently by Goll (Goll et al. 2003). In general the literature data indicates that the calpains cleave target proteins at a limited number of sites and produce large polypeptide fragments rather than small peptides or amino acids (Sasaki et al. 1984b). Early studies suggested that the calpains preferentially cleaved peptide bonds with a Leu or a Val residue in the P_2 position. A more complete data, however, indicated that subsite specificity of the calpains is controlled by the conformation of polypeptide chain and not by

amino acid sequence (Fischer et al. 1986a; Harris et al. 1988; Croall et al. 1996; Stabach et al. 1997).

5.3.2.6. Conclusions

Our present study has not revealed clear preferences for amino acid sequences, although in many cases a hydrophobic residue is present in the P_2 position (Table 11 and Fig. 5.39). For completeness, we also included in Table 2 two reports not covered by the reviews (Croall et al. 1991; Goll et al. 2003). These data pertain to the m-calpain cleavage of N-terminal propeptides during maturation of crystallins and activation of m-calpain. In these cases caplain seems to act on the amino-terminal region generating a set of large fragments with decreasing molecular mass. These pro-N-terminal amino acids are most probably highly mobile and in random coil conformations as, for example, no electron densities were observed for most of them in the X-ray structure of an unprocessed β-crystallin (PDB: 1E7N) (Clout et al. 2000).

In conclusion, we propose that calpains seem not to recognize amino acid sequences in target proteins but cleave with low sequence specificity at unstructured or solvent exposed fragments that connect folded, stable domains of target proteins suggesting that calpains may modulate functions of substrate proteins by cutting their interdomain regions.

5.3.3. Identification of cleavage sites of calpain in the G1 cyclin-dependent kinase inhibitor $p19^{INK4d}$

5.3.3.1. Proteolytic cleavage of p19 by μ-calpain and inhibiton by calpastatin

SDS-PAGE analysis as observed in Fig. 5.42 A, (lane 1 and 4), Fig .5.42 B, (lane 1) shows that the $p19^{INK4d}$ purified by our method was pure and not cleaved in the calpain assay buffer in the absence of μ-calpain. Incubation of p19 with μ-calpain in the presence of 1 mM $CaCl_2$ resulted in p19 fragmentation (Fig. 5.42 A, lane 2, 3, 5 and 6). $p19^{INK4d}$ was not cleaved in the presence of an endogenous calpain inhibitor, calpastatin, and calcium (Fig. 5.42, lane 5), or absence of calcium and calpastatin (Fig. 5.42 B, lane 4). Almost equal amount of p19 was cleaved by calpain in the presence of 5 mM (Fig. 5.42 B, lane 3) as compared to 1 mM $CaCl_2$ (Fig. 5.42 B, lane 2). Fig. 5.43 shows Western blot analysis of p19 and its cleavage products.

5.3.3.2. N-terminal amino acid analysis of fragments generated by calpain

The p19 cleavage products blotted on PVDF membrane were subjected to N-terminal amino acid analysis by Edman degradation and the sequence of various fragments obtained were as follows: LLHREL, KQGASP, EVRRLL, ALQVMM, IHLAVQ, FLAAES. Possible calpain cleavage sites in p19 were identified and are schematically shown in Fig. 5.44 A Fragments containing LLHREL and KQGASP as an N-terminal amino acid sequence were obtained in detectable amounts from reverse phase HPLC and hence we have concluded these two cleavage sites located between histidine 29 and arginine 30, glysine 64 and alanine 65 as major cleavage sites of calpain and remaining four fragments were obtained in low quantities and thus named as minor cleavage sites. Fig. 5.44 B shows the positions of the major calpain cleavage sites in the three-dimensional structure of p19.

Besides, synchronized cells which stably underexpress μ80K or m80K (Gil Parrado et al., manuscript in preparation) were used to analyze the effect of both catalytic subunits on p19 regulation in HeLa cells. Remarkably, downregulation of either *calpain 1* or *2* genes results in an

A **B**

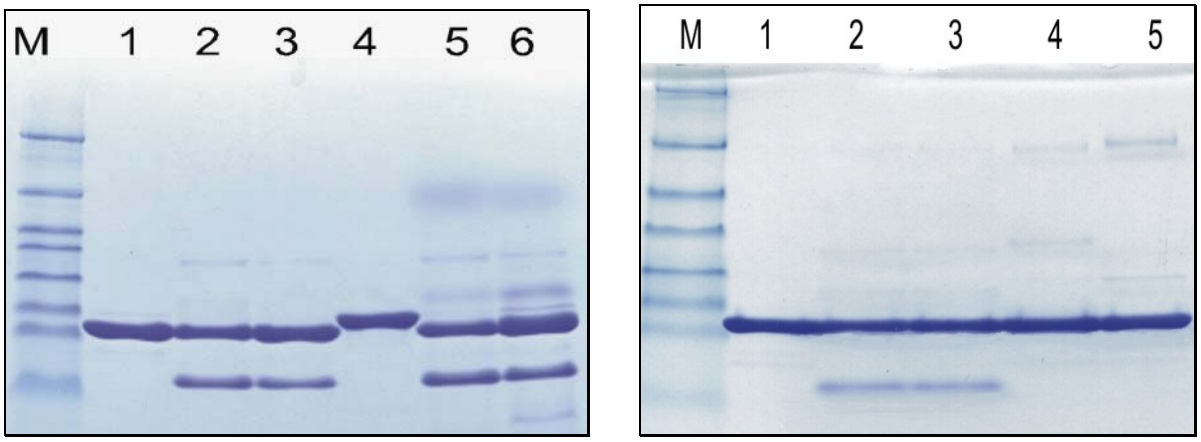

Figure 5.42 A *μ-calpain mediated proteolysis of p19: lane M, Prestained protein mass marker; lane1 and lane 4 are p19 without and with his-tag incubated in the calpain reaction buffer; lane 2 and lane 5 are p19 without and with his-tag digested with calpain in the presence of Ca^{2+} at a molar ratio of 50:1; lane 3 and 6 are p19 without and with his-tag digested with calpain in the presence of Ca^{2+} at a molar ratio of 100:1.*

B *Calpastatin blocks calpain mediated p19 degradation. Lane M, Prestained protein mass marker; lane 1, p19 incubated in the calpain reaction buffer; lane 2 and 3 registers p19 digested with calpain in the absence of calpastatin and presence of 1 mM and 5 mM Ca^{2+} subsequently; lane 4 and 5 shows p19 digested with calpain in the absence of calpastatin and Ca^{2+} and in the presence of calpastatin and Ca^{2+}.*

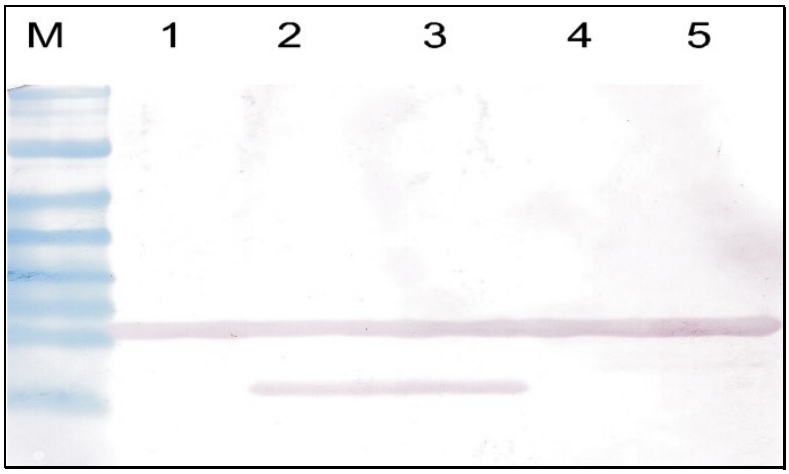

Figure 5.43 *Western blot of p19 fragments generated by calpain. p19 digested with calpain in the presence or absence of calcium and calpastatin, resolved on SDS-PAGE and transferred onto the nitrocellulose membrane. Non-cleaved and cleaved fragments of p19 were detected by immunoassaying with p19 polyclonal antibodies.*

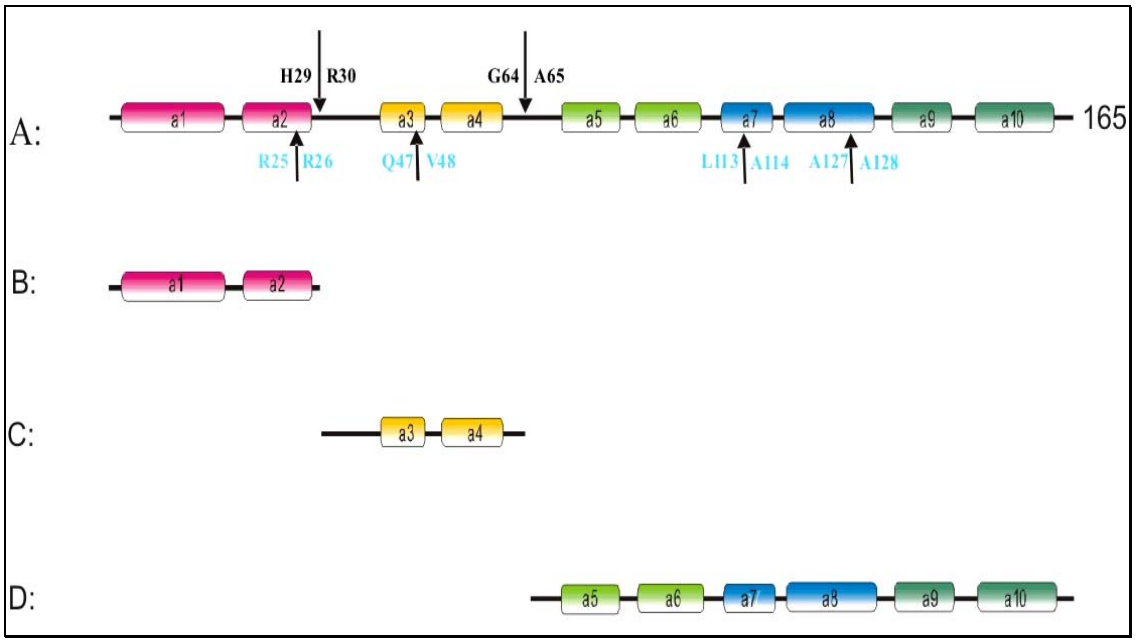

Figure 5.44 A *Schematic representation of domain organization and calpain cleavage sites of p19. Peptides generated from p19 in the calpain cleavage reaction were analyzed by N-terminal amino acid sequencing. Downward and upward arrows indicates major and minor calpain cleavage site subsequently. Fragments generated by calpain are schematically shown below the full-length sequence of p19.*

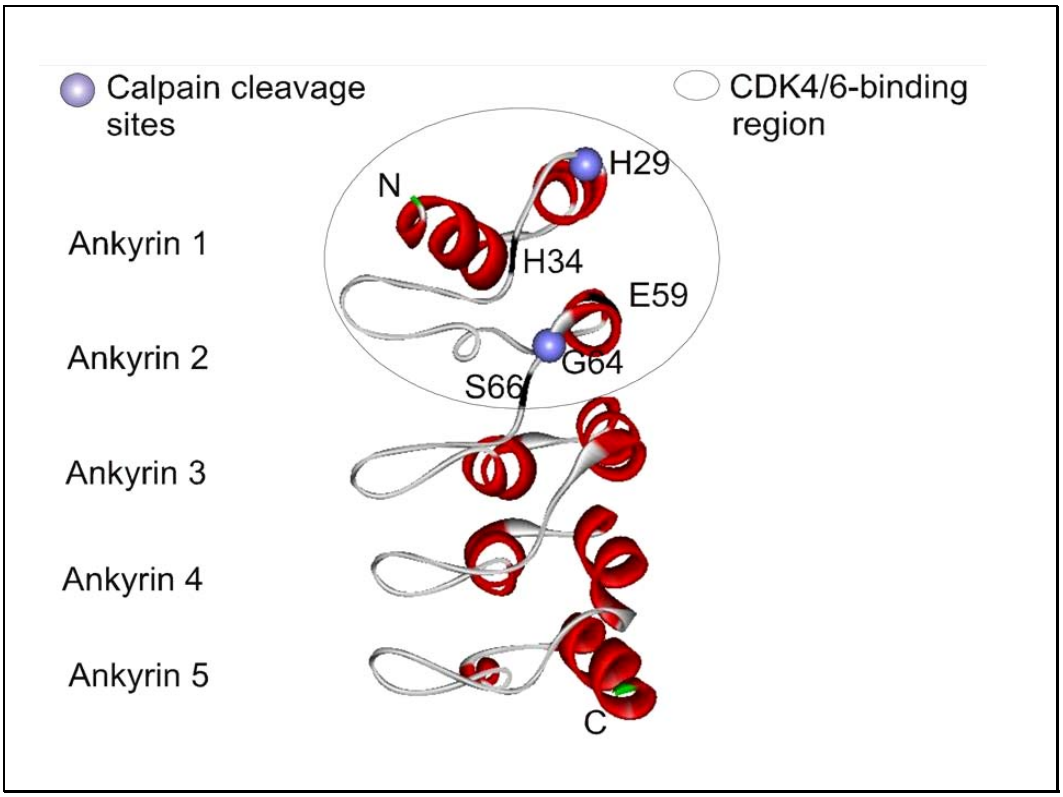

Figure 5.44 B *Ribbon diagram, schematically depicts p19 tertiary structure and its binding region to CDK4/CDK6. p19 consists of 10 α-helices assembled as five ankyrin repeats sequentially, forming an elongated structure. Ankyrin repeat 1 and 2 bind to CDK4/CDK6, represented with a circle. The calpain cleavage sites of p19 are denoted with blue colored spheres. Flexible amino acid residues detected by NMR relaxation studies (H 34, E 59 and S 66) are labeled and the regions corresponding to the respective amino acid residues are marked in black.*

increase of p19 levels in cell extracts when compared to those of mock cells (Fig. 5.45 A) Moreover, we could corroborate that p27 is also enriched in the antisense cell lines (Fig.5.45 B), implicating both ubiquitous calpains in the regulation of CDK inhibitors and as consequence of the cell cycle.

5.3.3.3. Discussion

Transition from the G1 to S phase of the mammalian cell cycle is regulated by the Rb/E2F pathway (Weinberg 1995). Cyclin D-cyclin dependent kinase-4/6 complexes phosphorylate the retinoblastoma protein (pRb), which frees E2F from the Rb/E2F complex. The freed E2F activates the transcription of genes involved in cell proliferation (Weinberg 1995; Leone et al. 1998), p53 dependent ((Bates et al. 1998) and independent apoptosis (Irwin et al. 2000). INK4

inhibitors specifically inhibit the G1 cyclin dependent kinase mediated phosphorylation of pRb and thus the normal function of Rb/E2F pathway is deregulated. INK4 inhibitors exert their action by binding directly to CDK4/6 through their two N-terminal ankyrin repeats (Brotherton et al. 1998; Russo et al. 1998). It is interesting to see that the major calpain cleavage sites in p19 are located exactly in these two ankyrin repeats. Calpains therefore should influence the INK4 inhibitor bindings to CDK4/6 and thus may take part in the regulation of this binding in vivo. This proposition is further backed up by the observation that CDK6 is resistant to calpain proteolysis. We have treated CDK6 with μ-caplain and observed that calpain does not affect CDK6. CDK4 and CDK6 have a typical overall bilobal fold found in many eukaryotic protein kinases, with the smaller N-terminal domain consisting predominantly of β-sheet structure and the larger C-terminal domain consisting primarily of α-helices (Pavletich 1999; Cheek et al. 2002). The structure is globular in contrast to the elongated rod-like structure of $p19^{INK4d}$. Resistance of CDK6 to calpain proteolysis, as compared to propensity of $p19^{INK4d}$ and cyclin D (Choi et al. 1997) for calpain degradation, suggests that calpain may be involved in the cell cycle by regulating the cell cycle regulatory protein turnover. $p19^{INK4d}$ may therefore be a substrate for calpains in these in vivo situations.

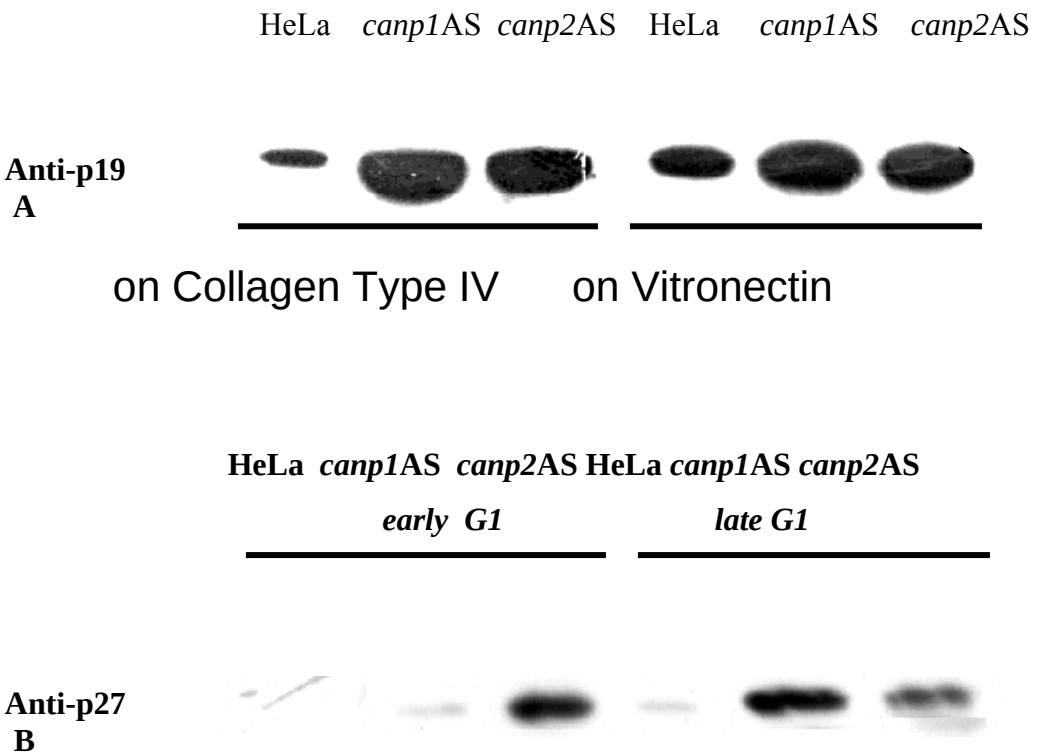

Figure 5.45 *Increase of p19 and p27 protein levels by downregulation of capn1 and capn2 genes. Representative immunoblots of cell lines stably expressing an antisense construct targeting calpain 1 or 2. Processing of endogenous p19 and p27 was detected using specific antibodies. Notice that levels of both CDK inhibitors increased in extracts from calpain 1 and 2 antisense cell lines, suggesting the calpain-mediated regulation of the protein levels of both inhibitors in vivo*

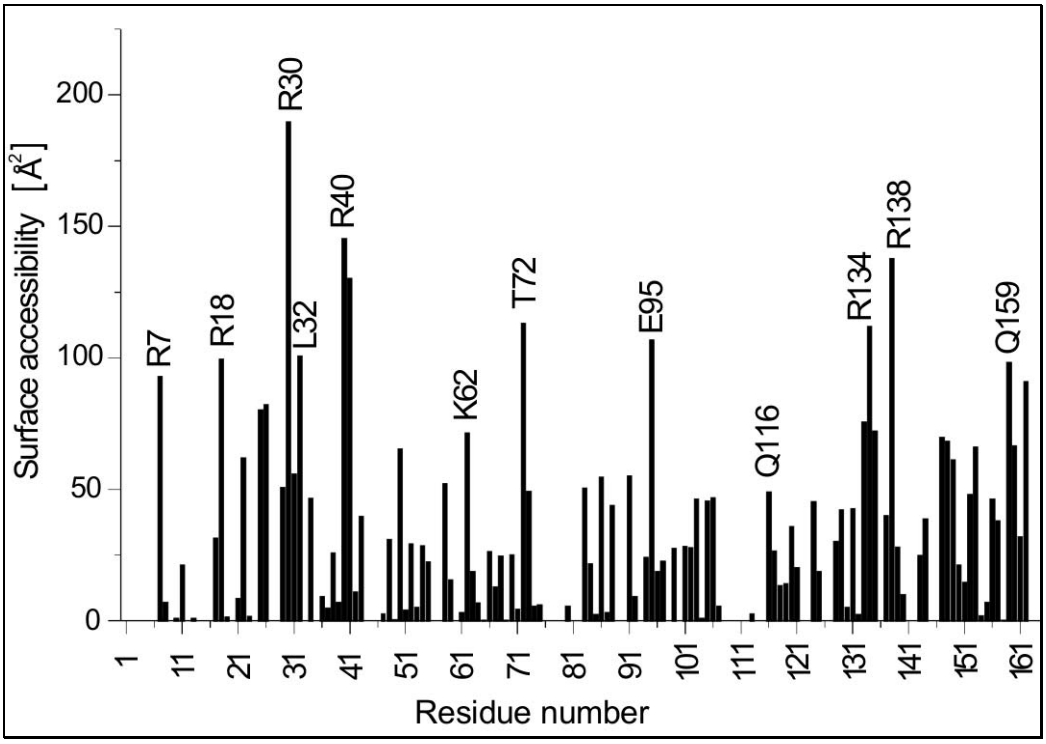

Figure 5.46 *Surface accessibility plot of p19: The above plot indicates the surface accessibility of each residue of p19 in square angstrom units [Å²]. The residues with higher surface accessibilities are labeled and are the most solvent exposed ones. The His29↓Arg30 cleavage site is one among the solvent exposed, however, the Gly64↓Ala65 site, although a calpain cleavage site, does not have a significant solvent exposed region.*

The p19 caplain cleavage seems to show still other features. The major calpain cleavage sites are located at the end of the second helix (α-2) of the first ankyrin repeat (His 29) and again at the end of the second helix (α-4) of the second ankyrin repeat Gly 64 (Fig. 5.42). His 29 and Arg 30 are in the α-helical conformation, the amide proton of His 29 makes a hydrogen bond with C=O of Arg 25 (Baumgartner et al. 1998). Gly 64 participates in a semi-helical loop, which follows helix α-4. Both major cleavage sites are therefore located immediately after well-structured, stable α-helices. Our previous NMR relaxation measurements on $p19^{INK4d}$ showed that

most of the backbone of $p19^{INK4d}$ exists in a well-defined structure of limited conformational flexibility on the nanosecond to picosecond time-scales. The exceptions were short stretches around residues Val 69 and Glu 129, which are flexible on this fast time scale. Also considerable amounts of slower exchange broadening were found for several residues throughout the sequence; these were located mostly in the second ankyrin repeat, and in the beginning and end of loops, connecting ankyrin repeats. Gly 64 is close to Val 69, and a minor cleavage site residue Ala 127 is close to Glu 129. However, we could not find any clear correlation between all "flexible" residues and their locations in the close neighborhood to the calpain cleavage sites. Fig. 5.46 show the residues which are solvent exposed in p19. The His 29/Arg 30 cleavage site is one of the most solvent exposed, however, the Gly 64/Ala 65 site is not; and therefore no correlation can again be detected.

Analysis of the *canp1*AS and *canp2*AS cell lines reveals a new candidate for calpain-regulated proteins which are known to be required for cellular proliferation ***e.g.***, p19. Interestingly, the relative amount of intact p19 was significantly increased in extracts from *canp1*AS and *canp2AS* clones, suggesting that ubiquitous calpains regulates the cell cycle by p19 cleavage thus preventing the phosphorylation of the pRb. We also note that other inhibitors of cyclin dependent kinases like p27 which have been repeteadly reported as calpain substrate might also contribute to the calpain-mediated regulation of the cell cycle. Notably both were enriched in the cytoplasma of antisense cell lines (Fig. 5.45).

In conclusion, our data seem to show new characteristics of calpain action in that calpains cleaved p19 immediately following stable α-helical segments of the protein, but not necessarily at the residues of linker polypeptide segments that are most exposed to solvent or that have highest flexibility.

6. Summary

This thesis is based on the studies that were carried out in the Department of Structural Research at the Max Planck Institute for Biochemistry from May 2001 to November 2004. The focus of my research involved structural and biochemical studies on proteins whose deregulation is associated with cancer. The protein included the tumor suppressor proteins p53, and pRb, the oncoprotein MDM2, the CDK inhibitor, $p19^{INK4d}$ and insulin like growth factor binding proteins (IGFBPs).

The oncoprotein MDM2 sequesters p53 by binding to its transactivation domain and thereby inhibiting both p53 mediated G_1 cell cycle arrest and apoptosis. It promotes the nuclear export of p53 and favors its rapid degradation by the proteosome pathway. MDM2 deregulation has been shown to be abnormally high in a variety of human tumors such as soft tissue sarcomas. The disruption of p53-MDM2 interaction with synthetic compounds has been shown to stabilize wild type p53 in the nucleus. In this study a series of novel boronic and cyano chalcones have been studied as possible inhibitors of the MDM2-p53 interactions. The protein-inhibitor interactions were characterized by ^{15}N HSQC spectroscopy and the binding sites of the inhibitor were mapped on MDM2. The results showed that these chalcone derivatives bind to a subsite of the p53-binding cleft of MDM2 with micromolar affinities and thus serve as potential starting compounds for the design of inhibitors with increased affinity. Preliminary studies were also carried out on expression of various C terminal MDM2 constructs. Since it is known that tumour suppressor pRb binds to C-terminal domain of MDM2 and this binding is essential for pRb to overcome both the antiapoptotic function of MDM2 and the MDM2-dependent degradation of p53, attempts were also made to co-express pRb and MDM2.

Insulin-like growth factor binding proteins (IGFBPs) constitute a family of six proteins which control the bioavailability and distribution of IGFs in the serum. The amino and carboxy domains are the conserved and structured domains of IGFBPs. To gain a more detailed understanding of the IGFBPs' domain organization and structural requirements for binding to IGFs, we studied the inter- and intra-domain arrangement and the extent of folding within the domains of IGFBP-3, -4, -5 and -6. The results show that within the N-terminal domains, the IGFBPs bind IGF primarily using residues 40-50, and that the first six residues of IGFBPs prevent the IGF-I receptor access to IGF through steric hindrance. The amino- and carboxyl-terminal domains of IGFBPs cooperate to form a high affinity IGF-I complex and a 3-6 times

tighter binding to IGF is observed in the presence of the C-terminal domain. Understanding of the IGFBP domain structure and the structural insights of their binding to IGF provides a basis for drug discovery.

In the last part of the study we determined the proteolytic cleavage pattern of IGFBPs and $p19^{INK4d}$ by a Ca^{2+} dependent cysteine proteinase, calpain. The structural clues of substrate recognition by calpain are incompletely understood. Our results with IGFBPs (-4 and -5) show that calpain seems not to recognize amino acid sequences but instead cleave unstructured or solvent exposed fragments that connect folded, stable domains of IGFBPs. In the next part of this proteolytic study with $p19^{INK4d}$, we found new insights in the calpain cleavage pattern, where calpain cleaved $p19^{INK4d}$ immediately after stable α-helical segments of the protein, and not necessarily at residues of linker polypeptide segments that are most exposed to solvent or that have high flexibility.

7. Zusammenfassung

Die Doktorarbeit wurde in der Abteilung Strukturforschung des Max Planck Institutes für Biochemie in der Zeit von Mai 2001 bis November 2004 erstellt.

Das Hauptinterresse der Forschung galt der strukturellen und biochemischen Charakterisierung von Proteinen, deren Deregulierung in Verbindung mit der Krebsentstehung stehen. Darunter die Proteine: p53, pRb, das Oncoprotein MDM2, der CDK Inhibitor $p19^{INK4d}$ und die *Insulin like growth factor binding* Proteine (IGFBPs).

Das Oncoprotein MDM2, dessen Expression in vielen Tumoren abnormal hochreguliert ist, blockiert p53 in dem es an dessen Transaktivierungsdomäne bindet. Dadurch wird sowohl die p53 abhängige Arretierung des Zellzyklus in der G_1 Phase als auch die Apoptose verhindert. MDM2 fördert den Export von p53 aus dem Zellkern und beschleunigt dadurch den raschen Abbau von p53 über den Proteasom-Stoffwechselweg.

Die Störung der Interaktion zwischen p53 und MDM2 mit synthetischen Wirkstoffen stabilisiert p53 im Zellkern. In dieser Arbeit wurden eine Reihe neuer Boro- und Cyanochalkone als potentielle Inhibitoren der p53-MDM2 Interaktion getestet. Die Wechselwirkung zwischen Inhibitor und Protein wurde mit Hilfe von ^{15}N HSQC Spektroskopie charakterisiert und die Bindestellen auf der Proteinoberfläche bestimmt. Die Studien zeigten, dass die Chalkonderivate in die p53 Bindungstasche auf der MDM2 Oberfläche mit einer Affinität im mikromolaren Bereich binden und sich daher als Grundlage für die Synthese weiterer Inhibitoren mit größerer Affinität eignen.

In ersten Studien wurden auch verschiedene C-terminale Konstrukte von MDM2 getestet, da das Tumorsupressorprotein pRB an die C-terminale Domäne von MDM2 bindet. Diese Wechselwirkung ist wichtig, da durch die Interaktion von pRb mit MDM2 sowohl die antiapoptose Funktion von MDM2 als auch die MDM2 abhängige Degradierung von p53 aufgehoben werden. Es wurde auch versucht beide Proteine zu coexpremieren.

Die *Insulin like growth factor binding* Proteine (IGFBPs) sind eine Familie von sechs Proteinen, die die Bioverfügbarkeit und Verteilung von IGF im Serum steuern. Die Amino- und Carboxyterminalen Domänen sind in der Familie der IGFBP konserviert mit einer definierten dreidimensionalen Struktur. Beide Domänen zeigen eine hohe Affinität zu IGFs. Um ein detailierteres Verständnis über die IGFBP Domänen Organisation und die strukturellen Voraussetzungen für eine Bindung an IGF zu erhalten, wurden die inter- und intradomänen Anordnungen und der Faltungsbereich von IGFBP-3, -4, -5 und –6 untersucht. Es zeigte sich, dass in der N-terminalen Domäne der IGFBPs IGF hauptsächlich an die

Aminosäurenreste 40-50 bindet. Weiterhin blockieren die ersten sechs Aminosäuren von IGFBP über eine sterische Hinderung die Bindung von IGF an den IGF-I Rezeptor. Die N- und C-terminale Domäne koopereren um einen hoch affinen IGF/IGFBP Komplex zu bilden. Die Affinität zwischen IGF und IGFBP ist in Anwesenheit der C-terminalen Domäne um das 3-6fache höher. Das Verständnis über die Domänenstruktur der IGFBP und die Erkenntnisse wie IGF gebunden wird bilden die Grundlage für die Entwicklung neuer Wirkstoffe.

Im letzten Teil der Arbeit wurde das proteolytische Verdaumuster von IGFBPs und $p19^{INK4d}$ durch die Endopeptidase Calpain bestimmt. Calpain gehört zur Familie der Ca^{2+} abhängigen Serinproteasen. Die strukturellen Grundlagen der Substraterkennung durch Calpain sind nur teilweise verstanden. Die Ergebnisse mit IGFBP (-4 und-5) zeigt, dass Calpain nicht aminosäurespezifisch schneidet, sondern ungefaltete oder lösungsmittelzugängliche Fragmente spaltet, die stabile, gefaltete Domänen der IGFBP verbinden. Dies stimmt mit dem in der Literatur beschriebenen Spaltmuster von Calpain überein. Im Gegensatz dazu brachte der proteolytische Verdau von $p19^{INK4d}$ neue Erkentnisse über Calpain. Calpain schneidet $p19^{INK4d}$ sofort nach einem stabielen α-helicalen Segment des Proteins und nicht notwendigerweise an Resten in *linker*- Regionen die hoch flexibel und lösungsmittelzugängliche sind.

8. Appendix

Abbreviations and symbols

Amino acids and nucleotides are abbreviated according to either one or three letter IUPAC (International Union of Pure and Applied Chemistry) code.

- 1D one-dimensional
- 2D two-dimensional
- Å Ångstrom (10^{-10} m)
- ALS acid labile subunit
- APS ammonium peroxodisulfate
- BEVS baculovirus expression vectors system
- BSA bovine serum albumin
- CAK CDK activating kinase
- CDC cyclin-dependent kinase
- cDNA complimentary DNA
- CDK cyclin-dependent kinase
- COSY correlation spectroscopy
- δ chemical shift
- DHFR dihydrofolate reductase
- DMSO dimethylsulfoxide
- DMSO-d6 deuterated dimethylsulfoxide
- DNA deoxyribonucleic acid
- DNaseI deoxyribonuclease I
- DBD DNA binding domain
- DTT Dithiothreitol
- EDTA ethylenediamine tetraacetic acid
- FID free induction decay
- GH growth hormone
- GSH reduced glutathione
- GSSG oxidized glutathione
- GST glutathione S-transferase
- HAT histone acetyltransferase activity

- HDAC histone deacetylase activity
- HSQC heteronuclear single quantum coherence
- Hz Hertz
- IGF insulin-like growth factor
- IGFBP IGF binding protein
- IGFBPrP IGFBP related protein
- IGF-IR IGF receptor type I
- INK4 inhibitor of CDK4 and CDK6
- IPTG isopropyl-β-thiogalactopyranoside
- kDa Kilodalton
- K_D Dissociation constant
- KIP inhibitor of kinase
- LB Luria-Broth medium
- M $mol\ l^{-1}$
- MAP mitogen-activated protein kinase
- MBD MDM2 binding domain
- MDM2 murine double minute clone 2
- MM minimal medium
- MW molecular weight
- Ni-NTA nickel-nitrilotriacetic acid
- NES nuclear export signal
- NLS nuclear localization signal
- NoLS nucleolar localization signal
- NMR nuclear magnetic resonance
- NOE nuclear Overhauser effect
- NOESY nuclear Overhauser enhancement spectroscopy
- OD optical density
- P3K phosphatidylinositol 3-kinase
- PAGE polyacrylamide gel electrophoresis
- PBS phosphate-buffered saline
- POL DNA polymerase α
- ppm parts per million
- pRb retinoblastoma susceptibility protein

- RF RING finger motif, or radio frequency
- SDS sodium dodecyl sulfate
- Sf9 spodoptera frugiperda
- TAD transcription activation domain
- TEMED N,N,N’,N’-tetramethylethylendiamine
- TK thymidine kinase
- ZF zinc finger motif

Human IGFBPs sequence alignment

N-domains:

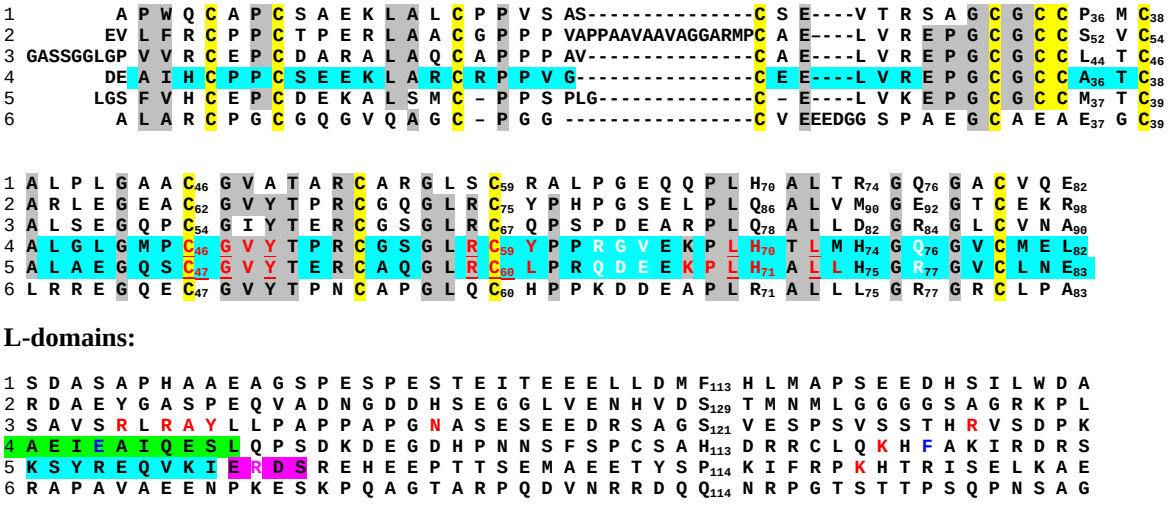

L-domains:

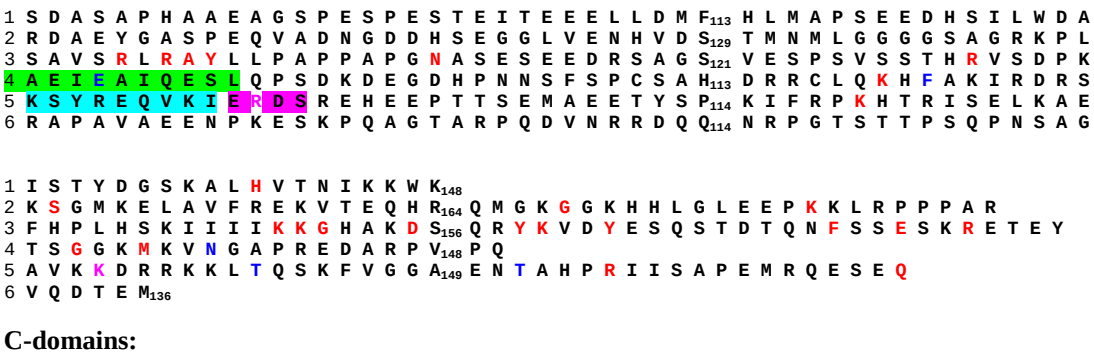

C-domains:

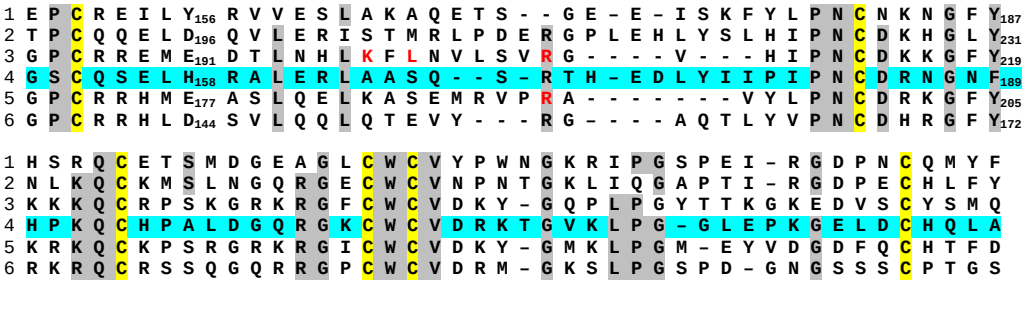

Sequence and structure alignment of human IGFBP-1 to -6. The N-terminal and C-terminal domains studied are marked by light blue. Conserved residues are indicated by gray shading and cysteines are in yellow. Residues that interact with IGF-I are highlighted in red (with primary sites underlined). Residues shown in white have no amino acid and structural homology between N-domains of IGFBP-4 and IGFBP-5.

BP-1

```
Homo sapiens                    A P W Q
Rattus norvegicus             A P Q P W H
Mus musculus                  A P Q P W H
Spermophilus                    Q P W H
Bos taurus                    S L Q P L H
Danio rerio                     Q E P I R
```

BP-2

```
Homo sapiens                    E V L F R
Rattus norvegicus               E V L F R
Mus musculus                    E V L F R
Sus scrofa                      E V L F R
Bos taurus                      E V L F R
Ovis aries                      E V L F R
Gallus gallus                   E V L F R
Danio rerio                     E M V F R
Sparus aurata                   D L A F R (gilthead seabream)
Oncorhynchus tshawytscha        D L V F Y (Chinook salmon)
```

BP-3

```
Homo sapiens        G A S S G G L G P V V R
Rattus norvegicus   G A G A V G A G P V V R
Mus musculus        A A G A V G - G P V V R
Sus scrofa          G S G A V G T G P V V R
Bos taurus          G A G T M G A G P V V R
Danio rerio               E S V S P V V R
consensus           G A G A V G L G P V V R
```

BP-4

```
Homo sapiens                    D E A I H
Rattus norvegicus               D E A I H
Mus musculus                    D E A I H
Ovis aries                      D E A I H
Sus scrofa                      D E A I H
Bos taurus                      D E A I H
Gallus gallus                   E E A T Q
```

BP-5

```
Homo sapiens                  L G S F V H
Rattus norvegicus             L G S F V H
Mus musculus                  L G S F V H
Pig taurus                    L G S F V H
Gallus gallus                 L G S F V Q
Danio rerio                     G S F V P
```

BP-6

```
Homo sapiens                    A L A R
Rattus norvegicus               A L A G
Mus musculus                    A L A G
```

Conserved IGFBP (1-6) residues among different species.

9. References

Andress, D.L., and Birnbaum, R.S. 1991. A novel human insulin-like growth factor binding protein secreted by osteoblast-like cells. *Biochem Biophys Res Commun* **176:** 213-218.

Argentini, M., Barboule, N., and Wasylyk, B. 2001. The contribution of the acidic domain of MDM2 to p53 and MDM2 stability. *Oncogene* **20:** 1267-1275.

Bach, L.A. 1999. Insulin-like growth factor binding protein-6: the "forgotten" binding protein? *Horm Metab Res* **31:** 226-234.

Bach, L.A., Hsieh, S., Sakano, K., Fujiwara, H., Perdue, J.F., and Rechler, M.M. 1993. Binding of mutants of human insulin-like growth factor II to insulin-like growth factor binding proteins 1-6. *J Biol Chem* **268:** 9246-9254.

Bach, L.A., and Rechler, M.M. 1996. Measurement of insulin-like growth factor (IGF)-II binding to purified IGF binding proteins 1-6: comparison of charcoal adsorption and high performance size exclusion chromatography. *Biochim Biophys Acta* **1313:** 79-88.

Barak, Y., Gottlieb, E., Juven-Gershon, T., and Oren, M. 1994. Regulation of mdm2 expression by p53: alternative promoters produce transcripts with nonidentical translation potential. *Genes Dev* **8:** 1739-1749.

Bartel, F., Pinkert, D., Fiedler, W., Kappler, M., Wurl, P., Schmidt, H., and Taubert, H. 2004. Expression of alternatively and aberrantly spliced transcripts of the MDM2 mRNA is not tumor-specific. *Int J Oncol* **24:** 143-151.

Bates, S., Phillips, A.C., Clark, P.A., Stott, F., Peters, G., Ludwig, R.L., and Vousden, K.H. 1998. p14(ARF) links the tumour suppressors RB and p53. *Nature* **395:** 124-125.

Baumgartner, R., Fernandez-Catalan, C., Winoto, A., Huber, R., Engh, R.A., and Holak, T.A. 1998. Structure of human cyclin-dependent kinase inhibitor p19INK4d: comparison to known ankyrin-repeat-containing structures and implications for the dysfunction of tumor suppressor p16INK4a. *Structure* **6:** 1279-1290.

Baxter, R.C. 2000. Insulin-like growth factor (IGF)-binding proteins: interactions with IGFs and intrinsic bioactivities. *American Journal of Physiology-Endocrinology and Metabolism* **278:** E967-E976.

Bayne, M.L., Applebaum, J., Chicchi, G.G., Miller, R.E., and Cascieri, M.A. 1990. The roles of tyrosines 24, 31, and 60 in the high affinity binding of insulin-like growth factor-I to the type 1 insulin-like growth factor receptor. *J Biol Chem* **265:** 15648-15652.

Binoux, M. 1996. Insulin-like growth factor binding proteins (IGFBPs): physiological and clinical implications. *J Pediatr Endocrinol Metab* **9 Suppl 3:** 285-288.

Blommers, M.J.J., Fendrich, G., GarciaEcheverria, C., and Chene, P. 1997. On the interaction between p53 and MDM2: Transfer NOE study of a p53-derived peptide ligated to MDM2. *J Am Chem Soc* **119:** 3425-3426.

Bois, F., Boumendjel, A., Mariotte, A.M., Conseil, G., and Di Petro, A. 1999. Synthesis and biological activity of 4-alkoxy chalcones: potential hydrophobic modulators of P-glycoprotein-mediated multidrug resistance. *Bioorg Med Chem* **7:** 2691-2695.

Booth, B.A., Boes, M., and Bar, R.S. 1996. IGFBP-3 proteolysis by plasmin, thrombin, serum: Heparin binding, IGF binding, and structure of fragments. *American Journal of Physiology-Endocrinology and Metabolism* **34:** E465-E470.

Bottger, A., Bottger, V., Garcia-Echeverria, C., Chene, P., Hochkeppel, H.K., Sampson, W., Ang, K., Howard, S.F., Picksley, S.M., and Lane, D.P. 1997. Molecular characterization of the hdm2-p53 interaction. *J Mol Biol* **269:** 744-756.

Brotherton, D.H., Dhanaraj, V., Wick, S., Brizuela, L., Domaille, P.J., Volyanik, E., Xu, X., Parisini, E., Smith, B.O., Archer, S.J., et al. 1998. Crystal structure of the complex of the cyclin D-dependent kinase Cdk6 bound to the cell-cycle inhibitor p19INK4d. *Nature* **395:** 244-250.

Brown, N., and Crawford, C. 1993. Structural Modifications Associated with the Change in Ca2+ Sensitivity on Activation of M-Calpain. *Febs Letters* **322:** 65-68.

Bunn, R.C., and Fowlkes, J.L. 2003. Insulin-like growth factor binding protein proteolysis. *Trends in Endocrinology and Metabolism* **14:** 176-181.

Burstein, E.A., Vedenkin.Ns, and Ivkova, M.N. 1973. Fluorescence and Location of Tryptophan Residues in Protein Molecules. *Photochem Photobiol* **18:** 263-279.

Calliste, C.A., Le Bail, J.C., Trouillas, P., Pouget, C., Habrioux, G., Chulia, A.J., and Duroux, J.L. 2001. Chalcones: structural requirements for antioxidant, estrogenic and antiproliferative activities. *Anticancer Res* **21:** 3949-3956.

Carafoli, E., and Molinari, M. 1998. Calpain: a protease in search of a function? *Biochem Biophys Res Commun* **247:** 193-203.

Carrick, F.E., Forbes, B.E., and Wallace, J.C. 2001. BIAcore analysis of bovine insulin-like growth factor (IGF)-binding protein-2 identifies major IGF binding site determinants in both the amino- and carboxyl-terminal domains. *J Biol Chem* **276:** 27120-27128.

Cascieri, M.A., and Bayne, M.L. 1993. Analysis of the interaction of IGF-I analogs with the IGF-I receptor and IGF binding proteins. *Adv Exp Med Biol* **343:** 33-40.

Cascieri, M.A., Hayes, N.S., Kelder, B., Kopchick, J.J., Chicchi, G.G., Slater, E.E., and Bayne, M.L. 1988. Inability of a mouse cell line transformed to produce biologically

active recombinant human insulin-like growth factor I (IGF-I) to respond to exogenously added IGF-I. *Endocrinology* **122:** 1314-1320.

Cheek, S., Zhang, H., and Grishin, N.V. 2002. Sequence and structure classification of kinases. *Journal of Molecular Biology* **320:** 855-881.

Chen, J., Marechal, V., and Levine, A.J. 1993. Mapping of the p53 and mdm-2 interaction domains. *Mol Cell Biol* **13:** 4107-4114.

Chen, J., Wu, X., Lin, J., and Levine, A.J. 1996. mdm-2 inhibits the G1 arrest and apoptosis functions of the p53 tumor suppressor protein. *Mol Cell Biol* **16:** 2445-2452.

Chernausek, S.D., Smith, C.E., Duffin, K.L., Busby, W.H., Wright, G., and Clemmons, D.R. 1995. Proteolytic Cleavage of Insulin-Like Growth-Factor Binding-Protein-4 (Igfbp-4) - Localization of Cleavage Site to Nonhomologous Region of Native Igfbp-4. *Journal of Biological Chemistry* **270:** 11377-11382.

Choi, Y.H., Lee, S.J., Nguyen, P., Jang, J.S., Lee, J., Wu, M.L., Takano, E., Maki, M., Henkart, P.A., and Trepel, J.B. 1997. Regulation of cyclin D1 by calpain protease. *J Biol Chem* **272:** 28479-28484.

Claussen, M., Kubler, B., Wendland, M., Neifer, K., Schmidt, B., Zapf, J., and Braulke, T. 1997. Proteolysis of insulin-like growth factors (IGF) and IGF binding proteins by cathepsin D. *Endocrinology* **138:** 3797-3803.

Clemmons, D.R. 2001. Use of mutagenesis to probe IGF-binding protein structure/function relationships. *Endocr Rev* **22:** 800-817.

Clout, N.J., Basak, A., Wieligmann, K., Bateman, O.A., Jaenicke, R., and Slingsby, C. 2000. The N-terminal domain of beta B2-crystallin resembles the putative ancestral homodimer. *Journal of Molecular Biology* **304:** 253-257.

Conover, C.A., Durham, S.K., Zapf, J., Masiarz, F.R., and Kiefer, M.C. 1995. Cleavage Analysis of Insulin-Like Growth-Factor (Igf)-Dependent Igf-Binding Protein-4 Proteolysis and Expression of Protease-Resistant Igf-Binding Protein-4 Mutants. *Journal of Biological Chemistry* **270:** 4395-4400.

Croall, D.E., Chacko, S., and Wang, Z. 1996. Cleavage of caldesmon and calponin by calpain: Substrate recognition is not dependent on calmodulin binding domains. *Biochimica Et Biophysica Acta-Protein Structure and Molecular Enzymology* **1298:** 276-284.

Croall, D.E., and DeMartino, G.N. 1991. Calcium-activated neutral protease (calpain) system: structure, function, and regulation. *Physiol Rev* **71:** 813-847.

De Vincenzo, R., Scambia, G., Benedetti Panici, P., Ranelletti, F.O., Bonanno, G., Ercoli, A., Delle Monache, F., Ferrari, F., Piantelli, M., and Mancuso, S. 1995. Effect of synthetic

and naturally occurring chalcones on ovarian cancer cell growth: structure-activity relationships. *Anticancer Drug Des* **10:** 481-490.

Dear, T.N., and Boehm, T. 2001. Identification and characterization of two novel calpain large subunit genes. *Gene* **274:** 245-252.

Dimmock, J.R., Elias, D.W., Beazely, M.A., and Kandepu, N.M. 1999. Bioactivities of chalcones. *Curr Med Chem* **6:** 1125-1149.

Dubaquie, Y., and Lowman, H.B. 1999. Total alanine-scanning mutagenesis of insulin-like growth factor I (IGF-I) identifies differential binding epitopes for IGFBP-1 and IGFBP-3. *Biochemistry* **38:** 6386-6396.

Fielder, P.J., Rosenfeld, R.G., Graves, H.C.B., Grandbois, K., Maack, C.A., Sawamura, S., Ogawa, Y., Sommer, A., and Cohen, P. 1994. Biochemical-Analysis of Prostate-Specific Antigen-Proteolyzed Insulin-Like Growth-Factor Binding Protein-3. *Growth Regulation* **4:** 164-172.

Firth, S.M., and Baxter, R.C. 2002. Cellular actions of the insulin-like growth factor binding proteins. *Endocr Rev* **23:** 824-854.

Fischer, S., Vandekerckhove, J., Ampe, C., Traub, P., and Weber, K. 1986a. Protein-Chemical Identification of the Major Cleavage Sites of the Ca2 Proteinase on Murine Vimentin, the Mesenchymal Intermediate Filament Protein. *Biological Chemistry Hoppe-Seyler* **367:** 1147-1152.

Fischer, S., Vandekerckhove, J., Ampe, C., Traub, P., and Weber, K. 1986b. Protein-chemical identification of the major cleavage sites of the Ca2+ proteinase on murine vimentin, the mesenchymal intermediate filament protein. *Biol Chem Hoppe Seyler* **367:** 1147-1152.

Fowlkes, J.L., Enghild, J.J., Suzuki, K., and Nagase, H. 1994. Matrix Metalloproteinases Degrade Insulin-Like Growth Factor-Binding Protein-3 in Dermal Fibroblast-Cultures. *Journal of Biological Chemistry* **269:** 25742-25746.

Freedman, D.A., Epstein, C.B., Roth, J.C., and Levine, A.J. 1997. A genetic approach to mapping the p53 binding site in the MDM2 protein. *Mol Med* **3:** 248-259.

Fuchs, E., and Weber, K. 1994. Intermediate Filaments - Structure, Dynamics, Function, and Disease. *Annual Review of Biochemistry* **63:** 345-382.

Goll, D.E., Thompson, V.F., Li, H., Wei, W., and Cong, J. 2003. The calpain system. *Physiol Rev* **83:** 731-801.

Goll, D.E., Thompson, V.F., Taylor, R.G., and Zalewska, T. 1992. Is calpain activity regulated by membranes and autolysis or by calcium and calpastatin? *Bioessays* **14:** 549-556.

Harris, A.S., Croall, D.E., and Morrow, J.S. 1988. The Calmodulin-Binding Site in Alpha-Fodrin Is near the Calcium-Dependent Protease-I Cleavage Site. *Journal of Biological Chemistry* **263:** 15754-15761.

Hashimoto, R., Ono, M., Fujiwara, H., Higashihashi, N., Yoshida, M., Enjoh-Kimura, T., and Sakano, K. 1997. Binding sites and binding properties of binary and ternary complexes of insulin-like growth factor-II (IGF-II), IGF-binding protein-3, and acid-labile subunit. *J Biol Chem* **272:** 27936-27942.

Ho, P.J., and Baxter, R.C. 1997. Characterization of truncated insulin-like growth factor-binding protein-2 in human milk. *Endocrinology* **138:** 3811-3818.

Hodgson, D.R., May, F.E., and Westley, B.R. 1996. Involvement of phenylalanine 23 in the binding of IGF-1 to the insulin and type I IGF receptor. *Regul Pept* **66:** 191-196.

Horikawa, Y., Oda, N., Cox, N.J., Li, X., Orho-Melander, M., Hara, M., Hinokio, Y., Lindner, T.H., Mashima, H., Schwarz, P.E., et al. 2000. Genetic variation in the gene encoding calpain-10 is associated with type 2 diabetes mellitus. *Nat Genet* **26:** 163-175.

Hsieh, J.K., Chan, F.S., O'Connor, D.J., Mittnacht, S., Zhong, S., and Lu, X. 1999. RB regulates the stability and the apoptotic function of p53 via MDM2. *Mol Cell* **3:** 181-193.

Hwa, V., Oh, Y., and Rosenfeld, R.G. 1999. Insulin-like growth factor binding proteins: a proposed superfamily. *Acta Paediatr Suppl* **88:** 37-45.

Iizuka, K., Kawaguchi, H., and Yasuda, H. 1991. Calpain is activated during hypoxic myocardial cell injury. *Biochem Med Metab Biol* **46:** 427-431.

Imai, Y., Busby, W.H., Smith, C.E., Clarke, J.B., Garmong, A.J., Horwitz, G.D., Rees, C., and Clemmons, D.R. 1997. Protease-resistant form of insulin-like growth factor-binding protein 5 is an inhibitor of insulin-like growth factor-I actions on porcine smooth muscle cells in culture. *Journal of Clinical Investigation* **100:** 2596-2605.

Irwin, M., Marin, M.C., Phillips, A.C., Seelan, R.S., Smith, D.I., Liu, W., Flores, E.R., Tsai, K.Y., Jacks, T., Vousden, K.H., et al. 2000. Role for the p53 homologue p73 in E2F-1-induced apoptosis. *Nature* **407:** 645-648.

Iwakuma, T., and Lozano, G. 2003. MDM2, an introduction. *Mol Cancer Res* **1:** 993-1000.

Jaques, G., Noll, K., Wegmann, B., Witten, S., Kogan, E., Radulescu, R.T., and Havemann, K. 1997. Nuclear localization of insulin-like growth factor binding protein 3 in a lung cancer cell line. *Endocrinology* **138:** 1767-1770.

Johnson, K.R., Young, K.K., and Fan, W. 1999. Antagonistic interplay between antimitotic and G1-S arresting agents observed in experimental combination therapy. *Clin Cancer Res* **5:** 2559-2565.

Kalus, W., Baumgartner, R., Renner, C., Noegel, A., Chan, F.K., Winoto, A., and Holak, T.A. 1997. NMR structural characterization of the CDK inhibitor p19INK4d. *FEBS Lett* **401:** 127-132.

Kalus, W., Zweckstetter, M., Renner, C., Sanchez, Y., Georgescu, J., Grol, M., Demuth, D., Schumacher, R., Dony, C., Lang, K., et al. 1998. Structure of the IGF-binding domain of the insulin-like growth factor-binding protein-5 (IGFBP-5): Implications for IGF and IGF-I receptor interactions. *Embo Journal* **17:** 6558-6572.

Khandwala, H.M., McCutcheon, I.E., Flyvbjerg, A., and Friend, K.E. 2000. The effects of insulin-like growth factors on tumorigenesis and neoplastic growth. *Endocr Rev* **21:** 215-244.

Khorchid, A., and Ikura, M. 2002. How calpain is activated by calcium. *Nat Struct Biol* **9:** 239-241.

Kohli, V., Gao, W., Camargo, C.A., Jr., and Clavien, P.A. 1997. Calpain is a mediator of preservation-reperfusion injury in rat liver transplantation. *Proc Natl Acad Sci U S A* **94:** 9354-9359.

Kumar, S.K., Hager, E., Pettit, C., Gurulingappa, H., Davidson, N.E., and Khan, S.R. 2003. Design, synthesis, and evaluation of novel boronic-chalcone derivatives as antitumor agents. *J Med Chem* **46:** 2813-2815.

Kussie, P.H., Gorina, S., Marechal, V., Elenbaas, B., Moreau, J., Levine, A.J., and Pavletich, N.P. 1996. Structure of the MDM2 oncoprotein bound to the p53 tumor suppressor transactivation domain. *Science* **274:** 948-953.

Lalou, C., Sawamura, S., Segovia, B., Ogawa, Y., and Binoux, M. 1997. Proteolytic fragments of insulin-like growth factor binding protein-3: N-terminal sequences and relationships between structure and biological activity. *Comptes Rendus De L Academie Des Sciences Serie Iii-Sciences De La Vie-Life Sciences* **320:** 621-628.

Laursen, L.S., Overgaard, M.T., Soe, R., Boldt, H.B., Sottrup-Jensen, L., Giudice, L.C., Conover, C.A., and Oxvig, C. 2001. Pregnancy-associated plasma protein-A (PAPP-A) cleaves insulin-like growth factor binding protein (IGFBP)-5 independent of IGF:

implications for the mechanism of IGFBP-4 proteolysis by PAPP-A. *Febs Letters* **504:** 36-40.

Lee, K.S., Frank, S., Vanderklish, P., Arai, A., and Lynch, G. 1991. Inhibition of proteolysis protects hippocampal neurons from ischemia. *Proc Natl Acad Sci U S A* **88:** 7233-7237.

Leone, G., DeGregori, J., Yan, Z., Jakoi, L., Ishida, S., Williams, R.S., and Nevins, J.R. 1998. E2F3 activity is regulated during the cell cycle and is required for the induction of S phase. *Genes & Development* **12:** 2120-2130.

Levine, R.A., and Fleischli, M.A. 2000. Inactivation of p53 and retinoblastoma family pathways in canine osteosarcoma cell lines. *Vet Pathol* **37:** 54-61.

Li, H., Thompson, V.F., and Goll, D.E. 2002. Effects of autolysis an properties of mu- and m-calpain. *Molecular Biology of the Cell* **13:** 304A-304A.

Li, Y., Chopp, M., Powers, C., and Jiang, N. 1997. Apoptosis and protein expression after focal cerebral ischemia in rat. *Brain Res* **765:** 301-312.

Lin, Y.M., Zhou, Y., Flavin, M.T., Zhou, L.M., Nie, W., and Chen, F.C. 2002. Chalcones and flavonoids as anti-tuberculosis agents. *Bioorg Med Chem* **10:** 2795-2802.

Lohrum, M.A., Ashcroft, M., Kubbutat, M.H., and Vousden, K.H. 2000. Identification of a cryptic nucleolar-localization signal in MDM2. *Nat Cell Biol* **2:** 179-181.

Lundberg, A.S., and Weinberg, R.A. 1998. Functional inactivation of the retinoblastoma protein requires sequential modification by at least two distinct cyclin-cdk complexes. *Mol Cell Biol* **18:** 753-761.

Malumbres, M., Ortega, S., and Barbacid, M. 2000. Genetic analysis of mammalian cyclin-dependent kinases and their inhibitors. *Biol Chem* **381:** 827-838.

Manes, S., Mira, E., Barbacid, M.D., Cipres, A., FernandezResa, P., Buesa, J.M., Merida, I., Aracil, M., Marquez, G., and Martinez, C. 1997. Identification of insulin-like growth factor-binding protein-1 as a potential physiological substrate for human stromelysin-3. *Journal of Biological Chemistry* **272:** 25706-25712.

Matsumura, Y., Saeki, E., Otsu, K., Morita, T., Takeda, H., Kuzuya, T., Hori, M., and Kusuoka, H. 2001. Intracellular calcium level required for calpain activation in a single myocardial cell. *J Mol Cell Cardiol* **33:** 1133-1142.

Mellgren, R.L. 1997. Evidence for participation of a calpain-like cysteine protease in cell cycle progression through late G(1) phase. *Biochemical and Biophysical Research Communications* **236:** 555-558.

Moldoveanu, T., Hosfield, C.M., Lim, D., Elce, J.S., Jia, Z., and Davies, P.L. 2002. A Ca(2+) switch aligns the active site of calpain. *Cell* **108:** 649-660.

Moldoveanu, T., Hosfield, C.M., Lim, D., Jia, Z., and Davies, P.L. 2003. Calpain silencing by a reversible intrinsic mechanism. *Nat Struct Biol* **10:** 371-378.

Montes de Oca Luna, R., Wagner, D.S., and Lozano, G. 1995. Rescue of early embryonic lethality in mdm2-deficient mice by deletion of p53. *Nature* **378:** 203-206.

Mori, S., Abeygunawardana, C., Johnson, M.O., and van Zijl, P.C. 1995. Improved sensitivity of HSQC spectra of exchanging protons at short interscan delays using a new fast HSQC (FHSQC) detection scheme that avoids water saturation. *J Magn Reson B* **108:** 94-98.

Oliner, J.D., Kinzler, K.W., Meltzer, P.S., George, D.L., and Vogelstein, B. 1992. Amplification of a gene encoding a p53-associated protein in human sarcomas. *Nature* **358:** 80-83.

Oliner, J.D., Pietenpol, J.A., Thiagalingam, S., Gyuris, J., Kinzler, K.W., and Vogelstein, B. 1993. Oncoprotein MDM2 conceals the activation domain of tumour suppressor p53. *Nature* **362:** 857-860.

Olson, D.C., Marechal, V., Momand, J., Chen, J., Romocki, C., and Levine, A.J. 1993. Identification and characterization of multiple mdm-2 proteins and mdm-2-p53 protein complexes. *Oncogene* **8:** 2353-2360.

Ono, Y., Sorimachi, H., and Suzuki, K. 1998. Structure and physiology of calpain, an enigmatic protease. *Biochem Biophys Res Commun* **245:** 289-294.

Pal, G.P., De Veyra, T., Elce, J.S., and Jia, Z. 2003a. Crystal structure of a micro-like calpain reveals a partially activated conformation with low Ca2+ requirement. *Structure (Camb)* **11:** 1521-1526.

Pal, G.P., De Veyra, T., Elce, J.S., and Jia, Z.C. 2003b. Crystal structure of a mu-like calpain reveals a partially activated conformation with low Ca2+ requirement. *Structure* **11:** 1521-1526.

Patel, Y.M., and Lane, M.D. 2000. Mitotic clonal expansion during preadipocyte differentiation: calpain-mediated turnover of p27. *J Biol Chem* **275:** 17653-17660.

Pavletich, N.P. 1999. Mechanisms of cyclin-dependent kinase regulation: structures of Cdks, their cyclin activators, and Cip and INK4 inhibitors. *J Mol Biol* **287:** 821-828.

Payet, L.D., Wang, X.H., Baxter, R.C., and Firth, S.M. 2003. Amino- and carboxyl-terminal fragments of insulin-like growth factor (IGF) binding protein-3 cooperate to bind IGFs

with high affinity and inhibit IGF receptor interactions. *Endocrinology* **144:** 2797-2806.

Perry, M.E., Piette, J., Zawadzki, J.A., Harvey, D., and Levine, A.J. 1993. The mdm-2 gene is induced in response to UV light in a p53-dependent manner. *Proc Natl Acad Sci U S A* **90:** 11623-11627.

Pollak, M.N. 1998. Endocrine effects of IGF-I on normal and transformed breast epithelial cells: potential relevance to strategies for breast cancer treatment and prevention. *Breast Cancer Res Treat* **47:** 209-217.

Pollak, M.N., Schernhammer, E.S, and Hankinson, S.E. 2004. Insulin-like growth factors and neoplasia. *Nature Rev Cancer* **4:** 505 518.

Pontremoli, S., Viotti, P.L., Michetti, M., Sparatore, B., Salamino, F., and Melloni, E. 1990. Identification of an endogenous activator of calpain in rat skeletal muscle. *Biochem Biophys Res Commun* **171:** 569-574.

Rami, A., and Krieglstein, J. 1993. Protective effects of calpain inhibitors against neuronal damage caused by cytotoxic hypoxia in vitro and ischemia in vivo. *Brain Res* **609:** 67-70.

Rehm, T., Huber, R., and Holak, T.A. 2002. Application of NMR in structural proteomics: screening for proteins amenable to structural analysis. *Structure (Camb)* **10:** 1613-1618.

Renner, C., Baumgartner, R., Noegel, A.A., and Holak, T.A. 1998. Backbone dynamics of the CDK inhibitor p19(INK4d) studied by 15N NMR relaxation experiments at two field strengths. *J Mol Biol* **283:** 221-229.

Richard, I., Roudaut, C., Saenz, A., Pogue, R., Grimbergen, J.E., Anderson, L.V., Beley, C., Cobo, A.M., de Diego, C., Eymard, B., et al. 1999. Calpainopathy-a survey of mutations and polymorphisms. *Am J Hum Genet* **64:** 1524-1540.

Rodriguez, M.S., Desterro, J.M., Lain, S., Lane, D.P., and Hay, R.T. 2000. Multiple C-terminal lysine residues target p53 for ubiquitin-proteasome-mediated degradation. *Mol Cell Biol* **20:** 8458-8467.

Roth, J., Dobbelstein, M., Freedman, D.A., Shenk, T., and Levine, A.J. 1998. Nucleo-cytoplasmic shuttling of the hdm2 oncoprotein regulates the levels of the p53 protein via a pathway used by the human immunodeficiency virus rev protein. *Embo J* **17:** 554-564.

Ruas, M., Brookes, S., McDonald, N.Q., and Peters, G. 1999. Functional evaluation of tumour-specific variants of p16INK4a/CDKN2A: correlation with protein structure information. *Oncogene* **18:** 5423-5434.

Rudolph, R., and Lilie, H. 1996. In vitro folding of inclusion body proteins. *Faseb J* **10:** 49-56.

Russo, A.A., Tong, L., Lee, J.O., Jeffrey, P.D., and Pavletich, N.P. 1998. Structural basis for inhibition of the cyclin-dependent kinase Cdk6 by the tumour suppressor p16INK4a. *Nature* **395:** 237-243.

Saido, T.C., Shibata, M., Takenawa, T., Murofushi, H., and Suzuki, K. 1992. Positive regulation of mu-calpain action by polyphosphoinositides. *J Biol Chem* **267:** 24585-24590.

Salahifar, H., Firth, S.M., Baxter, R.C., and Martin, J.L. 2000. Characterization of an amino-terminal fragment of insulin like growth factor binding protein 3 and its effects in MCF-7 breast cancer cells. *Growth Hormone & Igf Research* **10:** 367-377.

Salvesen, G., Parkes, C., Abrahamson, M., Grubb, A., and Barrett, A.J. 1986. Human low-Mr kininogen contains three copies of a cystatin sequence that are divergent in structure and in inhibitory activity for cysteine proteinases. *Biochem J* **234:** 429-434.

Sasaki, T., Kikuchi, T., Yumoto, N., Yoshimura, N., and Murachi, T. 1984a. Comparative specificity and kinetic studies on porcine calpain I and calpain II with naturally occurring peptides and synthetic fluorogenic substrates. *J Biol Chem* **259:** 12489-12494.

Sasaki, T., Kikuchi, T., Yumoto, N., Yoshimura, N., and Murachi, T. 1984b. Comparative Specificity and Kinetic-Studies on Porcine Calpain-I and Calpain-Ii with Naturally-Occurring Peptides and Synthetic Fluorogenic Substrates. *Journal of Biological Chemistry* **259:** 2489-2494.

Schedlich, L.J., Nilsen, T., John, A.P., Jans, D.A., and Baxter, R.C. 2003. Phosphorylation of insulin-like growth factor binding protein-3 by deoxyribonucleic acid-dependent protein kinase reduces ligand binding and enhances nuclear accumulation. *Endocrinology* **144:** 1984-1993.

Schon, O., Friedler, A., Bycroft, M., Freund, S.M., and Fersht, A.R. 2002. Molecular mechanism of the interaction between MDM2 and p53. *J Mol Biol* **323:** 491-501.

Shand, J.H., Beattie, J., Song, H., Phillips, K., Kelly, S.M., Flint, D.J., and Allan, G.J. 2003. Specific amino acid substitutions determine the differential contribution of the N- and

C-terminal domains of insulin-like growth factor (IGF)-binding protein-5 in binding IGF-I. *Journal of Biological Chemistry* **278:** 17859-17866.

Sherr, C.J. 1996. Cancer cell cycles. *Science* **274:** 1672-1677.

Sherr, C.J., and DePinho, R.A. 2000. Cellular senescence: mitotic clock or culture shock? *Cell* **102:** 407-410.

Sherr, C.J., and Roberts, J.M. 1999. CDK inhibitors: positive and negative regulators of G1-phase progression. *Genes Dev* **13:** 1501-1512.

Shih, M., Lampi, K.J., Shearer, T.R., and David, L.L. 1998. Cleavage of beta crystallins during maturation of bovine lens. *Mol Vis* **4:** 4.

Sorimachi, H., Imajoh-Ohmi, S., Emori, Y., Kawasaki, H., Ohno, S., Minami, Y., and Suzuki, K. 1989. Molecular cloning of a novel mammalian calcium-dependent protease distinct from both m- and mu-types. Specific expression of the mRNA in skeletal muscle. *J Biol Chem* **264:** 20106-20111.

Sorimachi, H., and Suzuki, K. 2001. The structure of calpain. *J Biochem (Tokyo)* **129:** 653-664.

Stabach, P.R., Cianci, C.D., Glantz, S.B., Zhang, Z.S., and Morrow, J.S. 1997. Site-directed mutagenesis of alpha II spectrin at codon 1175 modulates its mu-calpain susceptibility. *Biochemistry* **36:** 57-65.

Stewart, Z.A., Leach, S.D., and Pietenpol, J.A. 1999. p21(Waf1/Cip1) inhibition of cyclin E/Cdk2 activity prevents endoreduplication after mitotic spindle disruption. *Mol Cell Biol* **19:** 205-215.

Stoll, R., Renner, C., Hansen, S., Palme, S., Klein, C., Belling, A., Zeslawski, W., Kamionka, M., Rehm, T., Muhlhahn, P., et al. 2001. Chalcone derivatives antagonize interactions between the human oncoprotein MDM2 and p53. *Biochemistry* **40:** 336-344.

Stott, F.J., Bates, S., James, M.C., McConnell, B.B., Starborg, M., Brookes, S., Palmero, I., Ryan, K., Hara, E., Vousden, K.H., et al. 1998. The alternative product from the human CDKN2A locus, p14(ARF), participates in a regulatory feedback loop with p53 and MDM2. *Embo J* **17:** 5001-5014.

Strelkov, S.V., Herrmann, H., Geisler, N., Wedig, T., Zimbelmann, R., Aebi, U., and Burkhard, P. 2002. Conserved segments 1A and 2B of the intermediate filament dimer: their atomic structures and role in filament assembly. *Embo Journal* **21:** 1255-1266.

Strobl, S., Fernandez-Catalan, C., Braun, M., Huber, R., Masumoto, H., Nakagawa, K., Irie, A., Sorimachi, H., Bourenkow, G., Bartunik, H., et al. 2000. The crystal structure of

calcium-free human m-calpain suggests an electrostatic switch mechanism for activation by calcium. *Proceedings of the National Academy of Sciences of the United States of America* **97:** 588-592.

Takano, E., Ma, H., Yang, H.Q., Maki, M., and Hatanaka, M. 1995. Preference of calcium-dependent interactions between calmodulin-like domains of calpain and calpastatin subdomains. *FEBS Lett* **362:** 93-97.

Tompa, P., Emori, Y., Sorimachi, H., Suzuki, K., and Friedrich, P. 2001. Domain III of calpain is a ca2+-regulated phospholipid-binding domain. *Biochem Biophys Res Commun* **280:** 1333-1339.

Torres-Aleman, I., Barrios, V., Lledo, A., and Berciano, J. 1996. The insulin-like growth factor I system in cerebellar degeneration. *Ann Neurol* **39:** 335-342.

Tsutsui, T., Hesabi, B., Moons, D.S., Pandolfi, P.P., Hansel, K.S., Koff, A., and Kiyokawa, H. 1999. Targeted disruption of CDK4 delays cell cycle entry with enhanced p27(Kip1) activity. *Mol Cell Biol* **19:** 7011-7019.

Vanderklish, P.W., and Bahr, B.A. 2000. The pathogenic activation of calpain: a marker and mediator of cellular toxicity and disease states. *Int J Exp Pathol* **81:** 323-339.

Vassilev, L.T. 2004. Small-molecule antagonists of p53-MDM2 binding: research tools and potential therapeutics. *Cell Cycle* **3:** 419-421.

Vassilev, L.T., Vu, B.T., Graves, B., Carvajal, D., Podlaski, F., Filipovic, Z., Kong, N., Kammlott, U., Lukacs, C., Klein, C., et al. 2004. In vivo activation of the p53 pathway by small-molecule antagonists of MDM2. *Science* **303:** 844-848.

Vermeulen, K., Berneman, Z.N., and Van Bockstaele, D.R. 2003. Cell cycle and apoptosis. *Cell Prolif* **36:** 165-175.

Vogelstein, B., and Kinzler, K.W. 2001. Achilles' heel of cancer? *Nature* **412:** 865-866.

Wang, H., Oliver, P., Zhang, Z., Agrawal, S., and Zhang, R. 2003. Chemosensitization and radiosensitization of human cancer by antisense anti-MDM2 oligonucleotides: in vitro and in vivo activities and mechanisms. *Ann N Y Acad Sci* **1002:** 217-235.

Wang, J.F., Hampton, B., Mehlman, T., Burgess, W.H., and Rechler, M.M. 1988. Isolation of a Biologically-Active Fragment from the Carboxy Terminus of the Fetal-Rat Binding-Protein for Insulin-Like Growth-Factors. *Biochemical and Biophysical Research Communications* **157:** 718-726.

Wang, K.K. 2000. Calpain and caspase: can you tell the difference? *Trends Neurosci* **23:** 20-26.

Wattenberg, L. 1995. Chalcones, myo-inositol and other novel inhibitors of pulmonary carcinogenesis. *J Cell Biochem Suppl* **22:** 162-168.

Weinberg, R.A. 1995. The Retinoblastoma Protein and Cell-Cycle Control. *Cell* **81:** 323-330.

Wu, L., and Levine, A.J. 1997. Differential regulation of the p21/WAF-1 and mdm2 genes after high-dose UV irradiation: p53-dependent and p53-independent regulation of the mdm2 gene. *Mol Med* **3:** 441-451.

Wuthrich, K., Billeter, M., and Braun, W. 1984. Polypeptide secondary structure determination by nuclear magnetic resonance observation of short proton-proton distances. *J Mol Biol* **180:** 715-740.

Xiao, Z.X., Chen, J., Levine, A.J., Modjtahedi, N., Xing, J., Sellers, W.R., and Livingston, D.M. 1995. Interaction between the retinoblastoma protein and the oncoprotein MDM2. *Nature* **375:** 694-698.

Yamamoto, S., Shimizu, K., Suzuki, K., Nakagawa, Y., and Yamamuro, T. 1992. Calcium-dependent cysteine proteinase (calpain) in human arthritic synovial joints. *Arthritis Rheum* **35:** 1309-1317.

Yu, H., and Rohan, T. 2000. Role of the insulin-like growth factor family in cancer development and progression. *J Natl Cancer Inst* **92:** 1472-1489.

Zauberman, A., Flusberg, D., Haupt, Y., Barak, Y., and Oren, M. 1995. A functional p53-responsive intronic promoter is contained within the human mdm2 gene. *Nucleic Acids Res* **23:** 2584-2592.

Zeslawski, W., Beisel, H.G., Kamionka, M., Kalus, W., Engh, R.A., Huber, R., Lang, K., and Holak, T.A. 2001. The interaction of insulin-like growth factor-I with the N-terminal domain of IGFBP-5. *Embo Journal* **20:** 3638-3644.

Zheng, B., Clarke, J.B., Busby, W.H., Duan, C.M., and Clemmons, D.R. 1998. Insulin-like growth factor-binding protein-5 is cleaved by physiological concentrations of thrombin. *Endocrinology* **139:** 1708-1714.

Zhu, Q., Yao, J., Wani, G., Wani, M.A., and Wani, A.A. 2001. Mdm2 mutant defective in binding p300 promotes ubiquitination but not degradation of p53: evidence for the role of p300 in integrating ubiquitination and proteolysis. *J Biol Chem* **276:** 29695-29701.

Ziemka-Nalecz, M., Zalewska, T., Zajac, H., and Domanska-Janik, K. 2003. Decrease of PKC precedes other cellular signs of calpain activation in area CA1 of the hippocampus after transient cerebral ischemia. *Neurochem Int* **42:** 205-214.

Acknowledgements

I am grateful to Professor Robert Huber for providing me with the opportunity to work in his department as a research scholar.

I am indebted to my supervisor Dr. Tad A. Holak, for his unfailing support and encouragement which helped me through this thesis.

I am thankful to all the members of our structural research group for providing a stimulating research environment. A special thanks goes to my lab members, Igor Siwanowicz, Marcin Krajewski Ulli Rothweiler, Grzegorz Popwicz, Dr. Dorota Ksiazek Dr. Chrystelle Mavoungou, Dr. Till Rehm, Dr. Pawel Smialowski, Dr. Narashimha Rao Nalabothula, Mahavir Singh, Sudipta Majumdar, Loyola D'Silva, Joma Kanikadu Joy, Aleksandra Mikolajka, Tomasz Sitar and Przemyslaw Ozdowy, for their help and good working atmosphere.

I wish to acknowledge the generosity and helpfulness of all those, whose names are not mentioned.

I owe my thanks to my friend, colleague and now my husband, Sreejesh, whose continuous support and endless love has finally resulted in this thesis.

Last but not the least I am deeply grateful to my mom whose sacrifice and love I can never repay.